Forschungszentrum Juelich GmbH , Institut für Bio- und Geowissenschaften
IBG-3: Agrosphäre.

Coupled hydrogeophysical inversion for soil hydraulic property estimation from time-lapse geophysical data

Inaugural-Dissertation
Zur

Erlangung des Grades

Doktor der Agrarwissenschaft
(Dr.agr.)

der

Landwirtschaftlichen Fakultät

Der

Rheinischen Friedrich-Wilhelms-Universität Bonn

von

Cho Miltin Mboh

aus

Bamenda, Cameroon

Referent: Prof. Dr. Harry Vereecken
Korreferent: Prof. Dr. Andreas Kemna
Tag der mündlichen Prüfung: 14. September 2012
Erscheinungsjahr: 2012

Acknowledgements

I am fortunate to have been supervised by a person of great scientific vigour. Besides constraining my thinking in the direction of coupled hydrogeophysical inversion, the supervisory advice and help of Prof. Sander Huisman even went beyond the academic domain to family life. He conceived the PhD project, applied for and credited the project with grant HU1312/2-1 and HU1312/2-2 of the Deutsche Forschungsgemeinschaft (DFG).

This PhD project had the privilege to be carried out in the Agrosphere Institute of Forschungszentrum Juelich. I am grateful to my promoter and head of the institute, Prof. Harry Vereecken for accepting me as a PhD candidate. Great thanks also go to Prof. Jan Vanderborght through whom I had the opportunity to know this great institute while doing my Msc.

I cannot underestimate the programming help of Horst Hardelauf. He made available a special version of parallel SWMS in which initial conditions in water content can be used. This enabled me to make rapid progress with the PhD project.

I would like to thank the former colleagues of my research group, Dr. Jörg Rings and Jürgen Sorg for the strong collaboration we shared. Whenever I was stuck in a local minimum, they helped me out in the absence of my supervisor.

If there is one way of moving forward, it is to talk to people working on similar topics like yours. Discussions with colleagues like Dr. Khan Zaib Jadoon, Michel Bechtold and Benedikt Scharnagl proved useful. Thank you Dr. C. Montzka for translating the summary of this thesis into German.

Thank you Thomas Schuster for coming to the rescue when there was a blackout on my computer. Your timely intervention helped me from drowning into a sea of discouragement.

I cannot forget the help of Dr. Roy Kasteel and his team for carrying out the multi-step outflow measurements on my soil cores.

Special thanks to Dr. Lutz Weihermüller and co-players of the IBG 3 football team. Our football encounters were a means to keep fit, stay healthy and work well.

The help of administrative staff like Gaby Pillert, R. Bley, and K. Beumers cannot go unnoticed .They helped me to sort out matters with my employment at the Forschungszentrum Jülich and my stay in Germany at the start of my PhD.

I wish to express profound gratitude to Dr. Egon Zimmermann of the central institute for electronics (ZEL) and his team. They set up the electrical impedance system upon which I carried out self potential measurements and spared no efforts to ensure that everything worked well.

I want to acknowledge the moral support and encouragement of my wife Felicia C. Mboh. She improved the English in parts of this manuscript and understood why she had to be alone with my son Promise Awa and my daughter Mercylove Khan when I was absent from home sometimes.

I am very grateful to my mother mama Alice Mafor, my brothers George Mboh, Eric Mboh, and Muluh Ibrahim and my sister Fonkou Sylvie. Although there are very far from me in Cameroon, they have always assured me that out of sight is not out of mind.

Above all, I am most greatful to the Almigthy God for sustaining me to face this challenge.

Summary

Good knowledge of the hydraulic properties of the vadose zone is important for understanding water flow and solute transport processes therein. This can help to promote sustainable use and mitigate anthropogenic threats to soil and water resources. The use of time-lapse geophysical data to constrain our understanding of the flow and transport properties of the vadose zone is now well recognised. Conventional use of geophysical data to estimate the hydraulic properties of the vadose zone is based on an uncoupled inversion approach including an ill-posed tomograhic inversion step which can lead to error propagation to the estimated hydraulic properties. One way of improving the accuracy of estimating soil hydraulic properties is to use a so-called coupled hydrogeophysical inversion approach. In this inversion approach, the tomograhic inversion step is avoided as geophysical measurements are directly used in the hydrological inverse problem by coupling a forward model of the geophysical measurements with a hydrological model describing the hydrologic processes under investigation. Although the potential benefits of the coupled inversion approach have been illustrated with synthetic data, there are very few applications of the approach to actual field or laboratory data. Moreover, most studies using this approach focused on electrical resistivity tomography (ERT) and ground penetration radar (GPR), and the usefulness of this inversion approach remains to be explored for a range of other geophysical methods. Although coupled hydrogeophysical inversion frameworks are flexible enough for the integration of multiple hydrologic and geophysical data types, this data fusion aspect has also received less attention. Therefore, the aim of this thesis was to develop inversion frameworks for the estimation of effective subsurface hydraulic parameters from: i) the fusion of ERT and inflow data obtained under constant head infiltration in a field sandy loam, ii) SP data acquired during primary drainage of a sandy soil column, and iii) TDR data obtained under falling head infiltration into an initially dry sandy loam.

Based on synthetic and actual data we showed that it is feasible to estimate three key Mualem-van Genuchten parameters (α, n and K_s), using the developed coupled hydrogeophysical inversion frameworks for ERT, SP and TDR. In all cases, the inversion results compared well with independently obtained values. With respect to the fusion of ERT and inflow data, it was observed that the success of the procedure depends on the choice of an appropriate objective function. The best results were obtained when an objective function defined as the sum of the root mean square error of both data types normalized by the standard deviation of the respective measurements was used. On the other hand, successful inversion of the SP data depended on efficient pre-treatment of the measured signals prior to inversion and the availability of an adequate model for the voltage coupling coefficient at partial saturation. By comparing different models for the voltage coupling coefficient at partial saturation to the experimental data, it was observed that models that relate the voltage coupling coefficient to the relative permeability of the porous medium in addition to the saturation in water were most appropriate. In the case of inversion of TDR data, a comparison of the coupled and uncoupled inversion approaches revealed that the coupled inversion approach is more practical and less uncertain. Particularly it was observed that coupled hydrogeophysical inversion enables simultaneous monitoring of ponding depth and water infiltration, which avoids the laborious task of manually measuring the ponding depths and can thus enable rapid estimation of the soil hydraulic parameters for multiple locations through automatic measurements of ponded infiltration for multiple rings through TDR multiplexing.

Future studies should focus on using the coupled hydrogeophysical inversion approach to estimate spatially varying hydraulic properties which are more characteristic of the vadose zone. At the expense of a higher computational cost, better estimates of parameter uncertainties can be obtained with the use of MCMC algorithms that provide posterior probability distributions of the inverted parameters.

Zusammenfassung

Die genaue Kenntnis der hydraulischen Eigenschaften der ungesättigten Zone ist wichtig für das Verständnis deren Wasser- und Stofftransportprozesse. Dies fördert eine nachhaltige Nutzung und mildert anthropogene Gefahren für die Ressourcen Boden und Wasser. Zeitabhängige geophysikalische Daten sind mittlerweile eine weithin akzeptierte Quelle zur Erweiterung unseres Wissens um Fluss- und Transporteigenschaften der ungesättigten Zone. Der herkömmliche Einsatz geophysikalischer Daten zur Abschätzung hydraulischer Eigenschaften der ungesättigten Zone folgt einem sequentiellen Ansatz, der als ungekoppelte hydrogeophysikalische Inversion bezeichnet wird. Diese Inversion ist typischerweise unterbestimmt und schlecht konditioniert, und erfordert Regularisierung zur Stabilisierung des inversen Problems. Ein Weg, um die Genauigkeit der Abschätzung bodenhydraulischer Eigenschaften zu verbessern ist daher, eine gekoppelte hydrogeophysikalische Inversion zu entwickeln. In diesem gekoppelten Inversionsansatz werden die geophysikalischen Messungen sofort im hydrologischen Inversionsproblem eingesetzt, indem das Vorwärtsmodell der geophysikalischen Messungen an ein hydrologisches Modell zur Beschreibung der beobachteten hydrologischen Prozesse gekoppelt wird. Obgleich die möglichen Vorteile der gekoppelten hydrogeophysikalischen Inversion an synthetischen Daten demonstriert wurden, gibt es bislang nur wenige Anwendungen der Methode auf reale Feld- oder Labordaten. Außerdem konzentrieren sich die meisten Studien, die den gekoppelten hydrogeophysikalischen Inversionsansatz einsetzen auf elektrische Widerstands-Tomographie (electrical resistivity tomography, ERT) und Bodenradar (ground penetrating radar, GPR). Die Möglichkeiten dieses Inversionsansatzes sollten für eine größere Vielfalt geophysikalischer Methoden untersucht werden. Obwohl gekoppelte hydrogeophysikalische Inversionssysteme flexibel genug sind, um mehrere hydrologische und geophysikalische Datentypen zu integrieren, hat dieser Aspekt der Datenverschmelzung bislang wenig Aufmerksamkeit erhalten. Daher war das Ziel dieser Dissertation, gekoppelte hydrogeophysikalische Inversionssysteme für die Abschätzung von effektiven hydraulischen Parametern zu entwickeln, mit Hilfe: i) einer Fusion von ERT und Zuflussdaten, die unter konstantem Druckbedingungen am Rand im Feld gemessen wurden, ii) der Beobachtung des Strömungspotentials (SP), und iii) der Zeitbereichsreflektometrie (time domain reflectometry, TDR).
Anhand von synthetischen und realen Daten wurde gezeigt, dass die Schätzung von drei Mualem-van Genuchten Parametern (α, n und K_s) mit dem gekoppelten hydrogeophysikalischen Inversionsansatz für ERT, SP und TDR möglich ist. In allen Fällen zeigten die Inversionsergebnisse signifikante Übereinstimmungen mit unabhängigen Daten. Bei der Fusion von ERT und Zuflussdaten wurde beobachtet, dass der Erfolg des Ansatzes von der Wahl einer adäquaten Zielfunktion abhängt. Die besten Ergebnisse wurden erzielt, wenn die Zielfunktion als Summe des mittleren quadratischen Fehlers beider Datentypen definiert wurde, normalisiert durch die Standardabweichung der jeweiligen Messungen. Im Falle der Strömungspotenzialmessungen hängt der Erfolg des Ansatzes davon ab, ob das gemessene Strömungspotentialsignal effizient vor der Inversion vorbehandelt wird und von der Verfügbarkeit eines angemessenen Modells des elektrokinetischen Kopplungskoeffizienten bei teilweiser Sättigung. Im Vergleich verschiedener Modelle für diesen Koeffizienten mit den Daten des Experimentes konnte beobachtet werden, dass diejenigen Modelle am erfolgreichsten waren, die den Kopplungskoeffizient zusätzlich zur Wassersättigung mit der relativen Permeabilität des porösen Mediums verbinden. Im Vergleich zur ungekoppelten Inversion ist die gekoppelte Inversion bei Einsatz von TDR genauer und besser für den praktischen Einsatz geeignet, unter anderem da der Wasserstand auf dem Boden nicht gemessen werden muss.

Zukünftige Untersuchungen sollten die gekoppelte hydrogeophysikalische Inversion verwenden, um räumlich variable hydraulische Parameter abzuschätzen, die typisch für die meisten Feldbedingungen sind

Contents

List of Tables

List of Figures

1. General introduction

1.1. Background and state of the art

Water is perhaps the most vital resource that makes life possible on earth, besides air. Although the total amount of fresh water on earth measures almost 35 million km^3, this represents less than 3% of the total amount of water on earth (Wetzel, 2001). Global fresh water consumption has increased dramatically with explosion in human population due to increases in municipal water supply, water need for agriculture, industry and urban development. Pearce (1992) predicted that access to sufficient water of good quality will be one of the major problems humanity will face in the 21st century. Presently, this finite and vital resource is frequently under threat by pollution, groundwater depletion and soil erosion.

As a transition zone between the atmosphere and the groundwater reservoirs, the vadose zone determines the quality and quantity of fresh water resources through the separation of precipitation into infiltration, evapotranspiration and runoff. Processes like plant growth, the exchange of energy between the earth's surface and the atmosphere, the aerobic degradation of solutes and nutrients, groundwater recharge, contaminant transport and river discharge are linked to the physico-chemical, biological and hydrological properties of the vadose zone.

For efficient soil and water resources management including the design of appropriate groundwater use, pollution control and remediation strategies, it is important to understand the flow and transport properties of the vadose zone. The flow and transport properties of the vadose zone are traditionally estimated with hydrological models by solving the equation of Richards (1931). To solve the Richards' equation, information on the retention and hydraulic conductivity functions characterising the vadose zone need to be provided. The soil water retention function expresses the relation between volumetric soil water content and matric potential. Similarly, the hydraulic conductivity function expresses the soil hydraulic conductivity as a function of matric potential. Constitutive relationships have been developed over the past decades to predict hydraulic conductivity and water retention functions (e.g. Burdine, 1953; Brooks and Corey, 1964; Mualem, 1976; van Genuchten, 1980). Conventionally these functions are determined either from time-consuming and costly direct measurement methods (Klute and Dirksen, 1986) or indirectly based on inverse modelling with hydrologic data. Examples of inverse modelling with hydrologic data for the estimation of hydraulic conductivity and water retention functions include the use cumulative outflow and/or pressure head measurements from multi-step drainage on undisturbed soil cores (e.g. Toorman et al., 1992; Eching and Hopmans, 1993; van Dam et al., 1994; Simunek et al., 1998). Similarly, matric head data from tensiometry (e.g. Timlin and Pachepsky, 1998; Sisson et al., 2002) , cumulative infiltration from pressure ring (e.g. Vauclin et al., 1994; Gérald-Marchant et al., 1997; Mertens et al., 2002), tension disc infiltrometry (Simunek and van Genuchten, 1996; Simunek et al., 1998a; Wang et al., 1998), and water content from time domain reflectrometry (TDR; Parkin et al., 1995; Zhang et al., 2000) has been used in inverse modelling to estimate these soil properties. Although some of these methods are very precise (e.g multi-step drainage on undisturbed soil cores) they all have the disadvantage of sampling a small (<dm^3) support volume. Due to variations in soil texture and structure (e.g. Ersahin and Brohi, 2006), topography (e.g., Brocca et al., 2007), vegetation cover (e.g., Hupet and Vanclooster, 2002), temperature (e.g., Behaegel et al., 2007), soil hydraulic properties also vary in space. To satisfactorily describe hydrological processes at scales like agricultural land and small catchments which are relevant for efficient soil and water management using the above-mentioned methods, numerous sampling locations are necessary to capture the spatial variability of hydraulic properties. The labor-intensive, invasive, time consuming and expensive nature of these conventional methods for field scale sampling has led to a continued quest for alternative methods.

Due to their ability to provide good views of the subsurface, geophysical methods (e.g. seismic, self-potential, induced polarization, nuclear magnetic resonance, electrical resistivity tomography, electromagnetic induction, ground penetration radar, etc.) are used to probe the earth for mineral and oil exploration and many other scientific disciplines (e.g. National academy of sciences, 2000). With the establishment of suitable petrophysical relations (e.g. Archie, 1942; Waxman and Smits, 1968; Rhoades et al., 1976; Topp et al., 1980) that link geophysical properties (e.g., electrical conductivity, dielectric permittivity, seismic wave velocity) to hydrogeological properties (e.g water content, porosity, permeability, solute masses), the applications of geophysical methods now span from geological to hydrogeological characterization (and therewith the emergence of the field of hydrogeophysics).

The advantages of geophysical measurement techniques like Electrical Resistivity Tomography (ERT), Ground Penetration Radar (GPR), Electromagnetic Induction (EMI) and Self-Potential (SP) monitoring over conventional measurement techniques like Time Domain Reflectometry (TDR), soil coring, and tensiometry for the acquisition of data necessary for the calibration of vadose zone flow and transport models is increasingly being recognised (Hubbard et al., 1999; Chen et al., 2001; Linde et al., 2006a). For instance, GPR (e.g. Binley and Beven, 2003; Cassiani and Binley, 2005; Looms et al., 2008; Jadoon et al., 2010) data can be used to determine the subsurface dielectric permittivity distribution while the subsurface electrical conductivity distribution can be determined from ERT (e.g. Daily et al., 1992; Deiana et al., 2007; Batlle-Aguilar et al., 2009), or EMI (e.g. Sheets and Hendrickx, 1995; Reedy and Scanlon, 2003; Martinez et al., 2009). The dielectric permittivity (e.g Topp et al., 1980) or the electrical conductivity (e.g., Archie, 1942) of the vadose zone can be converted into state variables like water content or solute masses using petrophysical relations. The distribution of subsurface water fluxes can be obtained from SP data (e.g., Jardani et al., 2007). Geophysical techniques can therefore be used to map subsurface hydrologic variables like water content, solute masses and water fluxes at intermediate scales between the small scale measurements such as core samples and TDR and the large scale remotely sensed variable like satellite imagery. This gives geophysical methods the ability to alleviate the cost and difficulty involved in acquiring direct hydrological data at these scales. Furthermore, the geophysical measurement techniques are typically non-invasive and therefore can provide information in regions where conventional techniques cannot sample.

Due to the advantages mentioned above, geophysical measurements are increasingly being used in vadose zone hydrology (e.g., Hubbard and Rubin, 2000; Vereecken et al., 2004). In most studies, geophysical results have been used for qualitative interpretations (e.g., observation of flow and transport patterns) of flow and transport processes (e.g., Binley et al., 1996a; Slater et al., 2000, 2002; Srayeddin and Doussan, 2009; Clément et al., 2010). Much less studies have attempted to obtain relevant quantitative information on hydraulic and transport properties from geophysical measurements. Conventional use of geophysical measurements to derive quantitative estimates of flow and transport properties from vadose zone flow and transport models follows a three-step sequential approach:

1) Geophysical data obtained during a monitored flow or transport process in the vadose zone are inverted to estimate subsurface images of the geophysical property of interest.
2) The obtained geophysical properties of interest are converted into subsurface images of vadose zone hydrologic state variables (e.g., water content or solute mass) using a petrophysical relation (e.g., Archie, 1942; Topp et al., 1980)
3) The estimated state variable distributions are either used independently or in combination with other measured hydrologic states to calibrate a flow or transport model for the estimation of flow or transport properties.

This three-step sequential approach is now referred to as uncoupled hydrogeophysical inversion (Ferre et al., 2009; Hinnell et al., 2010).

There are numerous applications of the uncoupled hydrogeophysical inversion approach. Rubin et al. (1992) used the approach to map the permeability of a heterogeneous aquifer from seismic wave velocities and hydraulic head data. Cassiani and Medina (1997) combined vertical electrical soundings and direct well data within a co-kriging framework to estimate parameters of the transmissivity and transverse formation factor random fields of an aquifer using the uncoupled hydrogeophysical inversion approach. Similarly, Gloaguen et al. (2001) used the approach to combine GPR and hydrostratigrahic data within a cokriging framework to estimate the hydraulic conductivity of an unconfined aquifer. From the first and second moments of water content changes inferred from 2D and 3D cross-bore hole ERT and GPR profiles, Binley et al. (2002a) applied the uncoupled hydrogeophysical inversion approach to estimate the effective hydraulic conductivity of a sandstone aquifer. Chen et al. (2004) used the approach to estimate sediment geochemical parameters from GPR. From time-lapse monitoring of natural infiltration from precipitation into a consolidated sandstone vadose zone with cross-hole zero-offset GPR, Cassiani and Binley (2005) attempted to retrieve subsurface hydraulic properties. Despite these and many other successful case studies, a number of shortcomings have been identified with the uncoupled hydrogeophysical inversion approach:

1) Artificial smoothing of tomograms from regularized geophysical inversion

The independent inversion of the geophysical data to subsurface tomographic images of the geophysical property of interest is generally ill-posed and underdetermined due to the spatial discretisation necessary to capture complex distributions of the property. To condition and stabilize the inverse problem, a regularization constraint (e.g. smoothness) is often applied. This regularization introduces an artificial smoothing of the images and this can lead to highly uncertain estimates of hydraulic and transport parameters when such tomograms are used for calibrating water flow and solute transport models (Day-Lewis et al., 2005, Slater et al., 2007). Besides the type and strength of regularization, the spatial variability of the geophysical property of interest observed within the tomograhic images strongly depends on the prescribed data noise level (LaBrecque et al., 1996; Slater et al., 2000). Overestimation of errors leads to an over-smooth image while underestimation of errors will lead to rough images. While a good assessment of the data noise level is possible with ERT using reciprocal measurements, the estimation of errors in the meaning of “how well can I fit the data” still remains problematic with other geophysical methods.

2) Spatially varying resolution of tomograms

Tomograms obtained from inversion of geophysical data have a spatially varying resolution. This variable resolution is often directly linked to the measurement physics, and in combination with the use of regularization constraints, areas with low resolution might be plagued by inversion artefacts. These artefacts are directly propagated to the estimated hydraulic or transport properties when such tomograms are used in the uncoupled hydrogeophysical inversion approach. For example in borehole GPR tomography, objects located in the middle between the borehole are well resolved, whereas in borehole ERT objects close to the borehole are well resolved, but objects in the middle between boreholes are poorly resolved (Day-Lewis et al., 2005). In a synthetic two well pumping injection experiment, Singha and Gorelick (2005, 2006a) used ERT to monitor the migration of a saline tracer. Although the tomograms provided valuable insights into field scale tracer migration, the standard tomographic inversion resulted in an underestimate of the tracer mass and an overestimation of the effective dispersion coefficient. The authors showed that the tracer mass recovered with ERT measurements can deviate more than 40% from the applied tracer mass and attributed this to the

effects of the varying spatial resolution and spatial smoothing (regularization) within the inversion. The tracer mass recovery was even lower for actual ERT measurements.

3) Lack of hydrologic constraints on geophysical inversion.

An obvious problem is that hydrological information is not used when the geophysical survey data are converted to geophysical properties, although information sharing will most likely improve the results. For example, when ERT measurements are used to monitor the development of a tracer plume during an injection experiment, the total applied mass of solute is not used to constrain the inversion problem of obtaining the spatial distribution of electrical conductivity from ERT measurements.

Much recent research has evolved around the improvement of the uncoupled hydrogeophysical inversion approach. The reviews of Day-Lewis et al. (2005), Looms et al. (2008) and Hinnell et al. (2010) classify the proposed methods into the following categories:

1) Temporal relaxation techniques
The ill-posedness of classical geophysical inversion can be reduced by limiting the number of free parameters through time-lapse inversion approaches (e.g. Oldenborger et al., 2007; Clément et al., 2009; Wilkinson et al., 2010) which allow for simultaneous treating of several spatio-temporal images.

2) Application of spatially variably petrohysical relations
As shown by Day-Lewis et al. (2005), Moysey et al. (2006) and Singha and Gorelick (2006b), one way of mitigating the effects of spatially varying resolution of tomograms is to derive field-scale or apparent petrophysical relationships that vary spatially. Although the tracer mass recovery in an injection experiment improved with these apparent relationships, the derivation of these relationships is cumbersome as they strongly rely on a priori information on field site hydrogeology (e.g. porosity and hydraulic conductivity).

3) Joint inversion approaches
Another method of counteracting resolution artefacts is to construct tomograms from two or more geophysical methods that compliment each other (e.g. Gallardo and Meju, 2003; Musil et al., 2003; Linde et al., 2006). Apart from this complimentary advantage, some joint inversion approaches allow for simultaneous determination of distributions of the geophysical property of interest and petrophysical relations (Hyndman et al., 1994; Hyndman and Gorelick, 1996; Chen et al., 2006; Linde et al., 2006b).

4) Stochastic inversion approaches
Due to the inherent uncertainty associated with the geophysical imaging step of uncoupled hydrogeophysical inversion, stochastic or geostatistical inversion approaches have been developed to estimate hydraulic property distributions based on statistical correlations (e.g correlation lengths) present in the tomographic images and to quantify the uncertainty on the estimated distributions (Cassiani et al., 1998; Hubbard et al., 1999; Yeh et al., 2002; Hansen et al., 2008). The inversion is mainly performed within Bayesian or co-kriging frameworks (e.g. McKenna and Poeter, 1995; Cassiani et al., 1998; Hubbard et al., 2001).

An alternative approach to uncoupled hydrogeophysical inversion which does not involve an intermediate geophysical imaging step was recently proposed (Kowalsky et al., 2004; Lambot et al., 2006; Hinnell et al., 2010; Huisman et al., 2010; Rings et al., 2010). This approach is now referred to as coupled hydrogeophysical inversion (Ferre et al., 2009; Hinnell et al., 2010). In the coupled

hydrogeophysical inversion approach, geophysical measurements are directly used in the hydrological inverse problem by coupling a forward model of the geophysical measurements with a hydrological model describing a hydrologic process under investigation. Figure 1.1 shows a flow chart of the coupled hydrogeophysical inversion approach applied to the estimation of subsurface hydraulic parameters from geophysical response data G_r and hydrologic response data I (e.g., cumulative inflow measurements). Firstly, by perturbing the hydraulic parameters in the hydrologic model, distributions of hydrologic responses (e.g water content, water fluxes, and cumulative infiltration) are simulated and converted into distributions of the geophysical properties G_p* (e.g dielectric permittivity, electrical conductivity) of interest using a suitable petrophysical relationship. Secondly, the simulated geophysical properties of interest are fed into the forward geophysical model to simulate geophysical data (e.g. electrical resistances, GPR travel times or waveforms, streaming potentials) that honour the hydraulic parameter set used for generating the distributions of hydrologic responses. Thirdly, as in classical non-linear inverse modelling, an objective function which expresses the misfit between the simulated geophysical measurements and the corresponding measurements is evaluated. The whole process is repeated with updates of hydraulic parameters sets using an optimization algorithm until a hydraulic parameter set for which there is a close fit between the simulated and the measured geophysical data is found.

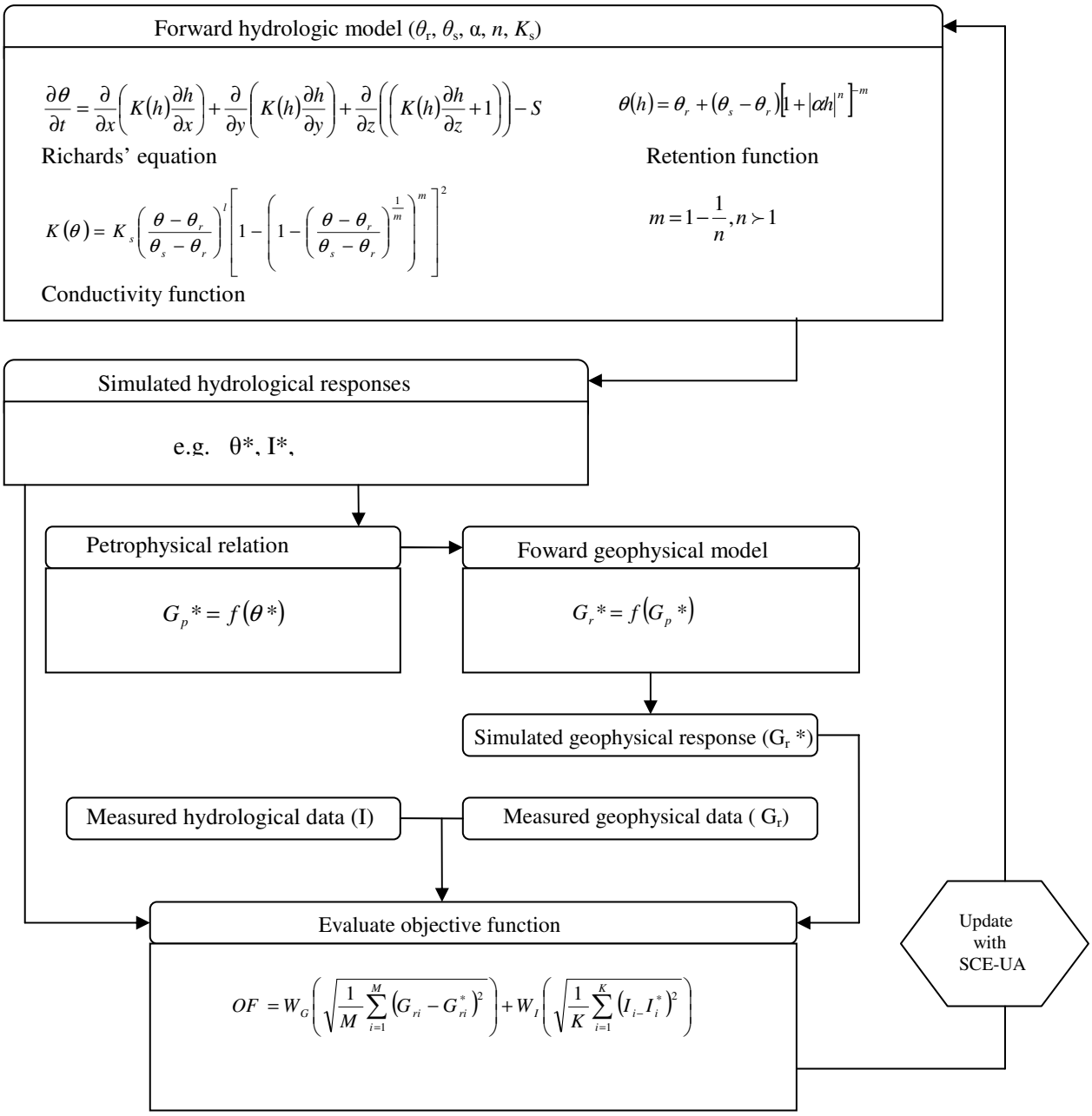

Figure 1.1: Workflow of coupled hydrogeophysical inversion approach applied to geophysical response data (G_r) and hydrological response data (I) and their corresponding simulations (G_r* and I*). G_p is a geophysical property of interest from which the geophysical responses are simulated and W_I and W_G are inversion weights. Although coupled inversion is illustrated for a single geophysical method here, it can easily be extended to consider multiple geophysical methods

As the coupled hydrogeophysical inversion approach does not require an intermediate tomograhic imaging step, it can avoid errors emanating from smoothing and resolution artefacts common to the uncoupled hydrogeophysical inversion approach. Most geophysical methods are sensitive to the spatial distribution of hydrologic states (Ferré et al., 1996; Furman et al., 2003). This implies that reliable core-scale petrophysical relations are sufficient to ensure a coupling between the hydrologic and the geophysical model. Consequently, there is no need to derive field-scale or apparent petrophysical relationships that vary spatially. Furthermore, because hydraulic information retrieval from geophysical measurements is directly constrained by the hydrologic model, the coupled

hydrogeophysical inversion approach provides a better means of assessing the consistency of the hydrologic model based on the geophysical measurements.

1.2. Problem statement

Recent research on the usefulness and applicability of the coupled hydrogeophysical inversion approach clearly illustrates the potential advantages of the method (Kowalsky et al., 2004; Rucker and Ferré, 2004; Lambot et al., 2006; Hinnell et al., 2010). However, very few studies have used the approach on actual field or laboratory data (Kowalsky et al., 2005; Looms et al., 2008; Huisman et al., 2010; Rings et al., 2010). Different geophysical methods differ in their sensitivity to different hydrologic states or soil types. For instance, GPR and ERT are more sensitive to water content while SP is also sensitive to water fluxes. On the other hand, GPR performs best on coarse grained soils, while methods like ERT, EMI and SP can be used in both fined-grained and coarse grained soils. Despites these observations, most studies focus on the use of GPR or ERT. There is clearly a need to develop and test the applicability of the coupled hydrogeophysical inversion approach on geophysical methods other than ERT and GPR. While coupled hydrogeophysical inversion frameworks potentially provide a suitable platform for the fusion of multiple geophysical and hydrological data sets, this has received even less attention (e.g. Kowalsky et al., 2005, Looms et al., 2008b).

1.3. Scientific objectives and thesis outline

The aim of this research project is to develop coupled hydrogeophysical inversion frameworks for ERT, streaming potential monitoring, and TDR, and to investigate the feasibility of retrieving subsurface hydraulic parameters from the developed frameworks using actual field or laboratory data. To achieve this aim, the following hydrologic experiments were designed:

1. A constant head infiltration experiment in the field was monitored with ERT. A coupled hydrogeophysical inversion framework was developed to estimate topsoil hydraulic parameters from the fusion of electrical resistances and cumulative inflow data. The objective was to investigate different methods for fusing ERT data and cumulative inflow within the coupled hydrogeophysical inversion scheme for the estimation of soil hydraulic parameters. The results from the coupled hydrogeophysical data fusion were benchmarked with hydraulic parameters from a multi-step outflow experiment on an undisturbed soil core from the experimental site. The results of this study are presented in chapter 2 and have been published in Near Surface Geophysics under the title “Coupled hydrogeophysical inversion of electrical resistances and inflow measurements for topsoil hydraulic properties under constant head infiltration” (Mboh et al., 2012 a)

2. A column scale drainage experiment on a sandy soil was monitored with the Self Potential (SP) method and tensiometers. Two objectives were envisaged for this experiment. The primary objective of this experiment was to use the streaming potential component of the SP measurements to estimate the hydraulic properties of the sandy soil using the coupled hydrogeophysical inversion approach. In order to so, an adequate model for the behavior of the voltage coupling coefficient at partial saturation is required. The voltage coupling coefficient links the measured streaming potentials to the hydraulic potential gradient. As the behaviour of this coefficient at partial saturation is still a subject of current debate, a secondary objective was to compare different models for the voltage coupling coefficient at partial saturation with the experimental data. The coupled hydrogeophysical inversion results are benchmarked with hydraulic properties obtained from inverse modeling of matric potential data obtained using tensiometers. The findings from this experiment are presented in

chapter 3 and have been published in the Vadose Zone Journal under the title “Coupled hydrogeophysical inversion of streaming potential signals for unsaturated soil hydraulic properties”. (Mboh et al., 2012 b)

3. A falling head infiltration experiment into initially dry loamy sand in a laboratory column was monitored with a vertically inserted TDR probe. The primary objective of this experiment was to investigate the feasibility of both the uncoupled and coupled hydrogeophysical inversion approaches to infer the hydraulic properties of the soil material using TDR data. A secondary objective was to examine the influence of initial conditions on the uncoupled and coupled inversion approaches developed for this experiment. The results were benchmarked with hydraulic parameters from a multi-step outflow experiment performed with a packed soil column. Because Time Domain Reflectometry (TDR) is frequently used to provide ground truth information when using other geophysical methods that easily enable field scale sampling (e.g. ERT, GPR, EMI), the findings provided a non-invasive way of acquiring local estimates of soil hydraulic properties which can be used for benchmarking spatially variable estimates of soil hydraulic parameters obtained using other geophysical methods. The results of this experiment are presented in chapter 4 and have been published in Soil Science Society of America Journal (Mboh et al., 2011).

Each chapter deals with the development of a separate coupled hydrogeophysical inversion framework. Therefore, each chapter is structured according to the classical presentation of research findings with an introduction including a formulation of the objectives, materials and methods, and the corresponding results, discussion and conclusions. After the research findings are presented in chapters 2 to chapter 4, a synthesis is presented in chapter 5 which summarises the general conclusions from the three research papers and provides an outlook on future research.

2. Coupled hydrogeophysical inversion of electrical resistances and inflow measurements for topsoil hydraulic properties under constant head infiltration[1]

Abstract

Accurate estimation of top soil hydraulic properties is important for understanding water flow and solute transport in the vadose zone. Coupled hydrogeophysical inversion schemes that enable the use of multiple geophysical and hydrologic data for the estimation of soil hydraulic properties have recently been proposed. In these coupled inversion schemes, a hydrologic model describing the process under investigation is coupled to a forward geophysical model and hydraulic parameters are directly estimated from geophysical measurements. While these schemes provide a suitable platform for the integration of multiple geophysical and hydrologic data, efficient methods to combine these data types for improved parameter estimation still warrant investigation. In this study, we investigated the feasibility of estimating three topsoil Mualem-van Genuchten parameters (α, n and K_s) from the fusion of inflow and electrical resistance measurements obtained under constant head infiltration. In addition to using only inflow or electrical resistances, we investigated three methods of combing these data for improved estimation of topsoil hydraulic parameters. Our results show that using inflow alone does not provide a unique solution to the inverse problem. Better results are obtained with the additional use of electrical resistances. We show that successful data fusion within the coupled hydrogeophysical inversion framework depends on the choice of an appropriate objective function. We obtained the best data fusion results when an objective function defined as the sum of the root mean square error of both data types normalized by the standard deviation of the respective measurements was used. In this case, the inverted hydraulic parameters were very comparable to reference values obtained from a multi-step outflow experiment carried out with undisturbed soil cores from the experimental site. It is concluded that the coupled hydrogeophysical inversion framework is a promising tool for non-invasive near surface hydrological investigations.

[1] Adapted from: Mboh, C.M., J.A. Huisman, N. Van Gaelen, J. Rings, and H. Vereecken. 2012. Coupled hydrogeophysical inversion of electrical resistances and inflow measurements for topsoil hydraulic properties under constant head infiltration. Near Surface Geophysics, 10: 413-426

2.1. Introduction

Accurate estimation of top soil hydraulic properties is important for understanding water flow and solute transport in the vadose zone, which affect many environmentally relevant processes like groundwater recharge and quality, flood generation and contaminant transport amongst many others. Consequently, sustainable ground water abstraction, mitigation of groundwater pollution and efficient irrigation and drainage strategies depend on good knowledge of top soil hydraulic properties.

Conventionally, in-situ topsoil hydraulic properties have been estimated from infiltrometry (Reynolds et al., 2002) or by inverting matric potential or soil water content measurements obtained from invasive techniques like tensiometry (Hendrickx et al., 1994; Faybishenko, 2000) and time domain reflectometry (TDR; Parkin et al., 1995; Huisman et al., 2002; Schwartz and Evett, 2002) during infiltration events. Although the water content and matric potential of the vadose zone can exhibit large spatial variation in the horizontal and vertical direction (e.g. Flury et al., 1994), tensiometry and TDR only provide limited spatial coverage (0.01 - 1 dm^3), requiring time-consuming measurements at many locations for field scale sampling. Geophysical methods like ground penetration radar (GPR; Binley and Beven, 2003; Cassiani and Binley, 2005; Looms et al., 2008a; Jadoon et al., 2010), electrical resistivity tomography (ERT; Daily et al., 1992; Deiana et al., 2007; Batlle-Aguilar et al., 2009), magnetic resonance imaging (Amin et al., 1993; Roy and Lubcynski, 2005; Vouillamoz et al., 2011) and electromagnetic induction (Sheets and Hendrickx, 1995; Reedy and Scanlon, 2003; Martinez et al., 2009) are increasingly being used for monitoring changes of water content and solute transport in the vadose zone. Unlike tensiometry and TDR, subsurface changes in water content and solute transport at larger scales like farm fields and small catchments can be quickly and non-invasively monitored with these geophysical methods. In this study, we focus on the use of ERT for non-invasive characterization of top soil hydraulic properties.

Despite the considerable promise of geophysical data in general and ERT in particular, interpretation of such data in a hydrological context is far from straightforward. Traditionally, ERT data (i.e. electrical resistances) are inverted into resistivity tomograms that provide qualitative insights into subsurface structure and the hydrological and transport processes therein. Based on resistivity tomograms, Binley et al. (1996) observed saturated flow paths in an undisturbed soil core. Slater et al. (2000, 2002) monitored a controlled saline tracer injection experiment in an experimental tank with ERT and gained valuable insights into the spatial variability of solute transport as they could visualize tracer accumulation, density-driven spill of tracer and preferential flow. The spatial variability of sorghum and maize root water uptake (Srayeddin and Doussan, 2009) and leachate recirculation in waste landfills (Clément et al., 2010) have also been successfully studied using qualitative interpretation of electrical resistivity tomograms.

Electrical resistivity tomograms are increasingly being converted into quantitative estimates of water content or solute mass using petrophysical relationships. These converted tomograms are then used for the calibration of subsurface flow and transport models (e.g. White, 1988; Daily et al., 1992; Binley et al., 2002; French et al., 2002; Kemna et al., 2002; Singha and Gorelick, 2005; Müller *et* al., 2010). This sequential approach in which resistivity tomograms are converted to hydrologic state variables (e.g. water content or solute concentration) which are then used for the estimation of soil hydraulic and transport properties in flow and transport models is referred to as uncoupled hydrogeophysical inversion (Ferre et al., 2009; Hinnell et al., 2010). A number of shortcomings have been identified with the quantitative use of tomographic images for the calibration of subsurface flow and transport models in the uncoupled hydrogeophysical inversion approach. The independent geophysical inversion from electrical resistances to subsurface electrical resistivity tomograms is

generally ill-posed and underdetermined. To condition and stabilize the inverse problem, a regularization constraint (e.g. smoothness) is applied. This regularization introduces artifacts that can lead to highly uncertain estimates of hydraulic and transport parameters when such tomograms are used for calibrating water flow and solute transport models (Day-Lewis et al., 2005, Slater et al., 2007). For example, Rings et al. (2008) observed that in the presence of strong resistivity contrasts, especially low sensitivity areas can often be plagued by inversion artifacts. Besides artifacts linked to the type and strength of regularization, electrical resistivity tomograms also have a spatially variable resolution. Targets closer to the high sensitivity areas near the electrodes are more resolved than those in the low sensitivity areas further away from the electrodes (Singha and Gorelick, 2005). In cross-borehole ERT surveys, Singha and Gorelick (2006) associated a tracer mass balance error of about 75% to the poor resolution of the electrical resistivity tomogram in the inter well region.

As a consequence of these shortcomings, vadose zone flow and transport properties obtained using the uncoupled hydrogeophysical inversion approach maybe very uncertain. Much recent research has evolved around the improvement of the uncoupled hydrogeophysical inversion approach. Time-lapse geophysical inversion approaches (Oldenborger et al., 2007; Clément et al., 2009; Wilkinson et al., 2010) now allow for simultaneous treatment of several spatio-temporal subsurface images, which limits some of the artifacts common to classical sequential geophysical inversion. Another approach to limit artifacts due to the spatially varying resolution of electrical resistivity tomograms is the use of spatially variable apparent petrophysical relations (Day-Lewis et al., 2005; Singha and Moysey, 2006; Singha and Gorelick, 2006a). Finally, joint inversion approaches (Gallardo and Meju, 2004; Linde et al., 2006) have been developed to construct tomograms from multiple geophysical methods that compliment each other and lessen the effect of varying spatial resolution.

An alternative approach that does not require intermediate geophysical tomograms for the estimation of subsurface flow and transport properties called coupled hydrogeophysical inversion was recently proposed (Kowalsky et al., 2004; Lambot et al., 2006; Hinnell et al., 2010; Huisman et al., 2010; Rings et al., 2010). Figure 2.1 shows the work flow of the coupled hydrogeophysical inversion approach applied to the use of electrical resistance (R) and cumulative inflow (I) measurements for the estimation of soil hydraulic properties. First, a forward geophysical model is coupled to a hydrologic model with the use of a suitable petrophysical relation. This allows the simulation of hydrologic state variables (e.g. water content distributions, θ^*) that can be converted into simulated geophysical properties (e.g. bulk electrical conductivity distributions, σ_b) using the petrophysical model. The simulated geophysical properties are then used to simulate geophysical data (e.g. electrical resistances, R*) using the forward geophysical model. By perturbing the hydrological model parameters using a suitable optimization algorithm, the simulated geophysical measurements are compared with the measured geophysical data (e.g. electrical resistances, R) until a close fit is found. As the geophysical data are not inverted into resistivity tomograms, the coupled hydrogeophysical inversion approach has potential to overcome the shortcomings associated with the direct use of electrical resistivity tomograms.

Despite the potential advantages of coupled hydrogeophysical inversion, relatively few studies have used this approach for the estimation of subsurface flow and transport properties from actual data (e.g. Kowalsky et al., 2005, Looms et al., 2008b; Lambot et al., 2009; Huisman et al., 2010; Rings et al., 2010; Mboh et al., 2011). While coupled hydrogeophysical inversion frameworks potentially provide a suitable platform for the fusion of multiple geophysical and hydrological data sets, this has received even less attention (e.g. Kowalsky et al., 2005, Looms et al., 2008b). In this study, we use surface ERT to monitor a constant head infiltration experiment and apply the coupled hydrogeophysical inversion approach on electrical resistances and inflow data for the estimation of topsoil hydraulic properties. We aim to compare three coupled hydrogeophysical data fusion techniques using inflow and electrical resistance measurements. The inversion results are

benchmarked by comparing the hydraulic parameter estimates with independently obtained parameters from a multi-step outflow laboratory experiment performed on undisturbed soil cores from the experimental site.

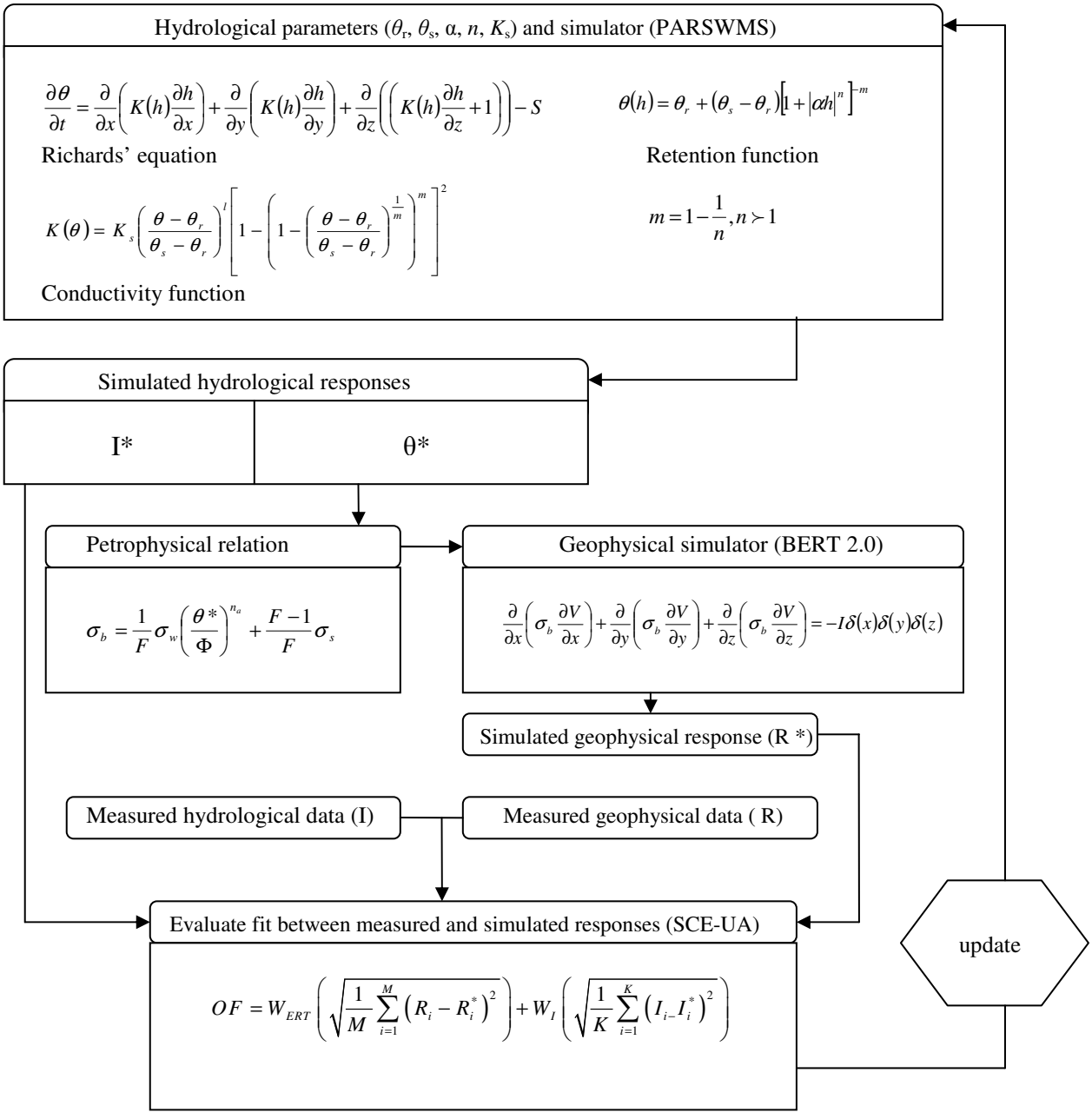

Figure 2.1: Workflow of coupled hydrogeophysical inversion approach applied to electrical resistances (R) and cumulative inflow measurements (I) and their corresponding simulations (R* and I*). W_I and W_{ERT} are weights

2.2. Materials and Methods

2.2.1. Measurements

We used ERT to monitor constant head infiltration of water with an electrical conductivity of 194.7 μS cm^{-1} and a temperature of 18.3 °C into an auger hole in a field plot in Geel in the north-east of Belgium (Figure 2.2). The upper 1 m of soil of this site is sandy loam (73% sand, 23% silt and 4% clay) underlain by a sandy soil with lower silt content but a slightly higher clay content (92% sand, 2 % silt and 6% clay). The auger hole had a depth of 40 cm and a diameter of about 10.4 cm. The upper half of the hole was sealed with a polyvinylchloride (PVC) pipe. Twenty-six stainless steel electrodes with a length of 30 cm and a diameter of 1.2 cm spaced 16 cm apart where vertically inserted into the soil to a depth of about 5 cm below the soil surface. The augered hole was at the center of the electrode lay-out between electrode 13 and 14. A marriote reservoir was used to maintain a constant water head of about 54.4 cm above the bottom of the augered hole during infiltration.

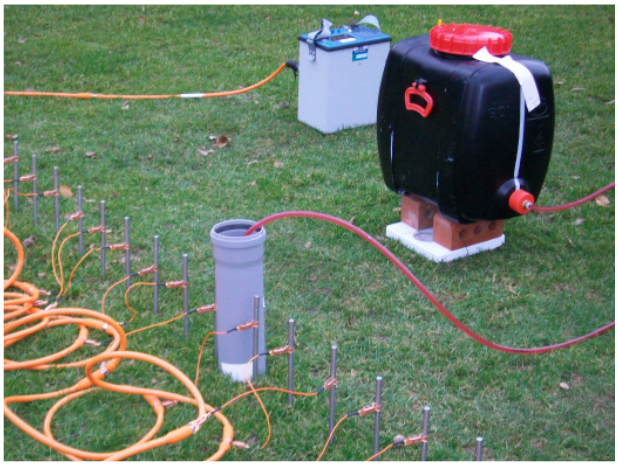

Figure 2.2: Field experimental set up. The black container is the mariotte reservoir and the gray box is the multi-electrode resistivity meter.

A multi-electrode resistivity meter (Syscal Pro, IRIS Instruments, France) was used to acquire electrical resistance measurements at 30 minutes intervals for 3 hours. Each time lapse measurement consisted of 420 electrical resistance values based on multi-gradient electrode arrays (Table 2.1). Apart from its suitability for multi-channel data acquisition in fast transient experiments like this, Dahlin and Zhou (2004) observed that the use of multi-gradient electrode arrays provides a better resolution than the commonly used Wenner arrays. Each of the 420 electrical resistance values was the average of an automated measurement cycle of up to 5 subsequent measurements. As an indication of measurement quality, the resistivity meter also reports the relative variation within each measurement cycle. This varies from 0.2% to 0.4% with an average of about 0.3%.

Table 2.1: Multi-gradient surface electrode arrays

Injection Spacing (m)	Injection (A-B)	Potential (M-N)	
		spacing =0.16 m	Spacing = 0.32 m
1.6	1-11	2-3, 3-4, 4-5 … 9-10	2-4, 3-5 , 4-6, … 8-10
	3-13	4-5, 5-6, 6-7, … 11-12	4-6, 5-7, 6-8, … 10-12
	5-15	6-7, 7-8, 8-9, … 13-14	6-8, 7-9, 8-10, … 12-14
	7-17	8-9, 9-10, 10-11, … 15-16	8-10, 9-11, 10-12, … 14-16
	9-19	10-11, 11-12, 12-13, … 17-18	10-12, 11-13, 12-14, … 16-18
	11-21	12-13, 13-14, 14-15, … 19-20	12-14, 13-15, 14-16, … 18-20
	13-23	14-15, 15-16, 16-17, … 21-22	14-16, 15-17, 16-18, … 20-22
	15-25	15-16, 16-17, 17-18, … 23-24	16-18, 17-19, 18-20, … 22-24
2.4	1-16	2-3, 3-4, 4-5, … 14-15	2-4, 3-5, 4-6 …13-15
	3-18	4-5, 5-6, 6-7, … 16-17	4-6, 5-7, 6-8, … 15-17
	5-20	6-7, 7-8, 8-9, … 18-19	6-8, 7-9, 8-10, … 17-19
	7-22	8-9, 9-10, 10-11, … 20-21	8-10, 9-11, 10-12, … 19-21
	9-24	10-11, 11-12, 12-13, … 22-23	10-12, 11-13, 12-14, … 21-23
	11-26	12-13, 13-14, 14-15, … 24-25	12-14, 13-15, 14-16, … 23-25
3.2	1-21	2-3, 3-4, 4-5, … 19-20	2-4, 3-5, 4-6, … 18-20
	3-23	4-5, 5-6, 6-7, … 21-22	4-6, 5-7, 6-8, … 20-22
	5-25	6-7, 7-8, 8-9, … 23-24	6-8, 7-9, 8-10, … 22-24
4	1-26	2-3, 3-4, 4-5, … 24-25	2-4, 3-5, 4-6, … 23-25

Apart from the electrical resistance data, time-lapse cumulative inflow measurements were also taken using a balance beneath the mariotte reservoir (Figure 2.2). Cumulative inflow for each time was determined from the weight loss of the marriotte reservoir relative to its initial weight. Prior to infiltration, several TDR measurements taken in the topsoil in the vicinity of the imaged plane showed a marginal water content variation from 0.281 cm^3cm^{-3} to 0.283 cm^3cm^{-3} with and an average of 0.282 cm^3cm^{-3}. Water content measurements obtained from oven-drying of core samples taken from the augered hole showed the same variation with a similar estimate of the average initial water content. Information from soil cores also indicate that the bulk density of the site marginally varies between 1.50 gcm^{-3} to 1.51 gcm^{-3}, which implies a saturated water content of about 0.38 cm^3cm^{-3}.

2.2.2. Forward Hydrologic Model

The Parallel Soil Water Modeling and Simulation model (PARSWMS, Hardelauf *et al*., 2007) was used to simulate the constant head infiltration experiment. A flow domain of 6 x 4 x 2 m (length x width x depth) was discretized into 4632 nodal points and 24052 tetrahedral elements. At the center of the flow domain, the cylindrical auger hole was included. A no flow boundary condition was imposed along the upper 0.2 m of the hole to represent the PVC pipe used to seal the upper section of the augered hole. A variable head boundary condition was used for the lower section of the hole. A free drainage boundary condition was used at the bottom of the flow domain while all other boundaries of the flow domain (i.e. the sides and the top) were imposed a no flow boundary condition. PARSWMS was used to simulate cumulative infiltration and water content distributions at a constant head of 54.4 cm above the bottom of the hole during the experimental period of 3 hours. We assumed a homogeneous top soil with an average initial water content of 0.282 cm^3cm^{-3} derived from in-situ TDR measurements.

PARSWMS numerically solves the 3D Richards' equation for variably saturated flow in a homogenous rigid porous medium:

$$\frac{\partial\theta(h)}{\partial t}=\frac{\partial}{\partial x}\left(K(h)\frac{\partial h}{\partial x}\right)+\frac{\partial}{\partial y}\left(K(h)\frac{\partial h}{\partial y}\right)+\frac{\partial}{\partial z}\left(\left(K(h)\frac{\partial h}{\partial z}+1\right)\right)-S \tag{2.1}$$

where z is the elevation (depth) coordinate, x are y are coordinates in the length and width directions of the flow domain, t is time, θ is the volumetric water content, h is the pressure head, $\theta(h)$ is the water retention function, $K(h)$ is the hydraulic conductivity function, and S is a sink term representing root water uptake. With estimated evapotranspiration levels less than 1% of the total cumulative inflow, the sink term was ignored in the simulations. It is assumed that the retention and conductivity functions that describe the hydraulic properties of the soil can be represented by the Mualem-van Genuchten model (MVG, Mualem, 1976; van Genuchten, 1980):

$$\theta(h)=\theta_r+(\theta_s-\theta_r)\left[1+|\alpha h|^n\right]^{-m} \tag{2.2}$$

$$K(h)=K_s\left(\frac{\theta-\theta_r}{\theta_s-\theta_r}\right)^l\left[1-\left(1-\left(\frac{\theta-\theta_r}{\theta_s-\theta_r}\right)^{\frac{1}{m}}\right)^m\right]^2 \tag{2.3}$$

where θ_r and θ_s are the residual and saturated water content respectively, α and n are empirical parameters which are respectively related to the air entry pressure value and the width of the pore size distribution, m is restricted by the Mualem condition $m = 1 - 1/n$ with $n > 1$, K_s is the saturated hydraulic conductivity, and l is a factor that accounts for pore tortuosity. A total of six MVG parameters (θ_r, θ_s, α, n, K_s and l) are therefore necessary to describe the soil hydraulic properties. The parameter l is commonly fixed to a value of 0.5 based on the recommendations of Mualem (1976). Theoretically considered as the soil water content for an infinitely large suction, θ_r is empirical and is sometimes fixed to a value of zero (Nimmo, 1991; Fuentes et al., 1992). Water content measurements in very dry field conditions or air-dried soil samples can provide a practical estimate of θ_r. Similarly, water content measurements in very wet field conditions or water-saturated undisturbed soil cores provide a direct estimate of θ_s. Based on water content measurements of air-dried and water-saturated undisturbed soil cores, θ_r and θ_s are fixed to 0.031 cm^3cm^{-3} and 0.380 cm^3cm^{-3}, respectively. We also fixed the tortuosity factor l to a value of 0.5. Based on these assumptions, three MVG parameters (α, n, K_s) remain to be estimated by inverse modeling. The model runs with PARSWMS used four processors in parallel, which enables rapid forward runs of the hydrological model with an average run time of about one minute. This is important for rapid estimation of the hydraulic parameters as inverse problems of this type typically require thousands of model runs to converge to the global minimum.

2.2.3. Forward Geophysical Model

Assuming a 3D distribution of isotropic conductivity, the forward model for ERT is defined by the Poisson equation that governs the behavior of electric current as:

$$\frac{\partial}{\partial x}\left(\sigma_b\frac{\partial V}{\partial x}\right)+\frac{\partial}{\partial y}\left(\sigma_b\frac{\partial V}{\partial y}\right)+\frac{\partial}{\partial z}\left(\sigma_b\frac{\partial V}{\partial z}\right)=-I\delta(x-x_s)\delta(y-y_s)\delta(z-z_s) \tag{2.4}$$

where σ_b is the bulk soil electrical conductivity, V is the electric potential, I is a point current source located at (x_s, y_s, z_s), and δ is a Dirac delta function. The electrical flow domain encloses the hydrologic domain and has a depth of about 2 m. To avoid boundary condition effects, the limits of the electrical flow domain in the length and width directions were set sufficiently far away (500 m) from the electrode domain. The electrical flow domain was discretized into 42000 tetrahedral elements with smaller elements near the surface and closer to the electrodes than at greater depths and regions further away from the electrodes. A no flow (Neumann) boundary condition was imposed at the surface and at the sides of the electrical flow domain, while a mixed type boundary condition was imposed at the bottom of the domain. Boundless Electrical Resistivity Tomography, BERT 2.0 (Rücker et al., 2006) was used to simulate time-lapse electrical resistances corresponding to the measurement arrays given in Table 1. The precision of the forward simulations was assessed by comparing an analytical solution for electrical resistances in a homogenous half space to that simulated by BERT. BERT simulated the electrical resistances with a numerical error less than 1%. As illustrated in Figure 2.1, the conductivity distributions required for BERT were derived from the water content distribution simulated by PARSWMS.

To gain further insights into the subsurface structure, resistivity tomograms were also obtained from a time-lapse inversion of the measured electrical resistances using BERT 2.0. BERT 2.0 handles the inversion for the resistivity distribution as a regularized least squares problem using a smoothness constraint and uses a Gauss-Newton method with inexact line search (DeGroot-Hedlin and Constable, 1990; Loke and Dahlin, 2002; Günther et al., 2006). A regularization parameter is used to find an appropriate compromise between data misfit and model roughness and the automated L-curve approach of BERT 2.0 was used here.

2.2.4. Petrophysical Model

The link between the forward hydrological and the geophysical model in the coupled hydrogeophysical inversion framework is a petrophysical relation which transforms simulated water content distributions into the corresponding electrical conductivity distributions. There are several petrophysical models of varying complexity to convert water content into electrical conductivity (e.g. Archie, 1942; Waxman and Smits, 1968; Rhoades et al., 1976; Mualem and Friedman, 1991). These petrophysical relations require site-specific calibration for any practical application. In this paper, we used the model of Jougnot et al. (2010) based on Revil et al. (2007) for variably saturated conditions:

$$\sigma_b = \frac{1}{F}\left(\sigma_w S_w^{n_a} + (F-1)\sigma_s\right) \tag{2.5}$$

where σ_b is the bulk electrical conductivity of the soil, σ_w is the pore water conductivity, σ_s is the surface conductivity associated with the electrical double layer surrounding the soil particles, S_w is the saturation defined as $\theta\Phi^{-1}$ where Φ is the porosity of the soil, F is the formation factor, and n_a is an empirical constant called the saturation exponent. While an average value of 2 is most often used for the saturation index of sandy soils (e.g. Friedman, 2005; Bänninger et al., 2009), values ranging between 1.1 and 2.7 for unconsolidated sands have been reported by Ulrich and Slater (2004). The pore water conductivity σ_w was assumed equal to the electrical conductivity of the water used for infiltration (0.0195 Sm^{-1}). The porosity, Φ, was assumed equal to the saturated water content of the soil (0.380 cm^3cm^{-3}). The parameters F, n_a, and σ_s were estimated in the laboratory from TDR-measured electrical conductivity in soil cores saturated to different levels. Water of three different conductivities (0.112 Sm^{-1}, 0.249 Sm^{-1} and 0.481 Sm^{-1}) was used for saturating three sets of the cores samples to different levels of saturation. For fully saturated core samples, eqn. 2.5 can be written as:

$$\sigma_{sat} = \frac{\sigma_w}{F} + \frac{(F-1)}{F}\sigma_s \tag{2.6}$$

where σ_{sat} is the conductivity of the soil at saturation. By fitting a straight line to a plot between solution conductivity (σ_w) and corresponding saturated bulk conductivity (σ_{sat}), F and σ_s were determined. These parameters were then fixed while fitting the saturation exponent, n_a, to bulk electrical conductivity measurements made on unsaturated core samples.

2.2.5. Objective Functions and Optimization

In optimization, an objective function which expresses a misfit between observations and predictions based on the inversion parameters is minimized. Generally, the parameters are perturbed within reasonably wide bounds (Table 2.2) and the generated predictions are compared to the corresponding observations until a close fit is found. In this paper, 5 scenarios were used for the inversion for the three hydraulic parameters (α, n, K_s) using objective functions based on the root mean square error (RMSE) between time-lapse predictions and the corresponding measurements. In the first scenario, the objective function was computed as the RMSE between K time-lapse cumulative infiltration (I) measurements and the corresponding predictions (I^*) from the hydrological model:

$$OF_1 = \sqrt{\frac{1}{K}\sum_{i=1}^{K}\left(I_i - I_i^{*(\alpha,n,Ks)}\right)^2} \tag{2.7}$$

In the second scenario, the coupled hydrogeophysical inversion approach was applied to M time-lapse electrical resistance (R) measurements and the objective function was similarly defined as:

$$OF_2 = \sqrt{\frac{1}{M}\sum_{i=1}^{M}\left(R_i - R_i^{*(\alpha,n,Ks)}\right)^2} \tag{2.8}$$

where R^* are predictions of electrical resistance measurements from the forward geophysical model coupled to the hydrological model.

In the last three scenarios, coupled hydrogeophysical inversion was used to estimate the hydraulic parameters (α, n, K_s) by fusing multiple data types, namely time-lapse cumulative infiltration and electrical resistance measurements. In this case, definition of the objective function requires the normalization of the RMSE for individual data types. Here, we explore three different normalization strategies: normalization with the standard deviation of measurements, the range of the measurements or the average of the measurements:

$$OF_3 = \frac{1}{\varepsilon_R}\sqrt{\frac{1}{M}\sum_{i=1}^{M}\left(R_i - R_i^{*(\alpha,n,Ks)}\right)^2} + \frac{1}{\varepsilon_I}\sqrt{\frac{1}{K}\sum_{i=1}^{K}\left(I_i - I_i^{*(\alpha,n,Ks)}\right)^2} \tag{2.9}$$

$$OF_4 = \frac{1}{\lambda_R}\sqrt{\frac{1}{M}\sum_{i=1}^{M}\left(R_i - R_i^{*(\alpha,n,Ks)}\right)^2} + \frac{1}{\lambda_I}\sqrt{\frac{1}{K}\sum_{i=1}^{K}\left(I_i - I_i^{*(\alpha,n,Ks)}\right)^2} \tag{2.10}$$

$$OF_5 = \frac{1}{\overline{R}}\sqrt{\frac{1}{M}\sum_{i=1}^{M}\left(R_i - R_i^{*(\alpha,n,Ks)}\right)^2} + \frac{1}{\overline{I}}\sqrt{\frac{1}{K}\sum_{i=1}^{K}\left(I_i - I_i^{*(\alpha,n,Ks)}\right)^2} \tag{2.11}$$

where ε_R and ε_I are respectively the standard deviation of the measurements for electrical resistances and cumulative infiltration, λ_R and λ_I are respectively the range (i.e. the difference between the maximum and the minimum value) of the electrical resistance and cumulative infiltration measurements, and $\bar{R}$ and $\bar{I}$ are respectively the average of the electrical resistance and cumulative inflow measurements. As these objective functions are highly non-linear, they are minimized using a global optimizer. In this paper we used the Shuffled Complex Evolution optimization algorithm (SCE-UA, Duan et al., 1993). SCE-UA is a genetic global optimizer which combines probabilistic and deterministic approaches with clustering and systematic evolution to randomly sample a population of parameter combinations from predefined parameter spaces of sufficiently wide ranges and evolve them to a global optimum. In this study, the SCE-UA was set to a convergence criterion in which an optimum was assumed to be reached when in 10 successive evolution loops, the objective function did not improve by more than 0.01%. To compare the accuracy of the different optimization scenarios, confidence intervals were computed around the optimum parameters based on a first order approximation (Kool and Parker, 1998).

Table 2.2: Inversion bounds for hydraulic parameters

Parameter	Maximum value	Minimum value
α [m^{-1}]	1.0	14.5
n [-]	1.2	3.2
K_s [ms^{-1}]	1.0e-6	1.0e-4

2.2.6. Numerical Experiments

Numerical investigations were carried out to gain further insight into the feasibility of obtaining plausible parameter estimates from the inversion of inflow and electrical resistance measurements obtained during constant head infiltration. For these simulations, a sandy loam soil with typical hydraulic parameters according to Carsel and Parish (1988) was considered (θ_s = 0.41 cm^3cm^{-3}, θ_r = 0.065 cm^3cm^{-3}, α = 0.075 cm^{-1}, n = 1.89, K_s = 4.421 cmh^{-1} and l = 0.5). For the petrophysical model (Eq. 2.5), we assumed the following parameters: σ_w = 0.02 Sm^{-1}, σ_s = 0.0003 Sm^{-1}, Φ = 0.41, F = 5.949, and n_a = 2. Using the forward models and the associated initial and boundary conditions, cumulative inflow and electrical resistance measurements corresponding to the measurement times of the constant head infiltration experiment were simulated. Gaussian noise with a standard deviation of 0.0001 m^3 and a mean of zero was added to the synthetic cumulative infiltration, while 3% relative random noise was added to the simulated electrical resistances. The simulations with noise were used as measurements and the feasibility of the five inversion scenarios was investigated. In each of the inversion scenarios, θ_r, θ_s, l and the petrophysical parameters were assumed to be known and were kept constant at their 'true' values while 2D objective function response surfaces in the α-n, α-K_s and n-K_s parameter planes were constructed for the other three hydraulic parameters by additionally fixing one of them and systematically varying two others within the inversion bounds given in table 2. For each parameter, the range was divided in 50 equidistant parts, which means that a single response surface consists of 2601 objective function evaluations.

2.2.7. Multi-Step Outflow Experiment

Independent estimates of the hydraulic parameters were obtained using a multi-step outflow (MSO) experiment. An undisturbed soil sample with a height of 10 cm and a diameter of 8.5 cm was obtained from the experimental site using a stainless steel cylinder. The sample was saturated to a water content of 0.380 m^3m^{-3} and six pressure increments were applied over a period of 483 hours while outflow and matric potential readings were recorded at 30 second intervals using two tensiometers located at 3 cm and 7 cm above the bottom of the sample. The outflow and matric head readings were filtered and used for the estimation of the hydraulic parameters (α, n and K_s) using the HYDRUS1D model (Simunek et al., 2008) and the SCE-UA optimization algorithm.

2.3. Results and Discussion

2.3.1. Numerical Experiments

Figure 2.3 shows the 2D objective function response surfaces in the α-K_s, α-n and n-K_s parameter planes for each of the five inversion scenarios. In the first inversion scenario (OF1) where only cumulative infiltration is used, it can be observed in the α-K_s and n-K_s parameter planes that the objective function minimum is constrained in a flat space in the K_s direction. This theoretically indicates that cumulative infiltration obtained using a constant head well permeameter has enough information to constrain the inversion for K_s. On the other hand, the α-n parameter plane for OF1 shows a strong positive correlation between α and n when K_s is fixed. This implies that α and n cannot be simultaneously estimated from cumulative inflow measurements in a sandy loam soil.

In scenario OF2 where only electrical resistances are used, the α-K_s parameter plane also shows a greater sensitivity towards K_s. However, the α-K_s and n-K_s parameter planes show a reduction in the uncertainty associated with α and n for a given K_s. This implies that information on the spatio-temporal evolution of the water content provided by the electrical resistances helps to further constrain the inversion for these parameters. Unlike the case of scenario OF1, no correlation is observed between α and n in the α-n parameter plane.

Scenarios OF3 to OF5 show the response surfaces obtained through the fusion of electrical resistances and cumulative inflow within the coupled hydrogeophysical inversion scheme. In scenario OF3 where the standard deviation of the measurements is used for normalization, a well defined objective function minimum is observed in the α-n parameter plane while the α-K_s and n-K_s parameter planes indicate that an adequate estimate of K_s is also possible from the inversion strategy. Scenarios OF4 and OF5 exhibit similar objective function response surfaces with a well defined minimum in the n-K_s parameter plane. Compared to scenarios OF1 and OF2, the α-n parameter plane shows more reduction in the uncertainty associated with the estimation of α and n when inflow and resistance measurements are simultaneously considered during inversion.

These numerical experiments show that the data fusion strategy to be adopted will therefore depend on the availability of reliable prior information on K_s or α. Within the coupled hydrogeophysical inversion scheme, the prior information can be provided in the form of ranges in which these parameters vary. Where there is reliable prior information on K_s, scenario OF3 is preferred to scenarios OF4 and OF5. Where there is reliable prior information on α, scenarios OF4 or OF5 are preferable. This makes scenario OF3 particularly attractive as it is easier to independently obtain estimates of K_s than α. Scenarios 3 to 5 clearly illustrate the data fusion power of the coupled hydrogeophysical inversion scheme. Theoretically this implies that the fusion of electrical resistance and cumulative inflow measurements obtained under a constant head well permeameter can provide enough information to constrain the inversion for α, n and K_s.

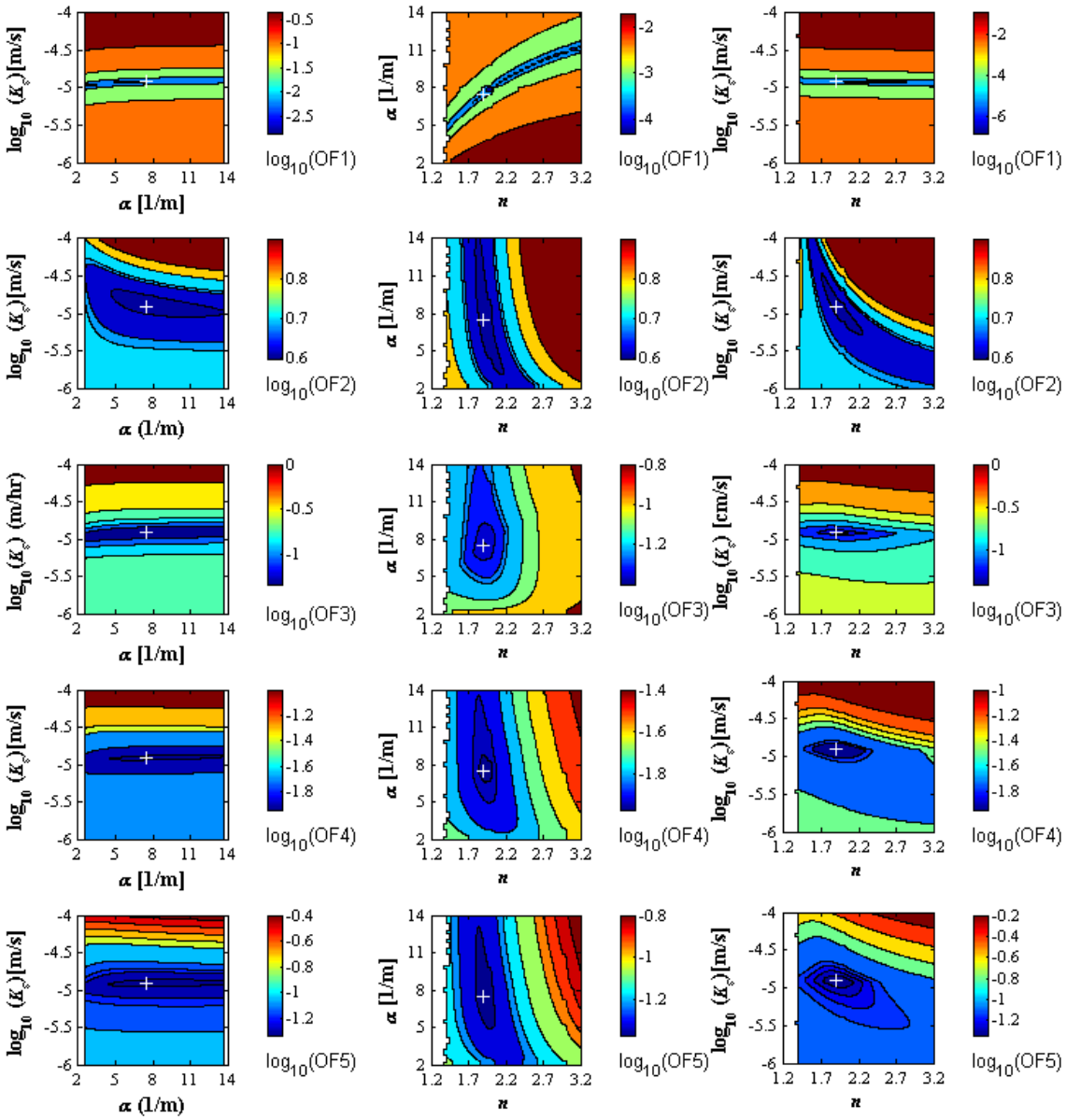

Figure 2.3: Objective function response surfaces for the 5 inversion scenarios. White spaces indicate parameter combinations for which the hydraulic model did not converge, while the white markers (+) indicate the objective function minimum

2.3.2. Laboratory and Field Experiments

Table 2.3 presents the optimization results from the MSO experiment. In addition to the optimized parameters (α, n and K_s) and the fixed parameters (θ_r, θ_s and l), the 95% confidence intervals of the optimized parameters are also reported. Figure 2.4 compares the measured and modeled outflow and matric potential. Clearly, the fit between the measured and predicted outflow is excellent while an appreciably good fit is also observed between the measured and the predicted matric potential.

Therefore, the hydraulic parameters from the MSO experiment are considered as independent reference in the remainder of this study.

Table 2.3: Optimized MVG parameters for MSO and the five inversion scenarios (OF1 - OF5)

Method	Parameters ± 95% confidence limits[¶]					
	θ_r [†] [cm^3cm_{-3}]	θ_s [†] [cm^3cm^{-3}]	α [cm^{-1}]	n [-]	K_s [cmh^{-1}]	l [†] [-]
MSO	0.031	0.380	0.023 ± 0.002	1.503 ± 0.005	1.660 ± 0.031	0.5
OF1	0.031	0.380	0.061 ± 0.011	1.552 ± 1.236	1.039 ± 0.007	0.5
OF2	0.031	0.380	0.030 ± 0.009	2.983 ± 0.104	0.837 ± 0.067	0.5
OF3	0.031	0.380	0.025 ± 0.006	1.652 ± 0.416	0.945 ± 0.047	0.5
OF4	0.031	0.380	0.014 ± 0.025	2.232 ± 0.628	0.809 ± 0.052	0.5
OF5	0.031	0.380	0.022 ± 0.010	2.998 ± 0.567	0.869 ± 0.050	0.5

[¶] θ_r is residual water content; θ_s is saturated water content; α, n and K_s are Mualem van Genuchten hydraulic parameters. The values in brackets are 95% confidence intervals on the associated parameters. [†] fixed during optimization

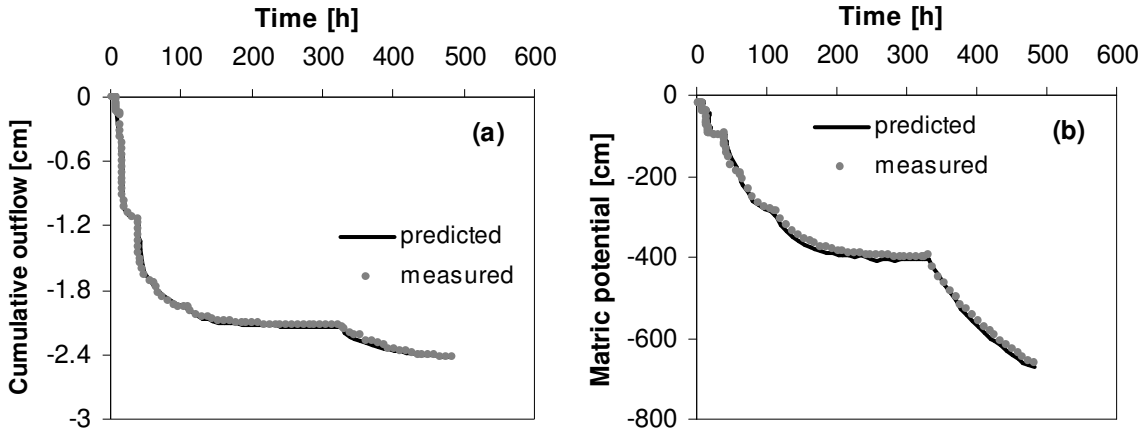

Figure 2.4: **Measured versus predicted cumulative outflow and (b) Measured versus predicted matric potential from the multi-step outflow experiment.**

Figure 2.5(a) shows the initial or background electrical resistivity distribution across the imaged plane obtained by inverting the ERT data and Figure 2.5(b) shows the resistivity distribution after three hours of infiltration. As can be seen from Figure 2.5, the soil is composed of two layers. The first layer has an average resistivity of 500 Ωm and extends from the surface to a depth of about 0.75 m and it is underlain by a second layer with an average resistivity of about 375 Ωm. Although approximately 23 litres of water was infiltrated into the soil in three hours, the resulting infiltration bulb is not very perceptible from from Figure 2.5(b). Nevertheless, Figure 2.5(b) shows lower resistvity values below the borehole at the point of inflow compared to Figure 2.5(a). To track

changes to the initial resistivity and to obtain a better understanding of the infiltration process, a relative difference between the final and the initial electrical resistivity distribution is presented in Figure 2.6. This relative difference was calculated as $1-\frac{\Delta\rho}{\rho_i}$, where ρ_i is the initial resistivity and $\Delta\rho$ is the absolute difference between the initial and the final resistivity distribution. The relative difference varies between approximately 1.00-0.74 corresponding to water content changes between approximately 0.28-0.38 cm^3cm^{-3}. It is worth noticing in Figure 2.6 that the infiltration plume extends to a depth of about 0.60 m below the soil surface within the first horizon. The infiltration is almost symmetric around the augered hole and the infiltration bulb has an approximate height and width of 0.60 m by 0.60 m. These tomograms (Figures 2.5 and 2.6) are only of qualitative importance to this study as they give us an appraisal of the subsurface structure and the possible size of the infiltration bulb. They were not used in the inversion for soil hydraulic parameters.

The petrophysical relation between water content and bulk electrical conductivity was derived in the laboratory by fitting the petrophysical model (eqn. 2.5) to bulk electrical conductivity and water content measurements made in the laboratory (Figure 2.7). The fitted empirical parameters are F = 5.858, n_a = 1.94 and σ_s = 0.00084 Sm^{-1}. Considering the conductivity of the water used for infiltration (0.0195 Sm^{-1}), the porosity of the soil (0.38 cm^3cm^{-3}), and the initial average water content of the topsoil (0.282 cm^3cm^{-3}), the determined petrophysical model gives us an initial conductivity of the topsoil of about 0.0026 Sm^{-1}. This compares well with conductivity of the topsoil estimated from the resistivity tomogram (Figure 2.5), which is about 0.002 Sm^{-1}. This suggests that the derived petrophysical model can be considered as a satisfactory link between the forward hydrologic and geophysical models within the coupled hydrogeophysical inversion framework.

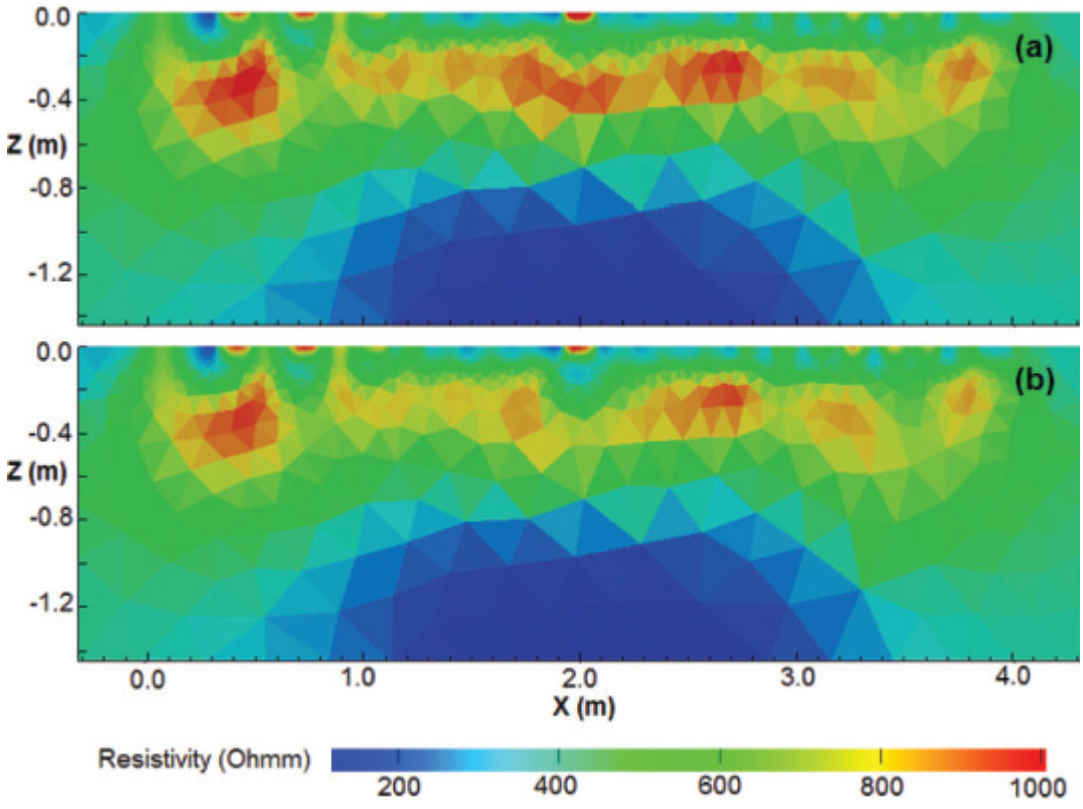

Figure 2.5: a) Background resistivity distribution and b) resistivity distribution after three hours of infiltration. Results are presented as slices through 3D tomograms directly below and in the direction of the electrode array.

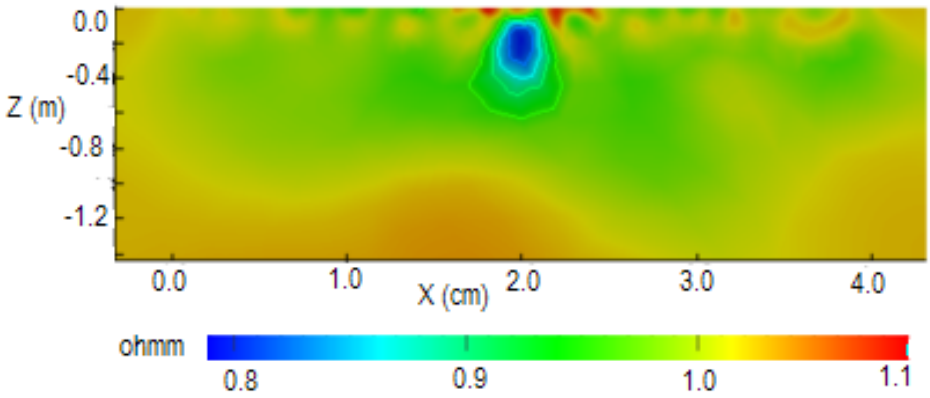

Figure 2.6: Extent of infiltration into the imaged plane. The outermost contour indicates the most probable extent of the infiltration plume.

Table 2.3 summarizes the inversion results for the five scenarios considered here. For scenario OF1 where only inflow measurements are used, n and K_s compare well with the MSO results (Table 2.3). However, the optimum α value for this scenario overestimates the value obtained with MSO. Therefore, the constant head cumulative inflow measurements seem to contain information on only two of the three MVG parameters (n and K_s). Similar results have been reported by Russo *et al.* (1991), Simunek and van Genuchten (1996), and Mboh et al. (2011) for infiltration measurements only. Despite the non-unique solution to the inverse problem, a good fit between the measured and modeled cumulative inflow is obtained (Figure 2.8). Clearly, a good fit does not imply that the hydraulic parameters are uniquely estimated.

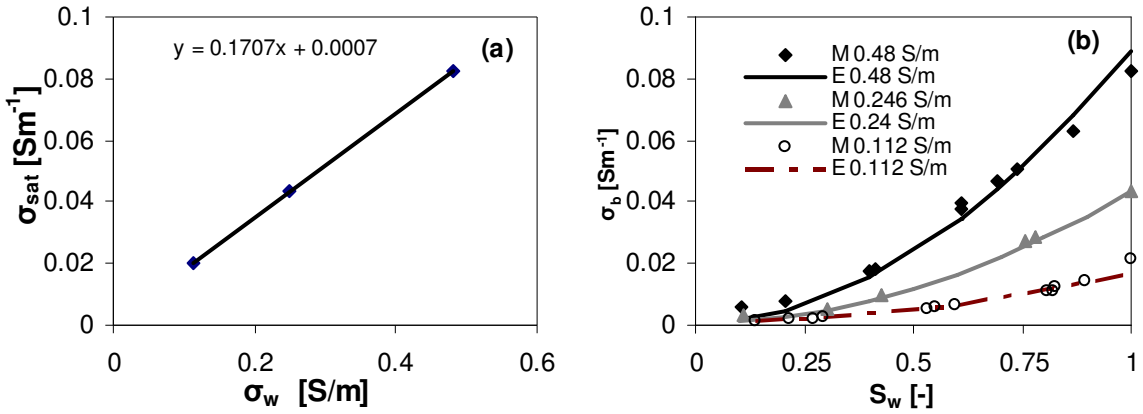

Figure 2.7: Plot of bulk electrical conductivity of a saturated sample against pore water conductivity. Intercept provides the surface conductivity ($\frac{F-1}{F}\sigma_s = 0.0007\ \mathrm{Sm^{-1}}$) and the slope is related to the formation factor ($F^{-1} = 0.1707$); (b) measured (M) and fitted (E) Archie's law for three water conductivities σ_w (0.48 $\mathrm{Sm^{-1}}$, 0.246 $\mathrm{Sm^{-1}}$, 0.112 $\mathrm{Sm^{-1}}$).

In scenario OF2 where only electrical resistances are used, K_s and α values that correspond well with those of MSO are obtained (Table 2.3). The value of n is overestimated compared to that of MSO. In scenario OF2, α is estimated with a narrower confidence interval than in the case of scenario OF1. Therefore, an inversion considering both data sources simultaneously is a logical next step. The results from scenario OF3 clearly illustrate the power of data fusion in coupled hydrogeophysical inversion. The optimum values for α, n and K_s all correspond well with those of the MSO experiment. As examined by Hinnell et al. (2010), such good estimates are only possible when the hydrologic model represents the main features of the hydrological process being monitored. Hence, we interpret this good match as a confirmation of the plausibility of the applied boundary and initial conditions and the assumptions used for setting up the hydrologic model (e.g. homogeneous top soil layer). In scenario OF4, α is underestimated compared to the MSO value but is still within a comparable range. There is an overestimation of n while K_s is close to the reference value from MSO. In scenario OF5, α and K_s are well estimated but n is overestimated compared to the value from MSO.

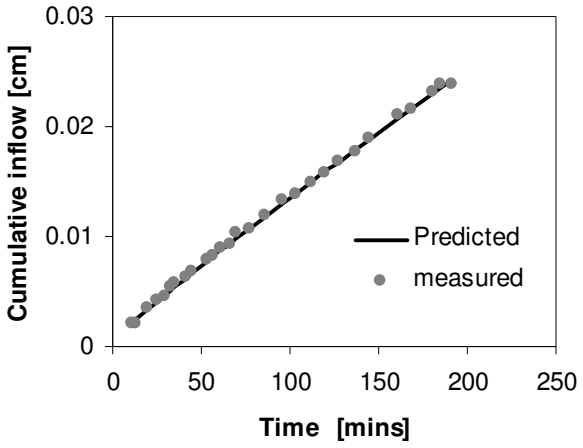

Figure 2.8: Comparison of measured and predicted cumulative inflow with the optimized parameters of scenario OF1.

The different results for scenarios OF3 to OF5 are a consequence of different weights for the objective function leading to trade-offs in fitting the inflow and electrical resistance measurements. The estimated hydraulic parameters for each of the 5 inversion scenarios were used to calculate the root mean square errors (RMSE) based on the ERT and the cumulative inflow data. A plot of RMSE associated with ERT and inflow for all five inversion scenarios (Figure 2.9) provides a Pareto front (e.g. Vrugt and Robinson, 2007) which illustrates the trade-off in fitting both measurement types. The extreme ends of the Pareto front represent the inversion results for scenarios OF1 and OF2 in which only a single data type was used for optimization. Scenarios OF3 to OF5 represent various compromise solutions along the Pareto front. In scenarios OF4 and OF5, there is a better fit to the ERT measurements than in scenario OF3, but a relatively poor fit to the inflow measurements. The Pareto front also shows that scenario OF3 is an almost equitable compromise between fitting the inflow and the ERT measurements. While it is not a general rule that this equitable scenario is the best, in this case scenario OF3 also produced hydraulic parameter estimates which are the closest to our MSO benchmark.

Figure 2.10 compares the water retention and hydraulic conductivity functions of the 5 inversion scenarios to those from the MSO experiment. Based on the coefficient of determination (R^2) which established the correlation between the MSO results and the other inversion scenarios, it can be observed from Figure 2.10(a) that the hydraulic function from scenario OF2 ($R^2 = 0.92$) is the closest

to that of MSO followed by scenario OF3, OF4 and OF5 which have similar R^2 values (R^2 = 0.87). The hydraulic conductivity function from scenario OF1 (R^2 = 0.6) is the least correlated to that from MSO. None of the five inversion scenarios predict a hydraulic conductivity function close to that from MSO at pF = 0. It is common to find differences in hydraulic parameters obtained using laboratory and field methods. Despite this observation, the K_s value predicted from the five inversion scenarios are all in the same order of magnitude as the K_s obtained from the MSO experiment (Table 2.3). Compared to the MSO method (Figure 2.10(b), the water retention functions from scenarios OF3 (R^2 = 0.98), and OF4 (R^2 = 0.94) are the best, followed by those from scanarios OF1 (R^2 = 0.91), OF5 (R^2 = 0.82) and OF2 (R^2 = 0.75). Therefore we conclude that the fusion of cumulative inflow and electrical resistances within the coupled hydrogeophysical inversion framework using scenario OF3 allowed the retrieval of plausible α , n and K_s comparable with those from an MSO experiment

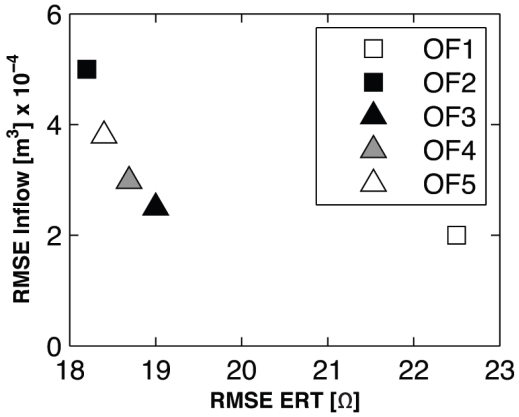

Figure 2.9: Pareto front showing the Root Mean Square Error (RMSE) between measured and predicted inflow and resistance measurements for the 5 inversion scenarios

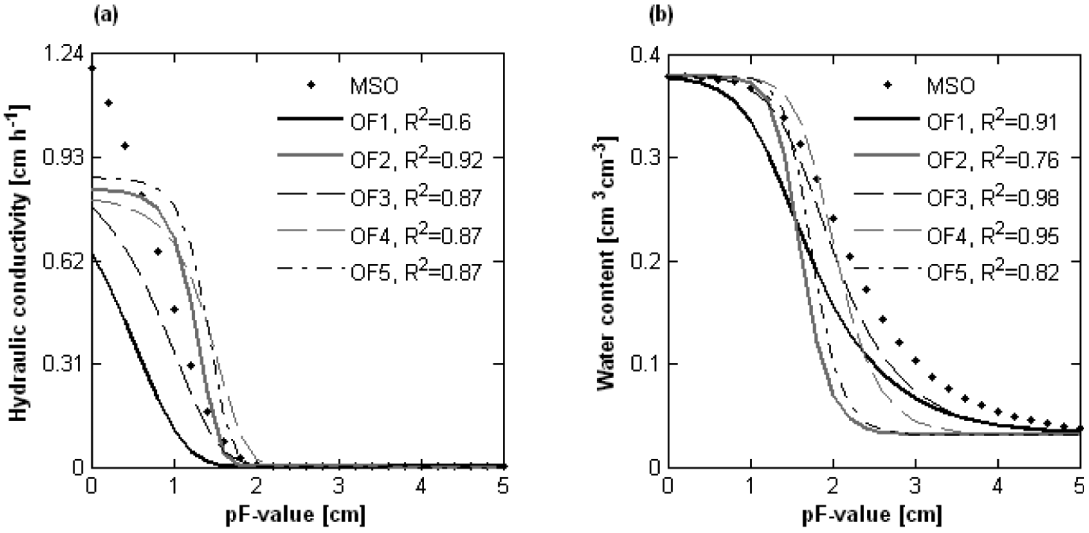

Figure 2.10: Comparison of (a) hydraulic conductivity and (b) water retention functions from optimized parameters of the MSO method and the five inversion scenarios (OF1 - OF5).

2.6. Conclusions

We have developed a coupled hydrogeophysical inversion framework for fast and accurate estimation of three key Mualem-van Genuchten (MVG) parameters (α, n and K_s) from electrical resistances and inflow measurements obtained under a constant head infiltration. Using synthetic data, we numerically investigated the feasibility of 5 inversion scenarios to estimate three MVG parameters (α, n and K_s) namely: (i) OF1, where only inflow measurements are used within the objective function ; (ii) OF2, where only electrical resistances are used within the objective function; (iii) OF3 where inflow and electrical resistances are used within an objective function normalized by the standard deviation of the resistance and inflow measurements; (iv) OF4, where inflow and electrical resistances are used in an objective function normalized by the range of the measurements, and (v) OF5, where both inflow and electrical resistance measurements are used within an objective function normalized by the mean of the measurements. The numerical experiment indicated that all the five inversion scenarios can enable reasonably good estimates of K_s. However, using inflow measurements alone does not provide a unique solution to the inverse problem due to a positive correlation between α and n. The results also showed that using only electrical resistance can provide reasonably good constraints on the estimation of α and n in addition to K_s.

By applying the coupled hydrogeophysical inversion procedure to real inflow and electrical resistances measured during a constant head infiltration experiment, and comparing the results with those from a MSO experiment carried out with undisturbed soil from the site of investigation, we observed that all 5 scenarios enable reasonably good estimates of K_s. The use of inflow data only enabled plausible estimates of n and K_s while reasonably good estimates of α and K_s were obtained using electrical data only. In scenario OF3, estimates of α, n and K_s closer to those obtained from MSO were retrieved. Fairly good estimates of α and n were possible with scenario OF4, while α and K_s could be appreciably estimated with scenario OF5. Hence, scenario OF3 was the best inversion method.

The results showed that the coupled hydrogeophysical inversion framework is a fast and efficient way of estimating unknown model parameters from geophysical data. The ability for data fusion of the developed coupled hydrogeophysical inversion scheme was also clearly shown. The joint interpretation of inflow and resistance measurements resulted in hydraulic parameter estimates that were more appropriate than the parameters obtained from the individual data. In the fusion of data sources, the choice of an appropriate objective function is a prerequisite and the multi-objective interpretation using the Pareto front indicated that the compromise solution that simultaneously fitted the inflow and the resistances also resulted in the most plausible hydraulic parameters. In future studies, it will be interesting to investigate the applicability of the method to estimate spatially varying soil hydraulic parameters.

3. Coupled hydrogeophysical inversion of streaming potential signals for unsaturated soil hydraulic properties [2]

Abstract
Streaming potential (SP_s) is the electric potential generated by fluid flow in a charged porous medium. SP_s signals are related to pore water velocity, bulk electrical conductivity, excess of charge in pore water and soil porosity. Several studies have estimated hydraulic properties of the saturated zone from SP_s signals but there are much less studies that attempt to infer hydraulic properties from SP_s signals obtained under variably saturated flow conditions. In this study, we aim to investigate the feasibility of inferring three key Mualem-van Genuchten hydraulic parameters (α, n, K_s) and the Archie's saturation exponent (n_a) from SP_s measurements obtained during a falling head infiltration experiment followed by primary drainage using a coupled hydrogeophysical inversion approach. Numerical and laboratory experiments were performed in which infiltration and subsequent drainage was monitored with non-polarizable Ag/AgCl electrodes and tensiometers. The synthetic case study showed that SP_s data obtained under variably saturated flow conditions can provide good information on the hydraulic parameters (α, n, and K_s) and n_a. In addition to a reasonably good estimate of n_a, coupled hydrogeophysical inversion of actual SP_s measurements during drainage of a sandy soil column provided estimates of α, n and K_s which were comparable to those obtained from an independent inversion of the tensiometric data (matric heads). It was concluded that coupled hydrogeophysical inversion of time-lapse SP_s signals is a promising method for hydraulic characterization of the vadose zone. Accurate modeling of SP_s signals is essential for reliable inversion results, but there still is debate about the appropriate model for the voltage coupling coefficient at partial saturation. Our experimental data showed a non-linear and monotonous decrease of the absolute voltage coupling coefficient with decreasing saturation. A comparison of several available models with our experimental data showed that models that consider the relative permeability and the relative electrical conductivity in addition to the saturated coupling coefficient and water saturation were most appropriate.

[2]Adapted from: Mboh, C.M., J.A. Huisman, E. Zimmermann, and H. Vereecken. 2012. Coupled hydrogeophysical inversion of streaming potential signals for unsaturated soil hydraulic properties. Vadose Zone Journal, 11(2). doi:10.2136/vzj2011.0115.

3.1. Introduction

Self-potential (SP) monitoring is a geophysical method based on the passive measurement of natural electrical potential fields on the surface or in the subsurface of the earth. Many processes cause spatio-temporal variations in these passively measured electric fields, including thermoelectric, electrochemical and electrokinetic processes (e.g., Marshall and Madden, 1959; Sato and Mooney, 1960), and often observed SP signals have more than one contributing effect. Nevertheless, SP signals have been used to delineate the lateral extent of hydrothermal zones associated with volcano activity (e.g., Ishido et al., 1997; Lénat et al., 2000; Finizola et al., 2002) or to image organic-rich contaminant plumes (Naudet et al., 2003, 2004; Linde and Revil, 2007), to name but a few of the potential applications. A dominant contribution to SP signals observed in many subsurface hydrological and hydrothermal processes is the so-called streaming potential, which is associated with fluid flow in charged porous medium (e.g., Zablocki, 1978; Ishido and Mizutani, 1981; Sill, 1983).

Streaming potential (SP_s) signals are related to the presence of an electrical double layer at the typically negatively charged interface of the solid phase in porous media (e.g., Stern, 1924; Overbeek, 1952; Dukhin and Derjaguin, 1974), which results in an excess of charge at the mineral-water interface. The drag on the excess of charge by the flow of water generates a macroscopic electric potential that can be measured. Because SP_s signals are proportional to water flow rates, they have found widespread applications in subsurface hydrological investigations. Most of these applications are limited to the saturated zone and include among others: monitoring of groundwater flow and determination of the location, nature, and geometry of electrokinetic sources from wavelet analysis and streaming potential inversion (Patella, 1997; Gibert and Pessel, 2001; Sailhac and Marquis, 2001; Rizzo et al., 2004); determination of the pattern of groundwater or subglacial water flow (Kulessa et al., 2003; Richards et al., 2010); detection of water leakages through dams (Bogoslovsky and Ogilvy, 1973; Al-Saigh et al., 1994; Panthulu et al., 2001; Bolève et al., 2009); and estimation of aquifer hydraulic properties from the inversion of surface SP_s anomalies (Darnet et al., 2003).

There are much less studies focusing at SP_s signals in variably saturated porous media. Some of the earliest experimental studies were carried out by Antraygues and Aubert (1993) and Sprunt et al. (1994). Recent research has focused on the development of models to predict SP_s for partially saturated conditions. Generally, these methods rely on the governing equations that apply to the saturated zone, but with a modification of the relationship between saturation and the voltage coupling coefficient that relates the driving pore pressure to the induced macroscopic potential. Several expressions have been proposed for this voltage coupling coefficient at partial saturation, but no consensus has been reached yet on what is the most appropriate model (e.g., Revil et al., 1999; Perrier and Morat, 2000; Guichet et al., 2003; Darnet and Marquis, 2004; Revil and Cerepi, 2004; Linde et al., 2007; Revil et al., 2007; Jackson 2008, 2010; Allègre et al., 2010).

Despite differences in the approaches for modeling streaming potential in unsaturated porous media, many studies have indicated that SP_s signals can provide information on the subsurface pore water velocity. This makes the SP method different from other geophysical methods (e.g., electrical resistivity tomography, ground penetrating radar, electromagnetic induction) that use changes in geophysical properties (e.g., electrical conductivity, dielectric permittivity) as proxies for changes in state variables, such as soil water content or solute concentration (e.g., Huisman et al., 2003; Samouelian et al., 2005; Robinson et al., 2008). In this context, an interesting research topic that remains vastly unexplored is the determination of subsurface unsaturated hydraulic properties from

SP_s signals. Theoretically, this can be achieved using two approaches. In the first approach, tomographic inversion is used to convert time-lapse SP_s signals into Darcy velocities (e.g., Jardani et al., 2006; Jardani et al., 2007; Minsley et al., 2007; Bolève et al., 2009), and these Darcy velocities are subsequently used to calibrate a hydrologic model. This process requires independent geophysical inversions for the subsurface streaming current density and electrical conductivity distributions at each measurement time. In the second approach, SP_s signals are directly used in model inversion without a prior inversion to Darcy velocities. These approaches are respectively referred to as uncoupled and coupled hydrogeophysical inversion approaches (Ferre et al., 2009; Hinnell et al., 2010).

Tomograhic inversion of SP_s signals for Darcy velocities is typically underdetermined and regularization with a smoothness constraint is applied to stabilize the inverse problem (e.g., Jardani et al., 2007). As has been observed with other geophysical methods like ground penetrating radar and electrical resistivity tomography (e.g., Day-Lewis et al., 2005), regularization can lead to errors on the Darcy velocity tomograms that will propagate to the estimated hydraulic properties when an uncoupled hydrogeophysical inversion approach is used. As the coupled hydrogeophysical inversion approach does not involve an intermediate tomographic inversion step, it has the advantage that this error propagation is avoided. Several other advantages of this inversion approach are discussed in Hinnell et al. (2010).

The coupled hydrogeophysical inversion approach has been successfully applied for the estimation of subsurface unsaturated hydraulic properties from ground penetrating radar (Kowalsky et al., 2005; Looms et al., 2008; Lambot et al., 2009), electrical resistivity tomography (Huisman et al., 2010; Rings et al., 2010) and time domain reflectometry (Mboh et al., 2011) data. In this study, we aim to investigate the feasibility of estimating soil hydraulic properties from SP_s signals obtained under variably saturated flow conditions using a coupled hydrogeophysical inversion approach. In particular, we analyze time-lapse SP_s signals made during falling head infiltration of water into a saturated sandy soil column followed by primary drainage similar to the experiments presented by Linde et al. (2007) and Allègre et al. (2010). This is one of the few attempts to use time-lapse SP_s signals to constrain the inversion for soil unsaturated hydraulic properties. Earlier attempts include Sailhac et al. (2004) who presented an approach to estimate unsaturated hydraulic properties based on analytical solutions for two-dimensional infiltration from a line source at steady state. As the behavior of the voltage coupling coefficient under unsaturated conditions is still under debate, our experimental results will also be used to compare the performance of several models for the voltage coupling coefficient at partial saturation.

3.2. Streaming potential theory

The distribution of streaming potentials (φ [V]) in porous media can be determined from the Poisson equation:

$$\nabla \cdot \sigma \nabla \varphi = \nabla \cdot \mathbf{j}_s \tag{3.1}$$

where $\mathbf{j}_s$ [A m^{-2}] and σ [S m^{-1}] are the streaming current density and electrical conductivity distributions of the porous medium, respectively. Eq. 3.1 results from the combination of the generalized Ohm's law $\mathbf{j} = -\sigma \nabla \varphi + \mathbf{j}_s$, which expresses the total electrical current density $\mathbf{j}$ [A m^{-2}] at the quasi-static limit of Maxwell equations, and the conservation equation $\nabla \cdot \mathbf{j} = 0$. From Eq. 3.1, it is evident that streaming potentials are created by electrokinetic sources that are characterized by a non-zero divergence of the streaming current density. As noted by Linde at al. (2007), such sources

may correspond to water tables and capillary fringes, geological boundaries or the confines of infiltration plumes in natural systems.

Linde et al. (2007) and Revil et al. (2007) proposed a model to relate the streaming current density ($\mathbf{j}_s$) to the Darcy velocity or flux $\mathbf{u}$ [m s^{-1}], the saturation S_w [-] and the excess of charge at saturation $Q_{v,sat}$ [C m^{-3}]:

$$\mathbf{j}_s = \frac{Q_{v,sat}\mathbf{u}}{S_w} \tag{3.2}$$

The saturation S_w is defined as $\theta\Phi^{-1}$, where θ [cm^3 cm^{-3}] is the water content and Φ [-] is the porosity of the medium, which we assumed to be equal to the saturated water content θ_s. The excess of charge at saturation $Q_{v,sat}$ is related to electrical conductivity at saturation σ_{sat} [S m^{-1}], the permeability of the medium k [m^2], the dynamic viscosity of water μ_w [Pa s], and the voltage coupling coefficient at saturation C_{sat} [V Pa^{-1}] according to (Revil and Leroy, 2004):

$$Q_{v,sat} = \frac{-C_{sat}\mu_w\sigma_{sat}}{k} \tag{3.3}$$

The permeability (k) is related to the saturated hydraulic conductivity of a water-filled porous medium by

$$k = \frac{K_s\mu_w}{\rho g} \tag{3.4}$$

where ρ [kg m^{-3}], and g [m s^{-2}] are the density of water and the gravitational constant, respectively. If surface conduction is negligible, C_{sat} is defined by the Helmholtz-Smoluchowski relation (Smoluchowski, 1905) as:

$$C_{sat} = \frac{\varepsilon_f\zeta}{\eta_f\sigma_f} \tag{3.5}$$

where ε_f [F m^{-1}] is the dielectric permittivity of the fluid, η_f [Pa s] is the fluid dynamic viscosity, σ_f [S m^{-1}] is the fluid electrical conductivity and ζ [V] is the zeta potential, which is defined as the electrical potential inside the electrical double layer (EDL) at the shear plane. The shear plane is a hypothetical slip plane slightly above a positively charged layer (Stern layer) in the EDL. C_{sat} can be determined experimentally by measuring the potential difference across a saturated sample with a known pressure gradient and assuming 1D flow conditions.

The model of Linde et al. (2007) and Revil et al. (2007) can be rearranged to obtain the following expression for the voltage coupling coefficient at partial saturation, $C(S_w)$ [V Pa^{-1}]:

$$C(S_w) = \frac{C_{sat}k_r}{S_w\sigma_r} \tag{3.6}$$

where σ_r [-] is the relative electrical conductivity of the porous medium defined as $\sigma_r = S_w^{n_a}$, and n_a [-] is the saturation exponent of Archie (1942). More details and extensions regarding the underlying equations leading to the proposed model of Linde et al. (2007) are examined in Revil et al. (2007). Several alternative models have been presented for $C(S_w)$. For example, Revil et al. (1999) presented the following model:

$$C(S_w) = \frac{C_{sat}}{S_e^{n_a}\left(1+2\left(\frac{F}{S_e^{n_a}}-1\right)\frac{\xi}{S_e}\right)} \tag{3.7}$$

where the effective saturation, S_e [-], is defined as:

$$S_e = \frac{\theta - \theta_r}{\theta_s - \theta_r} = \frac{S_w - S_w^r}{1 - S_w^r} \tag{3.8}$$

and F [-] is the electrical formation factor, ξ [-] is the ratio between mineral surface and pore fluid electrical conductivity, and S_w^r is the residual saturation defined as θ_r/θ_s with θ, θ_r and θ_s being the actual, residual and saturated volumetric water contents, respectively. Assuming that the surface electrical conductivity is negligible for silica dominated porous materials (i.e. ξ tends to zero), Darnet and Marquis (2004) simplified Eq. 3.7 to:

$$C(S_w) = \frac{C_{sat}}{S_e^{n_a}} \tag{3.9}$$

Guichet et al. (2003) presented a voltage coupling coefficient which is linearly dependent on the effective saturation S_e:

$$C(S_w) = C_{sat} S_e \tag{3.10}$$

Perrier and Morat (2000) used a model similar to Linde et al. (2007) where the voltage coupling coefficient also depends on the relative permeability of the porous medium:

$$C(S_w) = \frac{C_{sat} k_r}{\sigma_r} \tag{3.11}$$

Based on a bundle of capillary tubes model and assuming that the excess of charge is independent of saturation, Jackson (2008) also proposed Eq. 3.11 for the behavior of the voltage coupling coefficient at partial saturation. Commenting on Jackson (2008), Linde (2009) acknowledged that using a bundle of capillary tubes model can enable the development of a more accurate relation than the model of Linde et al. (2007) based on a representative elementary volume concept because the relative contribution of each capillary to the overall permeability can be determined. Linde (2009) however showed that the assumption of Jackson (2008) that excess of charge is independent of saturation is not physically plausible and proposed a correction in which the numerator of Eq. 3.11 is multiplied by the relative excess charge of the wetting phase. By assuming that the surface charge is constant in capillaries occupied by a given phase, Jackson (2010) investigated the impact of fluid and charge distribution on multiphase electrokinetic coupling. Again using a bundle of capillary tubes model, Jackson (2010) showed that the excess of charge at partial saturation depends on the pore scale distribution of fluid and charge, which is controlled by the thickness of the electrical double layers relative to the capillary radius, the capillary size distribution and the wettability. Relying on these results, he postulated that the excess of charge in real geologic media will also depend on these factors and argued that the model of Linde et al. (2007) should be considered as a first-order approximation because of the simplified assumption that the excess of charge at partial saturation scales inversely with water saturation. Notwithstanding these differences, Jackson (2008, 2010) equally acknowledges that a bundle of capillary tubes is not a good representation of the pore space of most geologic media.

3.3. Materials and Methods

3.3.1 Laboratory experiment

A falling head infiltration experiment followed by primary drainage was performed in a plexiglass tube with a length of 217.5 cm and an internal diameter of 5 cm. Quartz sand (F36, Quartzwerk Frechen GmBH, Germany) was evenly packed to a bulk density of about 1.5 g cm^{-3} and a height of 117.5 cm. According to the provider specifications, the material contains about 99% of sand with a mean grain size of 0.16 mm and is predominantly made of silica (99.3%). The sand column was

gradually saturated starting from the bottom for several hours to avoid air entrapment. At the start of the experiment, 56 cm of tap water with an electrical conductivity of 0.041 Sm^{-1} and a room temperature of 20.1 °C was ponded on top of the saturated sand column. The bottom of the column was closed for 22 minutes to obtain measurements under no flow conditions. Next, the bottom of the column was opened and a Marriotte reservoir was used to maintain a constant water level of 51 cm above the soil surface for 38 minutes. Finally, the Marriotte reservoir was closed to allow for falling head infiltration and subsequent drainage of the column until the end of the experimental period of 10 hours.

Ten custom-made non-polarizable Ag/AgCl electrodes and six T5 tensiometers (UMS GmbH, Munich, Germany) were horizontally installed in the soil column (Figure 3.1). The non-polarizable electrodes consist of plastic tubing of 50 mm length with a porous cylindrical ceramic tip of 25mm length and a diameter of 6 mm. The tubing was filled with the water used in the experiments and contained a silver wire partly coated with AgCl. Relative to a reference electrode at 5 cm, SP measurements were carried out for electrodes installed at 13.5, 25.5, 37.5, 49.5, 61.5, 73.5, 85.5, 97.5, and 109.5 cm from the bottom of the column. Tensiometers were installed at 10, 45, 65, 85, and 105 cm from the bottom of the column. SP measurements and tensiometric data were acquired using an Electrical Impedance Tomography (EIT) imaging system described in Zimmerman et al. (2008), which uses NI 4472 cards from National Instruments (www.ni.com) and amplifiers with very high input resistance (500 GΩ). The SP and tensiometric data were simultaneously acquired at a sampling frequency of 1 KHz and averaged to give signals every second. Next, the SP and tensiometric signals were filtered by calculating the median over six second intervals. This was done to reduce instrumental noise and improve the signal-to-noise ratio of the measurements. Even under well controlled laboratory conditions, interpretation of SP measurements can be challenging because apart from the streaming potential (SP_s) contribution, electrode responses can also vary due to drift terms that are related to the electrode design and age (Petiau and Dupis, 1980). Therefore, pre-processing of the SP measurements is required. By assuming that the drift is linear over time and that water flow is insignificant at the end of the experiment, we shifted the signals to give a zero voltage at the end while ensuring that signals at the beginning of drainage correspond to values directly determined based on the measured voltage coupling coefficient at saturation. The processed signals during drainage were sampled at 3.6 minute intervals and used for coupled hydrogeophysical inversion.

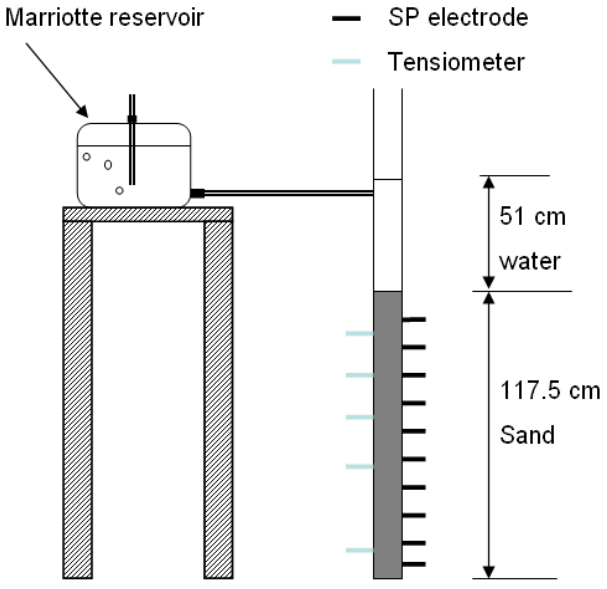

Figure 3.1: Illustration of the experimental setup. SP signals are measured relative to a reference electrode at 5cm from the bottom of the 117.5 cm sand column

The type of experimental set-up used here can be used to directly estimate the voltage coupling coefficient at partial saturation (Allègre et al., 2010). In order to do so, measured SP and tensiometric data were interpolated to obtain streaming potential and pressure head estimates at 45, 55, 65, 75, 85, 95, and 105 cm from the bottom of the column. From the interpolated streaming potentials φ [mV] and matric potentials h [m] at positions (x_1, x_2), the voltage coupling coefficient C_{x_1,x_2} [mV m^{-1}] for each data pair was calculated using:

$$C_{x_1,x_2} = \frac{\partial \varphi_{x_1,x_2}}{\partial P_{x_1,x_2}} = \frac{\varphi_{x_2} - \varphi_{x_1}}{\left(h_{x_2} + x_2\right) - \left(h_{x_1} + x_1\right)} \tag{3.12}$$

Based on Eq. 12 the voltage coupling coefficients were computed between successive electrode pairs in the unsaturated part of the column, that is, $C_{45,55cm}$, $C_{55,65cm}$, $C_{65,75cm}$, $C_{75,85cm}$, $C_{85,95cm}$, $C_{95,105cm}$. To investigate the variation of the voltage coupling with saturation, the average water content between these successive electrode pairs was calculated. It is important to note here that this method is only valid when water flow is strictly 1D.

The experimental set up can also be used for the direct estimation of the saturated hydraulic conductivity K_s [ms^{-1}] using the falling head method as described by Klute and Dirksen (1986):

$$K_s = \frac{L}{t_{in}} \ln \frac{b_0 + L}{b_1 + L} \tag{3.13}$$

where L [m] is the length of the saturated sandy soil column, and t_{in} [s] is the time it takes for a ponding water column of height b_0 [m] to fall to another height b_1 [m].

3.3.2. Coupled hydrogeophysical inversion

Figure 3.2 illustrates the coupled hydrogeophysical inversion approach for the estimation of soil hydraulic properties from time-lapse SP_s signals. A forward hydrologic model is coupled to a forward model for SP_s. Using a suitable optimization algorithm, varying sets of hydraulic parameters from predefined ranges are systematically fed into the hydrologic model, which provides simulations of Darcy velocity and water content distributions. The simulated Darcy velocity and water content distributions are converted into streaming currents and electrical conductivity distributions using the voltage coupling coefficient and a suitable petrophysical relation. Finally, the simulated streaming current and electrical conductivity distributions are fed into the geophysical model which predicts the corresponding streaming potentials associated with the set of hydraulic parameters being evaluated. The simulated streaming potential distributions are compared to the corresponding measurements by computing an objective function which expresses their misfit. The whole process is repeated until a hydraulic parameter set is found for which there is a close fit between measurements and simulations. The inversion of SP_s measurements for subsurface hydraulic parameters therefore requires petrophysical parameters and the voltage coupling coefficient at saturation. These can either be measured independently, or in some cases they can be included as additional inversion parameters in the coupled inversion approach. Maineult et al. (2005, 2006) used a similar approach to estimate the transport properties of salt fronts in saturated sand by manually fitting the Darcy velocity and the dispersion coefficient until the predicted and measured SP data fit together.

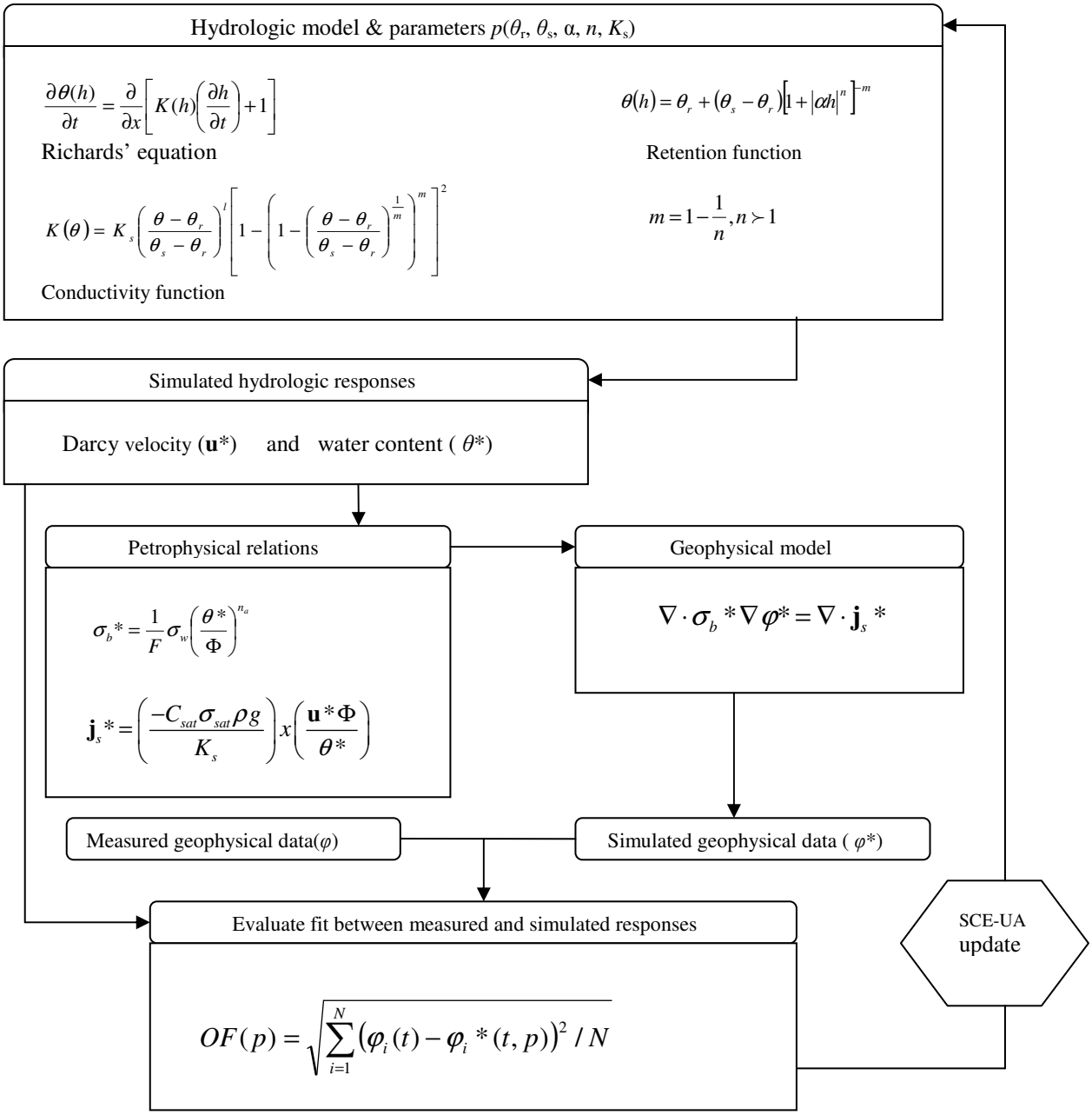

Figure 3.2: Work flow of coupled hydrogeophysical inversion of time-lapse streaming potentials (φ) to soil hydraulic properties p. *F* and n_a are respectively the formation factor and saturation exponent of the law of Archie (1942). C_{sat}, σ_{sat} and Φ are the voltage coupling coefficient at saturation, the saturated electrical conductivity, and the porosity of the soil while ρ and *g* are the density of water and the gravitational constant. $\mathbf{j}_s$* and σ_b* are simulated streaming current density and electrical conductivity distributions required to solve for the streaming potential distribution (φ*).

3.3.3. Forward hydrologic model

We modeled falling head infiltration and drainage using HYDRUS 1D (Simunek et al., 2008). The simulations were started with an atmospheric upper boundary condition and a measured ponding depth of 48 cm above the initially saturated soil column of 117.5 cm. A seepage face was applied as the bottom boundary condition. The 117.5 cm long soil column was discretized into 235 elements

with a thickness of 0.5 cm. HYDRUS 1D numerically solves the one-dimensional Richards' equation for variably saturated flow in rigid porous media:

$$\frac{\partial \theta}{\partial t} = \frac{\partial}{\partial x}\left[K(h)\left(\frac{\partial h}{\partial x} + 1\right)\right] \tag{3.14}$$

where $K(h)$ is the unsaturated hydraulic conductivity [cm d^{-1}]. We assumed that the material properties can be described by the classical Mualem-van Genuchten hydraulic model (Mualem, 1976; van Genuchten, 1980):

$$S_e(h) = \left[1 + |\alpha h|^n\right]^{-m} \tag{3.15}$$

$$K(h) = K_s k_r = K_s S_e^{\,l}\left[1 - \left(1 - S_e^{\,1/m}\right)^m\right]^2 \tag{3.16}$$

where k_r [-] is the relative permeability, S_e [-] is the effective saturation as defined in Eq. 8 while α [cm^{-1}] and n [-] are empirical parameters which are respectively related to the air entry pressure value (i.e the minimum pressure to overcome before drainage starts) and the width of the pore size distribution, m is restricted by the Mualem condition $m = 1 - 1/n$ with $n > 1$, K_s is the saturated hydraulic conductivity [cm d^{-1}], and l [-] is a factor that accounts for pore tortuosity. Of the six Mualem van Genuchten (MVG) parameters (θ_r, θ_s, α, n, K_s and l), we fixed l to its average value of 0.5 (Mualem, 1976) while θ_r and θ_s were respectively fixed to 0.05 cm^3cm^{-3} and 0.41 cm^3cm^{-3} based on TDR measurements in air-dried and water saturated samples of the material. Therefore, there are three hydraulic parameters (α, n and K_s) that remain to be estimated by inverse modeling.

3.3.4. Forward geophysical model for streaming potentials

We implemented the SP_s model outlined by Linde et al. (2007) in MATLAB (see section 3.2). The Darcy velocity distribution **u** and saturation S_w required to compute Eq. 3.2 and solve Eq. 3.1 are obtained from a forward hydrologic model run. The voltage coupling coefficient at saturation was estimated independently with a short sand column and the measurement set-up described by Suski et al. (2006) based on the relationship

$$C_{sat} = \left(\frac{\partial \varphi}{\partial H}\right)_{J=0} \tag{3.17}$$

where $\partial\varphi$ is the steady state difference of the streaming potential recorded between two electrodes in the sample and ∂H is the imposed hydraulic head difference between the two electrodes. Generally, the experiment is repeated using different hydraulic heads to obtain several pairs of $\partial\varphi$ and ∂H between the pair of electrodes in the sample. A plot of $\partial\varphi$ against ∂H gives a graph with a linear trend whose slope is equal to C_{sat}. An estimate of σ_{sat} was obtained by measuring the bulk conductivity of a sample packed to the same bulk density as the sand in the column and saturated with the same water (σ_w = 0.041 S m^{-1} at 20 °C) with TDR (Huisman et al., 2008).

The electrical conductivity distribution σ required to simulate SP_s signals was obtained by converting the simulated water content distributions using the model of Archie (1942):

$$\sigma = \sigma_w F^{-1} S_w^{n_a} \cong \sigma_{sat} S_w^{n_a} \tag{3.18}$$

where F [-] is the electrical formation factor and n_a [-] is the saturation exponent. Ulrich and Slater (2004) reported values for n_a varying between 1.1 and 2.7 from measurements made on unconsolidated sands. Glover (2009) also reports a similar range (1.5-2.5) for n_a. The exponent n_a was determined by fitting Eq. 3.18 to TDR-measured conductivities and saturations from samples variably saturated with the same water, and packed to a similar bulk density as in the laboratory experiment earlier described.

3.3.5. Objective function and inversion scenarios

Using the coupled hydrogeophysical inversion approach, the parameter set p is estimated by minimizing an objective function $OF(p)$ expressed as the root mean square error between N time-lapse simulated streaming potential distributions $\varphi^*(t,\mathbf{p})$ and the corresponding observations $\varphi(t)$:

$$\mathrm{OF}(p) = \sqrt{\sum_{i=1}^{N} \left(\varphi_i(t) - \varphi^*_i(t, p)\right)^2 / N} \qquad (3.19)$$

As vadose zone dynamics are non-linear, the objective function is expected to be non-linear and may be characterized by many local minima. To avoid the inversion from converging to a local minimum, we used a global search algorithm to minimize the objective function. For this purpose, the Shuffled Complex Evolution optimization algorithm SCE-UA (Duan et al., 1993) was used. This global optimizer from the family of genetic algorithms combines concepts of clustering, shuffling and systematic competitive evolution with a deterministic local search algorithm (Simplex) to find the global minimum. Initial parameter spaces varied over sufficiently wide ranges (Table 3.1). The uncertainty of the parameters obtained with coupled hydrogeophysical inversion was assessed by calculating the 95% confidence intervals based on a first order approximation (e.g., Kool and Parker, 1988; Vrugt and Bouten, 2002).

Table 3.1: Parameter inversion bounds

Parameter [1]	Lower bound	Upper bound
α [cm^{-1}]	0.005	0.165
n [-]	1.2	11.2
K_s [cmhr^{-1}]	0.2	100
n_a [-]	1.1	2.7

[1] α and n are hydraulic parameters which are respectively related to the air entry pressure value and the width of the pore size distribution. K_s is the saturated hydraulic conductivity and n_a is the saturation exponent of the law of Archie (1942).

Two inversion scenarios are considered in this study. In the first scenario, coupled hydrogeophysical inversion was performed to estimate the parameter set $p = \{\alpha, n \text{ and } K_s\}$. The remaining hydraulic parameters (θ_s, θ_r and l) and the petrophysical parameters (σ_{sat} and n_a) were fixed to literature or independently measured values. In the second scenario, n_a was also included in the inversion.

To benchmark the inversion of streaming potential signals for soil hydraulic properties, the tensiometric data obtained during the laboratory experiment were also inverted for α, n and K_s using HYDRUS1D and SCE-UA. The objective function was based on the root mean square difference between the time-lapse tensiometric measurements and the corresponding simulations of the matric potential (in analogy to Eq. 3.19)

3.3.6. Numerical experiments

Numerical experiments were performed to investigate the feasibility of estimating subsurface hydraulic properties from streaming potential signals obtained under falling head infiltration into an initially saturated soil and subsequent primary drainage. We considered a sandy soil with typical MVG hydraulic parameters (θ_r = 0.045 cm^3 cm^{-3}, θ_s = 0.43 cm^3 cm^{-3}, α = 0.145 cm^{-1}, n = 2.68, K_s = 29.7 cm h^{-1} and l = 0.5) according to Carsel and Parish (1988). For the petrophysical parameters and the voltage coupling coefficient at saturation, we assumed the values determined by Linde et al. (2007) for fine-grained sand. Namely, F = 4.26, σ_w = 0.051 S m^{-1}, n_a = 1.6, and C_{sat} = -2.9 x 10^{-7} V Pa^{-1}. Based on these hydraulic and petrophysical parameters, streaming potential signals corresponding to the measurement setup and duration of the laboratory experiment were simulated. Gaussian noise with a standard deviation of 2.73 x 10^{-5} V and a mean of zero was added to the simulated signals. This noise level was estimated from repeated measurements of streaming potential for long time series in the laboratory. The simulated data with added noise were used as measurements in the numerical experiments. To study the shape of the objective function in the vicinity of its minimum and to gain insights into the correlation and identifiability of the three key MVG hydraulic parameters (α, n, and K_s), we constructed 2D objective function response surfaces in the α-n, α-K_s and n-K_s parameter planes. This was done by fixing all other parameters and systematically varying the mentioned pairs between predefined ranges and computing the objective function (Eq. 3.19). In addition to the 2D objective function response surfaces, the simulated data were used to test the uniqueness of the parameter estimates that can be retrieved from the streaming potential signals considering the two inversion scenarios $p = \{\alpha, n, K_s\}$ and $p = \{\alpha, n, K_s, n_a\}$ under investigation.

3.4. Results and Discussions

3.5.1. Numerical Experiment

Figure 3.3 shows the synthetic data generated during falling head infiltration and drainage based on our experimental setup. As expected, the simulated SP_s data tend to zero voltage towards the end of the experiment where water flow is insignificant. The feasibility analysis using the synthetic data is summarized in 2D objective function response surfaces in Figure 3.4. The first column of Figure 3.4 shows the response surfaces when only SP_s measurement during falling head infiltration are considered. The second column shows the response surfaces when only SP_s measurement during drainage are considered, while the third column shows the response surfaces obtained when both data sets are combined. As expected, only K_s can be obtained from SP_s measurements obtained under falling head infiltration into a saturated soil. This is clearly observable in the α-K_s and n-K_s parameter planes where the objective function minimum is constrained in a space which is perpendicular to the K_s axis at the point where K_s is equal to its true value.

The response surfaces for the drainage phase of the experiment indicate that SP_s measurements obtained during drainage also contain enough information to adequately constrain the inversion for K_s. This is evident in the α-K_s and n-K_s response surfaces that illustrate that a slight change in log(K_s) in the vicinity of the objective function minimum is accompanied by a major increase in the misfit. This sensitivity of SP_s signals to K_s is obvious as streaming currents are induced by fluid motion and K_s is a parameter that strongly influences the pore water velocity and the associated drag on the excess of charge in the diffuse electrical double layer at the mineral-fluid interface. On the other hand, the α-n response surface during drainage revealed a correlation between these two parameters in the vicinity of the objective function minimum. It is worth noting that n varies over a narrow range

of values compared with the range of values for α. SP_s signals obtained from a 1D drainage experiment therefore seem to contain more information on n than α for the sandy soil investigated here. The response surfaces during drainage are similar to those obtained from the combination of drainage and falling head infiltration. Therefore, we only considered the drainage phase in the analysis of the actual experimental data.

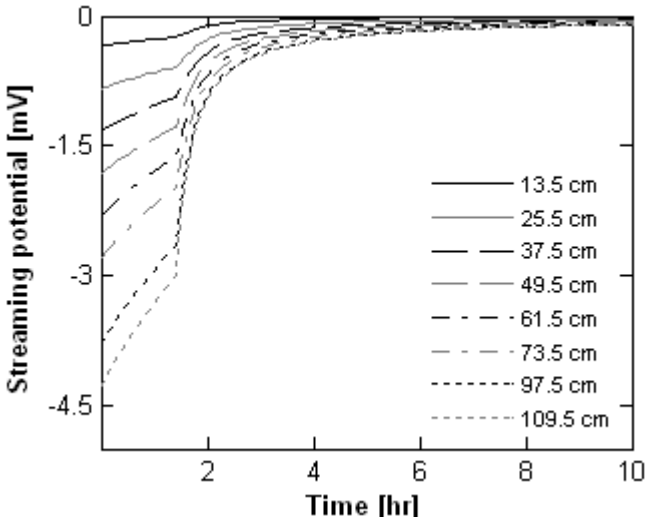

Figure 3.3: Synthetic streaming potential data during falling head infiltration and drainage. Distances are relative to the bottom of the column.

To investigate the uniqueness of the hydraulic parameter estimates, the synthetic data with added noise were used to invert for hydraulic parameters following the two inversion scenarios (Table 3.2). A comparison of prescribed and inverted parameters reveals that accurate estimates of n and K_s are possible for both scenarios. The inversion result for α is still reasonably good for most practical applications. It is worth noticing that the saturation exponent, n_a, is also accurately estimated in scenario 2. Theoretically this implies that SP_s signals obtained under variably saturated flow conditions contain enough information to uniquely constrain the inversion for n, K_s and n_a for a sandy soil. This finding is interesting because the independent estimation of n_a from soil cores is an error-prone procedure which may result in non-negligible error propagation in coupled hydrogeophyical inversion.

Table 3.2: Hydraulic and petrophysical parameres estimates from synthetic data

Scenarios	Pararameters[1]			
	α [cm^{-1}	n [-]	K_s [cm hr^{-1}]	n_a [-]
'True'	0.145	2.68	29.7	1.6
Scenario 1	0.137	2.69	29.7	-----
Scenario 2	0.138	2.69	29.7	1.59

[1] α and n are hydraulic parameters which are respectively related to the air entry pressure value and the width of the pore size distribution. K_s is the saturated hydraulic conductivity and n_a is the saturation exponent of the law of Archie (1942). In scenario 1, coupled hydrogeophysical inversion of synthetic streaming potential data is performed to estimate α, n and K_s while in scenario 2 n_a is additionally estimated.

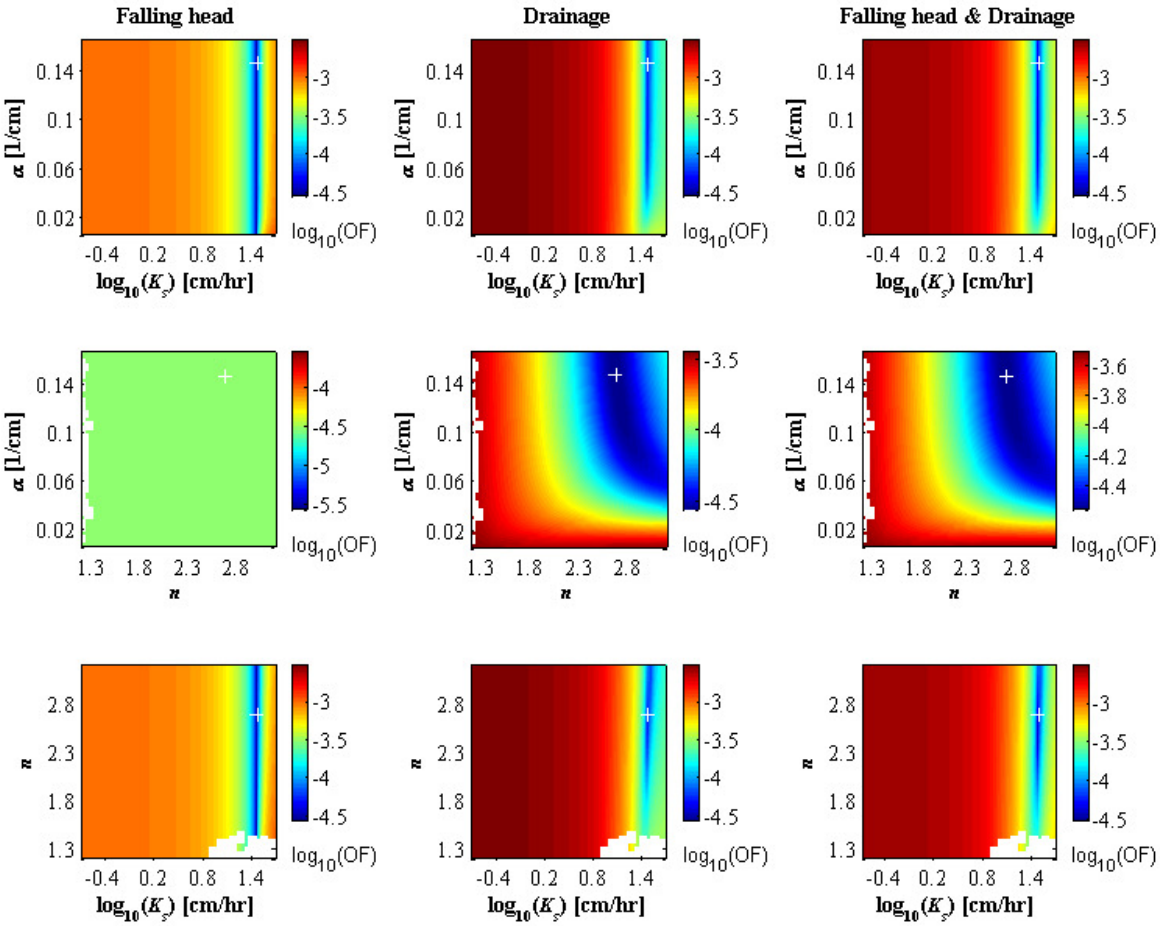

Figure 3.4: Simulated 2D objective function (OF) response surfaces during falling head infiltration infiltration (Column 1) into a saturated sandy soil column and subsequent drainage (Column 2). Column 3 considers both processes. The white (+) is the OF minimum while the white areas are parameter combinations for which the hydrologic model does not converge.

3.5.2 Laboratory experiments

The voltage coupling coefficient at saturation, C_{sat}, and the petrophysical properties of the sand were determined independently. C_{sat} was estimated to be -3.3 mV m^{-1} (Figure 3.5). This value is comparable to those obtained by Linde et al. (2007) and Allègre et al. (2010) on sands using tap water of similar electrical conductivity. The saturation exponent, n_a, was estimated to be 1.87 (Figure 3.6), which also is well within the range of previously reported values (e.g., Ulrich and Slater, 2004).

The hydraulic parameters of the sand were estimated from matric potential measurements made during the drainage phase. Previously, it has been shown that such measurements contain enough information to provide good estimates of soil hydraulic properties (Hopmans et al., 2002). A good fit between measured and simulated matric potential with a RMSE of 1.0 cm was obtained (Figure 3.7). Moreover, the estimated K_s of 31.5 cm hr^{-1} (Table 3.3) compares well with the value obtained from the falling head method (36.6 cm hr^{-1}). Therefore, the hydraulic parameters estimated from the matric potential data are used as an independent benchmark for the streaming potential-based inversions.

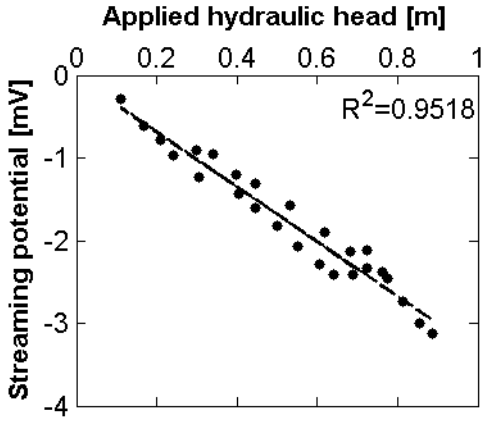

Figure 3.5: Estimation of the voltage coupling coefficient at saturation (C_{sat}).The slope of the linear regression (black line) leads to C_{sat} = 3.3 mV m^{-1} for a water conductivity of σ_w = 0.044 S m^{-1}.

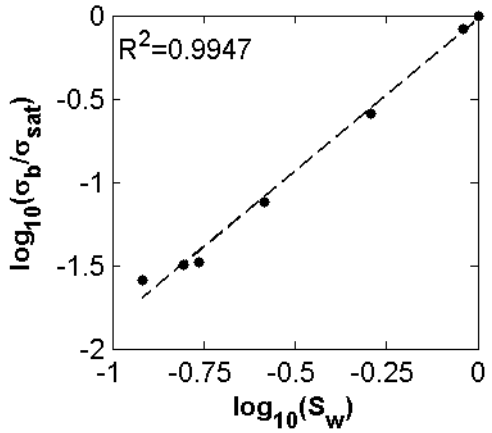

Figure 3.6: Estimation of Archie's saturation exponent (n_a) from bulk-to-saturated electrical conductivity ratio σ_b/σ_{sat} and water saturation S_w. The slope of the linear regression (black line) gives n_a = 1.87

Figure 3.8 shows the raw SP measurements acquired during the experiment. While the drainage phase of our experiment is similar to the experiment of Allègre et al. (2010), our data look very different from theirs. Our data show the same trends observed in the synthetic measurements (Figure 3.3) during falling head infiltration and drainage. Although the voltages do not tend to zero towards the end of the experiment as observed in the synthetic data, the first derivatives do. This indicates that negligible changes in the observed signals over time were recorded towards the end of the experiment. One of the reasons why the signals do not tend to zero towards the end of the experiment is because of SP contributions other than streaming potentials. This is evident from Figure 3.8 because constant signals that differ in magnitude for each electrode were observed under no flow conditions. These issues were handled with careful pre-processing of the SP signals prior to inversion. The resulting corrected SP_s signals are presented in Figure 3.9 for the drainage phase.

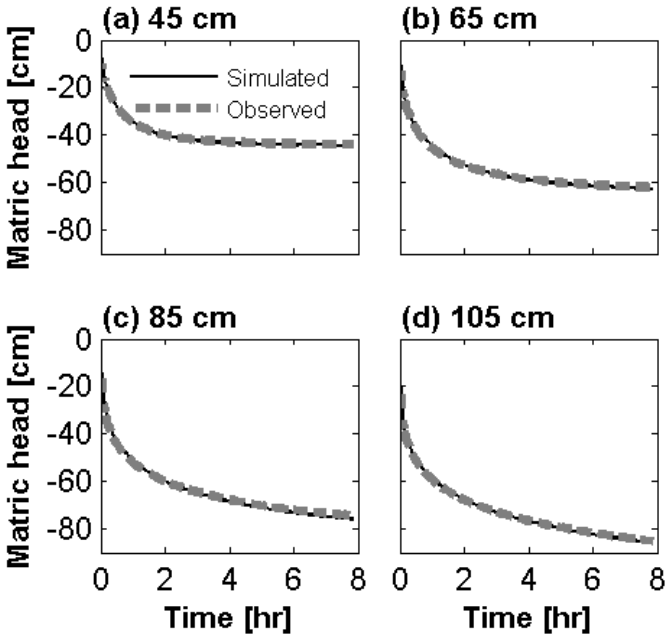

Figure 3.7: Measured (grey lines) versus simulated (black lines) matric potentials at four locations within the sand column during drainage. Distances are relative to the bottom of the column.

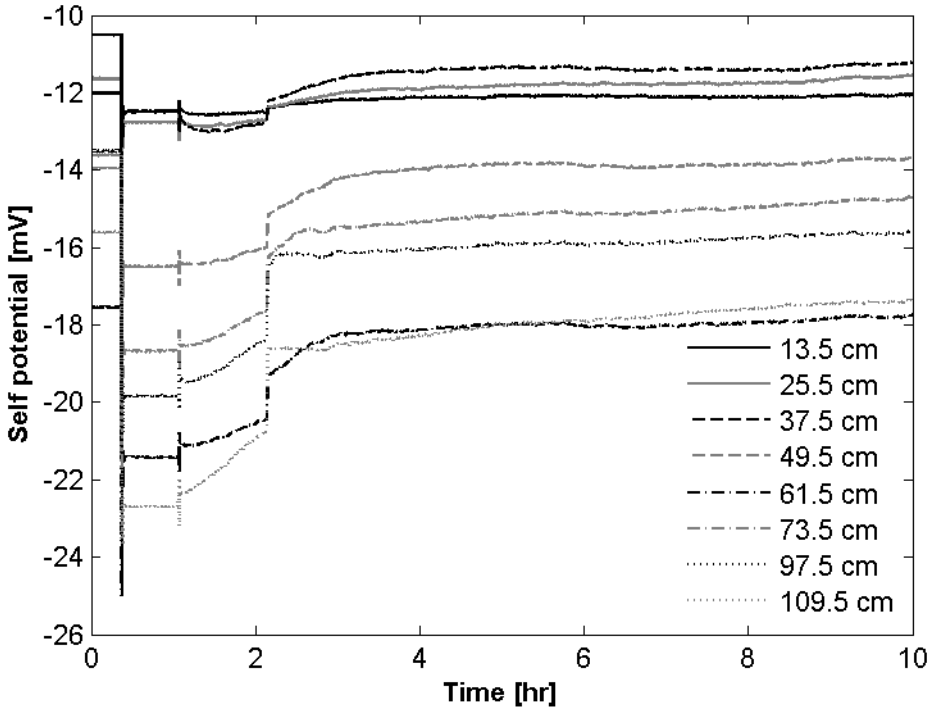

Figure 3.8: Raw SP measurements taken at distances relative to the bottom of the column. Signals from 0-0.36 hr, 0.36-1.06 hr, 1.06-2.14 hr, 2.14-10 hr were obtained under no flow, constant head, falling head and drainage conditions, respectively

The independently estimated C_{sat} and n_a were used within the coupled hydrogeophysical inversion to estimate the hydraulic properties of the sand from the processed streaming potential signals obtained during drainage. Table 3.3 compares the estimated parameters from streaming potential measurements to those independently obtained from the inversion of tensiometric data. The 95% confidence intervals on these estimates are also presented in Table 3.3. Figure 3.10 presents a comparison between the measured streaming potential and the corresponding simulations based on the estimated hydraulic parameters from scenario 1 (RMSE is 0.02 mV). An identical plot (not presented) was obtained using the hydraulic parameters from scenario 2. Scenarios 1 and 2 resulted in similar hydraulic properties which are comparable to those obtained from the inversion of matric heads. This is illustrated in Figure 11 which compares the predicted hydraulic conductivity and water retention functions of the three methods. In all three inversions, n and K_s are estimated with a relatively narrower 95% confidence interval than α. This confirms the numerical findings in which it was observed from 2D objective function response surfaces that SP_s signals obtained for our experimental conditions contained more information on K_s and n than α. The estimated saturation exponent, n_a, is 1.81 in scenario 2, which is close to the independently derived value of 1.87. Evidently, SP_s measurements obtained under variably saturated flow conditions contain ample information on the subsurface electrical conductivity distribution. The ability of the coupled hydrogeophysical inversion approach to also estimate petrophysical parameters determining this electrical conductivity distribution is due to the strong mass balance constraints provided by the hydrological model.

Table 3.3: Hydraulic and petrophysical parameters from actual data

Methods	Parameters[¶] ± 95% confidence limits			
	α [cm^{-1}]	n [-]	K_s [cm hr^{-1}]	n_a [-]
Matric head	0.020 ± 0.015	3.879 ± 0.0001	31.117 ± 1.000	
SP Scenario 1	0.021 ± 0.309	3.408 ± 0.011	33.266 ± 1.004	
SP Scenario 2	0.019 ± 0.444	3.203 ± 0.002	28.445 ± 1.005	1.812 ± 0.006

[¶] α and n are hydraulic parameters which are respectively related to the air entry pressure value and the width of the pore size distribution. K_s is the saturated hydraulic conductivity and n_a is the saturation exponent of the law of Archie (1942). In scenario 1, coupled hydrogeophysical inversion of streaming potential data is performed to estimate α, n and K_s while in scenario 2 n_a is additionally estimated.

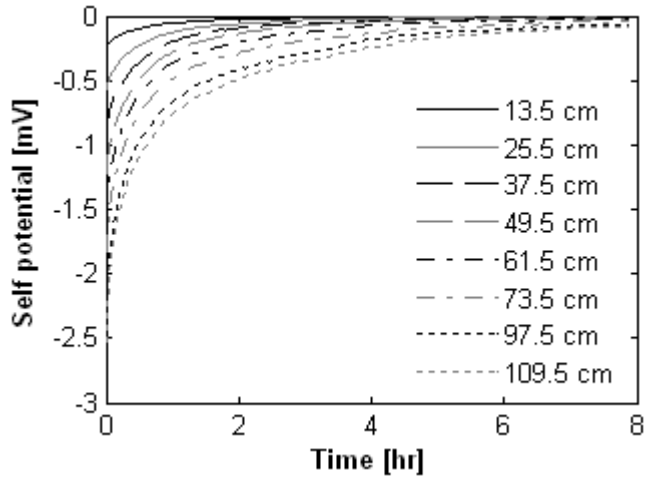

Figure 3.9: Pre-processed SP signals during drainage. The signals were shifted to zero voltage at the end of the experiment while ensuring that signals at the beginning of drainage correspond to values directly determined based on the voltage coupling coefficient at saturation.

The measured voltage coupling coefficient $C(S_w)$ between successive electrode pairs as a function of average saturation, S_w, between the pairs is shown in Figure 3.12a. The average saturation S_w was calculated from pressure head using the hydraulic parameters obtained from the inversion of tensiometric data. The calculated saturation varies between 0.325 and 1. In similar drainage experiments with sand (e.g., Revil et al., 2007; Allègre et al., 2010), this range was also observed as the saturation limits within which significant voltage coupling coefficients were measured. From this range, 13 bins with a step of 0.05 were constructed to obtain a plot of the average absolute voltage coupling coefficient as a function of average water saturation (Figure 3.12b). It can be observed that the absolute $C(S_w)$ decreases non-linearly with a decrease in saturation. Contrary to the observations of Allègre et al. (2010), our data does not show an increase in absolute $C(S_w)$ with decrease in saturation between 1 and 0.7. Our data are also inconsistent with the models of Darnet and Marquis (2004) and Revil et al. (1999) because these model predict an increase of absolute $C(S_w)$ in response to a decrease in saturation. Therefore, these models are not considered in detail in the following.

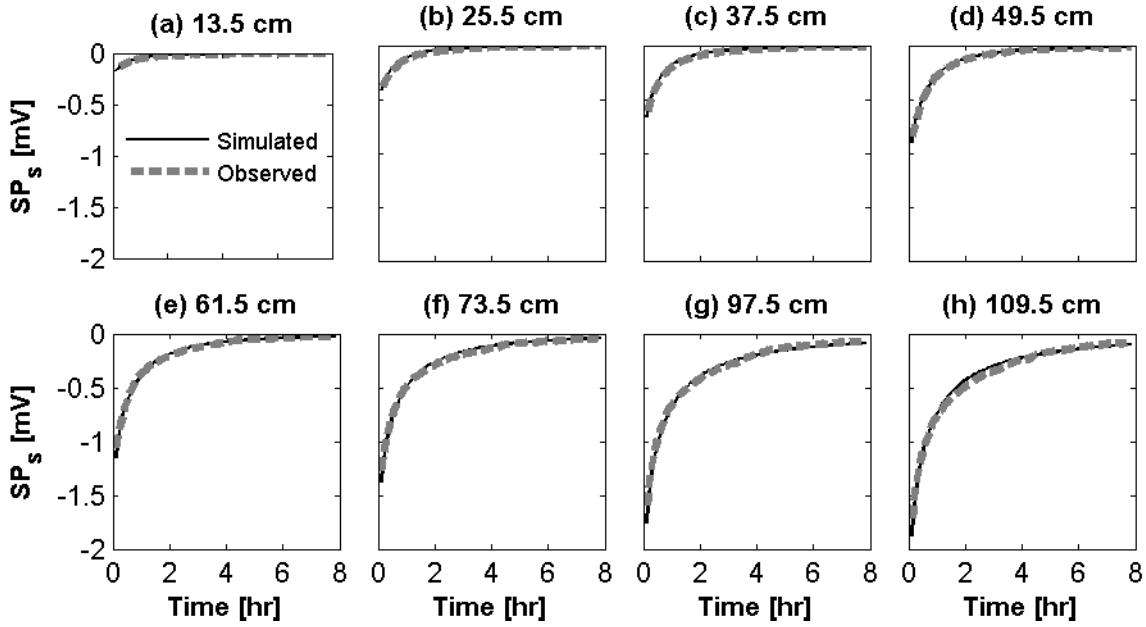

Figure 3.10: Simulated and observed streaming potentials (SP_s) at distances relative to the bottom of the column during drainage.

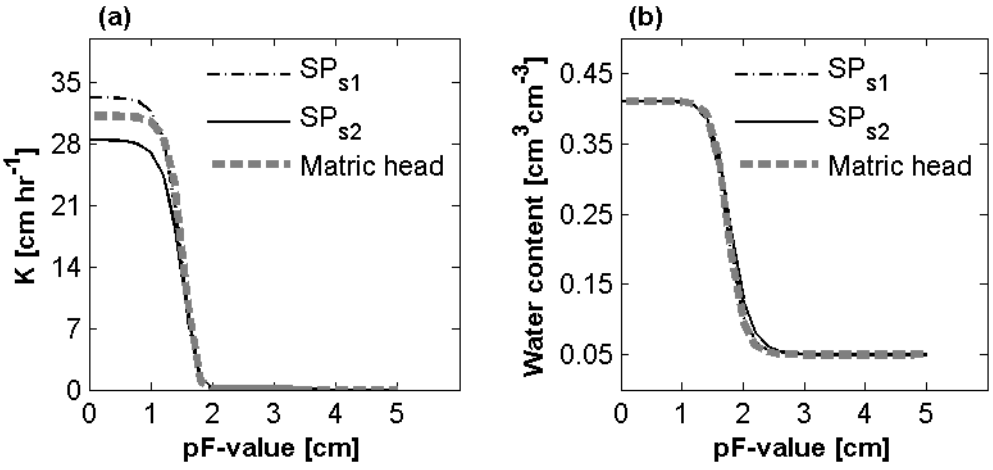

Figure 3.11: Comparison of (a) hydraulic conductivity and (b) water retention functions from the streaming potential inversion scenarios 1 and 2 (SP_{s1} and SP_{s2}) with those predicted from the inversion of matric head

Figure 12b compares the models of Guichet et al. (2003), Perrier and Morat (2000) and Linde et al. (2007) with the binned absolute $C(S_w)$. For the comparison of these models, we used the measured Archie's saturation exponent (n_a = 1.87) and prescribed the relative permeability k_r based on the hydraulic parameters obtained from the independent inversion of tensiometric data. The model of Guichet et al. (2003) deviates most from the measured absolute $C(S_w)$. Clearly, a simple linear decrease with decreasing saturation does not capture the non-linear behavior observed in our data. The model of Linde et al. (2007) fits the absolute $C(S_w)$ data well. The model of Perrier and Morat (2000) captures the shape of the measured curve but underestimates absolute $C(S_w)$. In conclusion, the results presented in Figure 3.12 inspire confidence in the approach of Linde et al. (2007) and Revil et al. (2007).

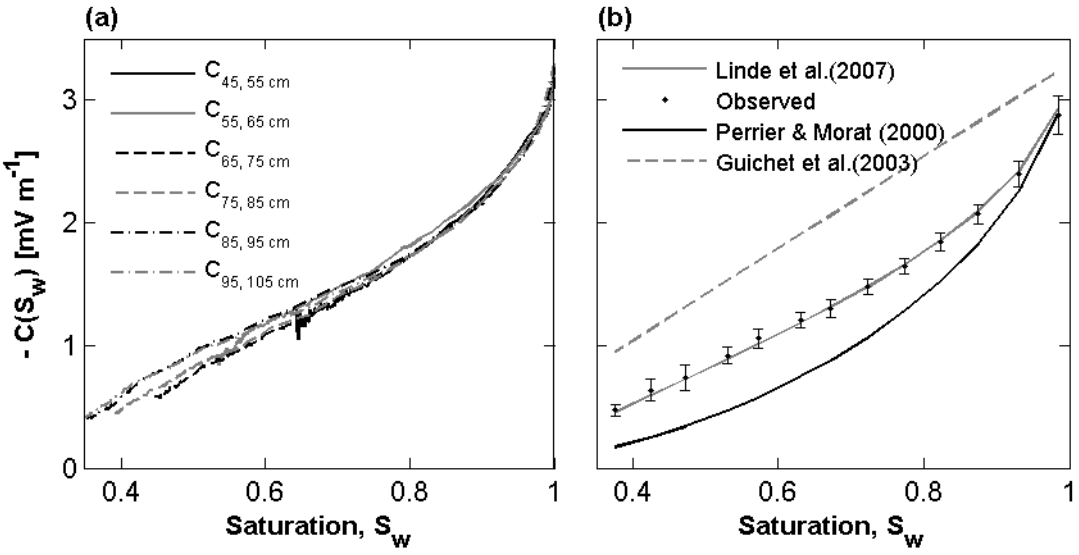

Figure 3.12: a) Variation of measured voltage coupling coefficient $C(S_e)$ with saturation. b) The models of Perrier and Morat (2000), Guichet et al. (2003) and Linde et al. (2007) are also presented. Hydraulic properties were obtained from the inversion of tensiometric data.

3.6. Conclusions

The primary objective of this study was to investigate the feasibility of estimating subsurface hydraulic and petrophysical properties from streaming potential signals (SP_s) obtained under variably saturated flow conditions using a coupled hydrogeophyical inversion approach while a secondary aim was to compare different models describing the voltage coupling coefficient under partially saturated conditions. In order to so, a laboratory experiment was performed in which falling head infiltration and drainage of an initially saturated sandy soil column was monitored with a vertical alignment of non-polarizable Ag/AgCl electrodes and tensiometers. As a first step, we numerically investigated the possibility of using this experimental set-up to estimate three Mualem-van Genuchten (MVG) parameters (α, n and K_s) and the Archie's saturation exponent n_a from time-lapse SP_s signals. It was concluded from these synthetic experiments that SP_s signals obtained under

drainage contained enough information to uniquely constrain the inversion for n, K_s, and n_a for the assumed experimental conditions. The synthetic data also enabled a reasonably good estimate of α.

In a next step, the actual time-lapse SP_s measurements were analyzed. Coupled hydrogeophysical inversion of SP_s signals obtained during drainage provided estimates of α, n and K_s that are similar to those obtained from the inversion of the tensiometer data. In addition, the fitted Archie's saturation exponent, n_a, was also close to the independently measured value. It was therefore concluded that coupled hydrogeophysical inversion of SP_s signals obtained under variably saturated flow conditions allows estimation of unsaturated hydraulic parameters. The success of this procedure relies on efficient pre-processing of the observed SP data prior to inversion. This is because the observed SP signals contain contributions like time varying electrode potentials and drift which are not of electrokinetic origin.

Recent developments now make it possible to use vertically aligned SP electrodes in boreholes (Pezard et al., 2009). This implies that variably saturated flow can be monitored in the field for the estimation of subsurface hydraulic properties from streaming potential signals. As outlined by Linde et al. (2011), this is, however, not trivial because of the superposition of a range of SP sources and the fact that electrode responses vary with temperature and electrochemical conditions in the vicinity of the electrode. In addition, non-linear drifts terms that are related to electrode design and age complicate field SP measurements and often hinder quantitative interpretations of field SP data. Notwithstanding these challenges, our results show that coupled hydrogeophysical inversion of SP_s signals under variably saturated flow conditions is a promising tool for cost-effective hydraulic characterization of the vadose zone.

From measurements of the voltage coupling coefficients at partial saturation, it was concluded that the absolute voltage coupling coefficient non-linearly and monotonously decreases with saturation. There was good agreement between measured and modeled voltage coupling coefficients using the approach of Linde et al. (2007). In contrast, the models of Darnet and Marquis (2004), Revil et al. (1999), Guichet et al. (2003), and Perrier and Morat (2000) did not adequately describe the observed variation of voltage coupling coefficient with saturation. In the ongoing debate on the modeling of streaming potentials in unsaturated porous media, it was concluded that the approach and model of Linde et al. (2007) performed best for our experimental data.

4. Feasibility of sequential and coupled inversion of TDR data to infer soil hydraulic parameters under falling head infiltration [3]

Abstract

Accurate estimation of soil hydraulic properties is a prerequisite for efficient soil and water management. On a small scale, time domain reflectometry (TDR) measurements obtained during an infiltration event can be used for estimating soil hydraulic properties either using a sequential or a coupled inversion approach. In the traditional sequential approach, the TDR measurements are inverted into water content averages based on travel time analysis and subsequently used for calibrating a hydrologic model. Travel time analysis has been reported to be subjective and difficult to use for analyzing TDR measurements obtained during infiltration. In this paper, we extend the sequential inversion approach by using water content profiles obtained via inverse modeling of TDR measurements and introduce a coupled inversion approach which directly uses the TDR measurements for constraining the inversion for hydraulic properties without first inverting them into water content profiles or averages. By comparing the feasibility of these approaches to infer three Mualem-van-Genuchten hydraulic parameters (α, n, K_s) from TDR measurements obtained under falling head infiltration, we concluded that the coupled approach is more practical and less uncertain than the sequential approach. In particular, the coupled inversion approach allows to simultaneously monitor ponding depth and water infiltration, which avoids the laborious task of manually measuring the ponding depths and can thus enable rapid estimation of the soil hydraulic parameters for multiple locations through automatic measurements of ponded infiltration for multiple rings through TDR multiplexing.

[3] Adapted from: Mboh, C. M., J.A. Huisman and H. Vereecken. 2011. Feasibility of sequential and coupled inversion of TDR data to infer soil hydraulic parameters under falling head infiltration. Soil Science Society of America Journal 75:775-786.

4.1. Introduction

Time Domain Reflectometry (TDR) has become a standard method for soil water content determination. This is because TDR can be used to accurately measure soil permittivity, which is strongly related to soil water content (Topp et al., 1980). In the last two decades there have been significant advances in the use of TDR to infer soil water content. These advances have gone from the acquisition of an average water content based on the permittivity estimated from TDR travel time (e.g. Topp et al., 1980) to spatially resolved water content profiles along the TDR probe based on modeling of TDR wave propagation (e.g. Heimovaara et al., 2004; Leidenberger et al., 2006; Greco, 2006; Bänninger et al., 2008; Bänninger et al., 2009).

An interesting application of TDR is to use the temporal development of soil water content to determine soil hydraulic properties. This temporal development of soil water content can be monitored either by vertically or horizontally installed TDR probes. Wang et al. (1998) used horizontally installed TDR probes to measure soil water contents under a tension infiltrometer and estimated the saturated hydraulic conductivity (K_s) and an empirical parameter used in the Gardner's exponential hydraulic conductivity function. As the probes were buried, this approach is intrusive and is therefore not applicable to situations where undisturbed soil conditions are required. As a consequence of this shortcoming, several studies have used vertically installed TDR probes to measure soil water content during infiltration experiments to infer soil hydraulic parameters. For instance, Parkin et al. (1995) used time-lapse water contents measured with TDR probes installed vertically beneath a constant-rate rainfall simulator to derive the cumulative infiltration and estimates of K_s and the inverse capillary length scale for a coarse-textured soil. Zhang et al. (2000) obtained estimates of K_s, the inverse capillary length scale and the saturated water content (θ_s) of a sandy soil from pressure heads and water content measurements measured by multi-purpose TDR probes vertically installed below a surface line source with a constant flux of water. Although multi-purpose TDR probes offer the possibility to obtain supplementary information like pressure head, they are not yet common and readily commercially available like the ordinary TDR probes. Schwartz and Evett (2002) combined TDR-measured soil water contents and cumulative infiltration under a tension disc infiltrometer to investigate the identifiability of the n, α and K_s parameter of the Mualem-van Genuchten hydraulic model (Mualem, 1976; van Genuchten, 1980) for a fine-textured field soil. Three parameter fits to field data yielded a non-unique solution due to a positive correlation between α and K_s. By fixing α to a value determined by fitting to laboratory water retention data, they obtained plausibly good estimates of n and K_s. However, the optimized water contents for early times were significantly larger than those measured with TDR.

The previous studies have typically relied on the average water content obtained via travel time analysis along a vertically installed TDR probe during an infiltration event. The interpretation of TDR measurements thus obtained requires considerable experience using classical travel time-based interpretation methods as the wetting front may manifest itself as an intermediate reflection on the TDR wave trace which may be difficult to differentiate from the reflection at the end of the probe (Topp et al., 1982; Parkin et al., 1995). Inverse modeling of TDR measurements now allows the determination of the soil water content variation along the wires of the probe, which eases the interpretation of TDR measurements made during infiltration and potentially results in additional information to estimate soil hydraulic properties.

Greco and Guida (2008) used inverse modeling of TDR measurements to monitor the temporal development of soil water content with depth during infiltration. However, the inversion of TDR waveforms to obtain soil water content profiles typically requires some kind of regularization of the

inverse problem. For example, Oswald et al. (2003) added an additional term to the objective function that penalized large fluctuations in the second derivative of the inverted permittivity and conductivity profiles. Greco (2006) proposed to describe the soil water content profile using a parametric function with a limited number of fitting parameters to obtain a well-posed inverse problem. This approach was used by Greco and Guida (2008) to interpret their TDR data. The soil water content profiles obtained by inversion of TDR measurements acquired during a hydrological process can be used in a second inversion of the hydrological model describing the process to obtain soil hydraulic properties. The disadvantage of such a sequential inversion approach is that all errors of the TDR inversion will propagate into the estimation of the hydraulic parameters in the second inversion step. In addition, this sequential inversion approach does not accommodate important hydrological information that might be available in the case of time-lapse monitoring of infiltration events (e.g. the total volume of water entering the soil).

Recently, coupled inversion approaches have been proposed for the interpretation of time-lapse geophysical data (e.g. Kowalsky et al., 2004; Hinnell et al., 2010; Huisman et al., 2010). In a coupled inversion approach, a hydrological model is coupled to a forward geophysical model and the geophysical data are directly inverted for hydraulic parameters. This has the advantage that hydrological information can be considered in the inversion of the geophysical data, amongst several other advantages discussed in Hinnell et al. (2010). To the best of our knowledge, a coupled inversion approach has not yet been used to estimate soil hydraulic properties from the TDR measurements.

The aim of this paper is to explore the possibility to estimate soil hydraulic properties from a single ring falling head infiltration experiment monitored with a single vertically installed TDR probe using inverse modeling. Three TDR-based inversion strategies are considered. In the first approach, the average water content along the TDR probe is used to determine cumulative infiltration and these data are then used to inversely estimate hydraulic parameters (i.e a sequential approach similar to Parkin et al., 1995). In the second approach, inverse modeling of the TDR data is used to determine the soil water content variation along the wire of the probe and this information is then used to inversely estimate the hydraulic parameters (i.e. a sequential inversion strategy). In the third approach, a variably saturated flow model is coupled to a TDR forward model and the hydraulic parameters are inversely estimated by minimizing the difference between measured and modeled TDR data (i.e. a coupled inversion strategy). To benchmark the inversion results, the optimized parameters are compared to those resulting from the cumulative infiltration determined from the ponding depth and from a multi-step outflow (MSO) experiment carried out with the same material and similar bulk density.

4.2. Materials and Methods

4.2.1 TDR wave propagation model

We use the TDR wave propagation model of Heimovaara et al. (2004) to simulate TDR measurements for a given complex permittivity profile along a TDR probe. In this model, the measured TDR data in the time domain, $r(t)$, is a convolution of an input signal, $v_0(t)$, generated by a cable tester and a system function, $s(t)$, that describes how the probe-soil system transforms the input signal (Heimovaara, 1994; Van Gemert, 1973):

$$r(t) = \int_{-\infty}^{\infty} v_0(t-\tau)s(t)d\tau \qquad (4.1)$$

where τ is an integration variable. Based on the convolution theorem, the frequency domain response R(*f*) is defined as:

$$R(f) = V_0(f)S(f) \tag{4.2}$$

in which *f* is the frequency (Hz) and *R*(*f*), $V_0(f)$ and *S*(*f*) are the Fourier transforms of *r*(*t*), v_0(t) and *s*(*t*), respectively. Procedures to transform the data from the time domain to the frequency domain are discussed in detail in Huisman et al. (2004). The input signal, $v_0(t)$, was described by the analytical function of Heimovaara et al. (2004):

$$v_0(t) = \frac{1 + erf\left[\psi(t - t_0)\right]}{2} \tag{4.3}$$

where *erf* is the error function, *t* is the time, t_0 is time at which the input signal starts to rise and ψ is a parameter which signifies the inverse of the rise time (i.e. the time it takes for the input signal to reach a stable input voltage). Heimovaara et al. (2004) outlines the advantages of using such an analytical function.

The Fourier-transformed system function, *S*(*f*) ,was described by the theoretical S_{11} multi-section scatter function (MSSF) (Heimovaara, 1994; Feng et al.,1999; Lin, 2003) of an open ended coaxial probe as:

$$S_{11}^{j}(f) = \frac{\rho^{j}(f) + S_{11}^{j-1}(f)\exp\left[-2\gamma_j(f)L_j\right]}{1 + \rho^{j}(f)S_{11}^{j-1}(f)\exp\left[-2\gamma_j(f)L_j\right]} \tag{4.4}$$

in which

$$\rho^{j}(f) = \frac{Z_{j-1}(f) - Z_j(f)}{Z_{j-1}(f) + Z_j(f)} \tag{4.5}$$

$$\gamma_j(f) = \frac{i2\pi f\left[\varepsilon^{j}(f)\right]^{1/2}}{c} \tag{4.6}$$

$$Z_j(f) = \frac{Z_0^{j}}{\sqrt{\varepsilon^{j}(f)}} \tag{4.7}$$

where $\rho^{j}(f)$ is the reflection coefficient of the j^{th} section with propagation coefficient, $\gamma_j(f)$, impedance $Z_j(f)$ and length, L_j. $Z_0{}^{j}$ is the characteristic impedance of the transmission line section in air, and $i = \sqrt{-1}$. The final section of the multisection scatter function describes TDR wave propagation in the coaxial cable connecting the cable tester to the TDR probe. For this section, we use the model extension of Lin and Tang (2007) in which

$$\gamma(f) = \frac{i2\pi f\left[\varepsilon(f)\right]^{1/2}}{c} A \tag{4.8}$$

$$Z(f) = \frac{Z_0}{\sqrt{\varepsilon(f)}} A \tag{4.9}$$

$$A = \sqrt{1 + (1 - i)\frac{\alpha_r}{\sqrt{f}}} \tag{4.10}$$

where α_r is the resistance loss factor ($s^{-0.5}$) that describes the combined effect of geometric factors and surface resistivity (Lin and Tang, 2007).

Assuming that all the materials in the transmission line do not show a relaxation in the TDR frequency range, the complex dielectric permittivity is described by:

$$\varepsilon^j(f) = \varepsilon_a + \frac{i\sigma_{dc}}{2\pi f \varepsilon_0} \tag{4.11}$$

in which ε_a[-] is the apparent dielectric permittivity of layer *j*, σ_{dc} (Sm^{-1}) is the bulk electrical conductivity at dc voltage (assumed to be equal to the TDR bulk conductivity), ε_0 the dielectric permittivity of free space (8.544 x 10^{-12} Fm^{-1}), and i = √-1. For most soils, this is a reasonable assumption (e.g. Campbell, 1992; Weerts et al., 2001).

Bänninger et al. (2009) proposed to relate the permittivity and the bulk electrical conductivity for each model section in the soil using a scaling approach:

$$\sigma_{r,j} = \theta_{Topp,j}^{c} \tag{4.12}$$

$$\sigma_j = \frac{\sigma_{dc}}{\sum_{j=1}^{Ns} \frac{\sigma_{r,j} L_{s,j}}{L_s}} \sigma_{r,j} \tag{4.13}$$

where σ_j is the electrical conductivity of the j^{th} slice of the soil ($L_{s,j}$) with relative electrical conductivity, $\sigma_{r,j}$, and *Ns* is the number layers used to discretize the soil of total depth L_s. $\sigma_{r,j}$ is estimated from the water content of the slice, $\theta_{Topp,j}$ and c, the saturation exponent of Archie's law (Archie,1942). For sandy soils, the saturation exponent is close to 2 (Friedman, 2005; Bänninger et al., 2009). The soil water content, $\theta_{Topp,j}$, of each slice is estimated from the permittivity using the equation of Topp et al. (1980). When using this scaling approach, it is assumed that the porosity of the soil profile and the pore water conductivity are constant along the TDR probe (Bänninger et al., 2009).

4.2.2. Calibration of the TDR system for inverse modeling

The TDR measurements in this study were made using the TDR100 cable tester (Campbell Scientific, USA) connected to a custom-made 19-cm long three-rod TDR probe with a cable of about 2.6 m. The use of inverse modeling of TDR waveforms requires the calibration of a number of model parameters in the wave propagation model described in Eqs. (4.3-4.10). As detailed in Heimovaara (1994), it is important to use a sufficiently long sampling window when acquiring TDR waveforms for inverse modeling. In this study, all measurements with the TDR100 used a sampling window starting at -2 m and ending at 25 m. In a first calibration step, the two parameters of the analytical input function (ψ and t_0 in Eq.4. 3) were determined using a TDR measurement of the initial step in the cable tester (see Heimovaara et al., 2004 for more details). This resulted in ψ = 6.61 ns^{-1} and t_0 = 0.058 ns. In a second calibration step, unknown cable and probe parameters were determined by minimizing the difference between measured and modeled TDR waveforms in two media with

known dielectric properties (air and water with known temperature and electrical conductivity). In total, seven model parameters were calibrated and these are listed in Table 4.1. The calibrated lengths of the cable, probe head and probe sections are close to the estimated physical lengths and the calibrated impedance in air (Z) for the probe is close to the value expected from the probe dimensions (Ball et al., 2002; Huisman et al., 2008).

Table 4.1: Calibrated parameters of the TDR wave propagation model

Parameter	Calibrated Value
Cable	
L [m]	2.616
α [$s^{-0.5}$]	29.165
Probe Head	
L [m]	0.030
Z [Ω]	154.687
ε_a [-]	2.764
Probe	
L [m]	0.191
Z [Ω]	184.216

4.2.3. Falling head infiltration experiment

A cylindrical laboratory column with a height of 35 cm and an internal diameter of 20 cm was tightly packed to a depth of 20 cm with artificial quartz substrate (Millisil W3, from Quartzwerke Frechen GmbH, Germany). The initial water content was about 0.03 $cm^3\ cm^{-3}$ and the bulk density was 1.54 g cm^{-3}. According to the manufacturer, the material contains 62 % sand, 35 % silt and 3 % clay (i.e. a sandy loam according to the USDA textural classification). A porous nylon cloth was placed at the bottom of the column to support the soil and to allow for seepage if required. The TDR probe was inserted to a depth of 15 cm at the center of the packed column. At the start of the experiment, 4 cm of tap water was ponded on the soil surface and the infiltration was monitored with TDR. TDR measurements were taken at 2 minute intervals until the ponded water was completely infiltrated. The depth of the ponded water at each TDR acquisition time was also measured with a graduated ruler.

4.2.4. Hydrological modeling

The HYDRUS1D model (Simunek et al., 2008) was used to simulate falling head infiltration into an initially dry material subject to an atmospheric upper boundary condition with an initial water layer of 4 cm. A seepage face was used as the bottom boundary condition of the model. This is a mixed boundary condition typically used for lysimeters where a no-flow boundary is assumed when the pressure head in the lower part of the soil column is below 0 and a fixed pressure head of 0 is assumed when the pressure head in the lower part of the soil column exceeds 0. The HYDRUS1D model numerically solves the 1-dimensional Richards' equation for variably saturated flow in rigid porous media:

$$\frac{\partial \theta(h)}{\partial t} = \frac{\partial}{\partial x}\left[K(h)\left(\frac{\partial h}{\partial t} + 1\right)\right] \tag{4.14}$$

where x is elevation, t is time, $\theta(h)$ is the water retention function, θ is the volumetric water content, h is the pressure head, and $K(h)$ is the hydraulic conductivity function. The 20 cm long soil column was discretized into 200 elements with a thickness of 0.1 cm. It is assumed that the retention and conductivity functions that describe the hydraulic properties of the material can be represented by the classical Mualem-Van Genuchten model (MVG) (Mualem, 1976; van Genuchten, 1980):

$$\theta(h) = \theta_r + (\theta_s - \theta_r)\left[1 + |\alpha h|^n\right]^{-m} \tag{4.15}$$

$$K(h) = K_s\left(\frac{\theta - \theta_r}{\theta_s - \theta_r}\right)^l \left[1 - \left(1 - \left(\frac{\theta - \theta_r}{\theta_s - \theta_r}\right)^{\frac{1}{m}}\right)^m\right]^2 \tag{4.16}$$

where θ_r and θ_s are respectively the residual and saturated water content, α and n are empirical parameters which are respectively related to the air entry pressure value and the width of the pore size distribution, m is restricted by the Mualem condition $m = 1 - 1/n$ with $n > 1$, K_s is the saturated hydraulic conductivity, and l is a factor that accounts for pore tortuosity. A total of six MVG parameters (θ_r, θ_s, α, n, K_s and l) are therefore necessary to describe the soil hydraulic properties. Due to its relatively small effect on hydrodynamic events, the parameter l is commonly fixed to its average value of 0.5. Defined as the water content of a sample under an infinitely large suction, θ_r is often regarded as empirical and is sometimes fixed to a value of zero (Nimmo, 1991; Fuentes et al., 1992). Under very dry field conditions, TDR-inferred average soil water content can be a practical estimate of θ_r. Similarly under saturated field conditions, θ_s can easily be measured with TDR. In this paper, θ_r and θ_s are fixed to the initial dry soil TDR-inferred water content (0.03 $m^3\ m^{-3}$), and the maximum TDR-measured water content at the topmost layer of the soil column (0.326 $m^3\ m^{-3}$). Using these assumptions, there are three MVG parameters (α, n, K_s) that remain to be estimated by inverse modeling.

4.2.5 General approach for inversion of data to obtain soil hydraulic properties

The parameter vector p is estimated by minimizing an objective function (OF) expressed as the root mean square error between N time-lapse observations $D(t)$ and model predictions $D^*(t, p)$:

$$OF(p) = \sqrt{\sum_{i=1}^{N} \left(D_i(t) - D^*_i(t, p)\right)^2 / N} \tag{4.17}$$

The parameters are perturbed within reasonably wide bounds (see Table 4.2) and the predictions are compared to observations until a close fit is found. As the objective function is very non-linear and may be characterized by many local minima, the misfit between predictions and observations is minimized using the Shuffled Complex Evolution optimization algorithm (SCE-UA) which is a global optimizer (Duan et al., 1993). According to Duan et al. (1993), the SCE-UA is a genetic optimizer which combines probabilistic and deterministic approaches with clustering and systematic evolution to randomly sample and evolve a population of parameter combinations to a global optimum. In this paper, the SCE-UA was set to convergence criteria by which an optimum was assumed to be reached when in 10 successive evolution loops the objective function did not improve by more than 0.01%. The confidence intervals of the inverted model parameters were determined by a first-order approximation (e.g. Kool and Parker, 1988; Vrugt and Bouten, 2002).

Table 4.2: Inversion bounds for hydraulic parameters

Parameter	Minimum value	Maximum value
α [cm^{-1}]	0.004	0.124
n [-]	1.2	2.8
K_s [cm h^{-1}]	0.095	31.63

4.2.6 Data inversion approaches to estimate hydraulic parameters

i) Inversion using inflow data determined from ponding depth

In the first approach, we use manually measured ponding depths to infer soil hydraulic parameters from falling head infiltration. A falling head infiltration model for the experimental conditions discussed in section 4.2.3 was set up in HYDRUS 1D. Using the SCE-UA algorithm, the hydraulic parameters in the infiltration model were perturbed within reasonably wide bounds (Table 4.2), generating predictions of inflow. These predictions were compared with the corresponding inflow measurements until a close fit was found.

ii) Sequential inversion using average water content (inflow) or soil water content profiles determined by inverse modeling of TDR

In the second and third inversion approach, a sequential inversion strategy consisting of two optimization step was used. In the first step, the TDR measurements are inverted to obtain average water content or water content profiles based on the TDR wave propagation theory discussed previously. In a second step, these data are then compared with predictions from the hydrological model to inversely estimate the hydraulic parameters. To determine water content profiles from TDR measurements, the length of the TDR probe inserted in the soil is discretized in 15 layers of 0.01 m. To account for the water layer ponding on the surface, the part of the TDR probe not inserted into the soil (0.04 m) was discretized in two layers: one representing air and one representing water as illustrated in Figure 4.1 for a water layer of 0.02 m.

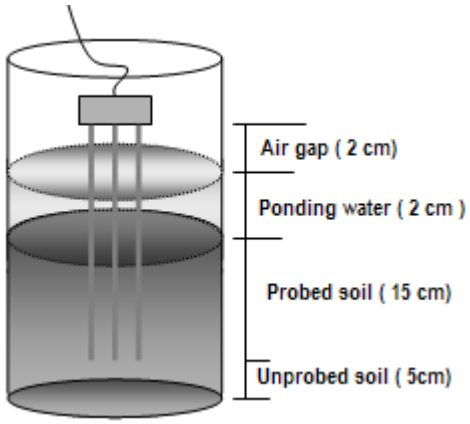

Figure 4.1: Soil column illustrating air gap and ponding water (Figure not to scale).

After specifying the measured depth of ponded water, the electrical conductivity of the water layer, and the water temperature, the water content of each of the 15 layers and the mean bulk electrical conductivity were inversely estimated by minimizing the difference between measured and modeled TDR waveforms using the SCE-UA algorithm. The permittivity of each of the 15 layers was obtained by calculating the permittivity from the soil water content using the equation of Topp et al. (1980). The bulk electrical conductivity of each layer was estimated using the scaling approach

outlined in Eqs. (4.12-4.13). Preliminary investigations showed that highly erratic water content profiles were obtained when the water content of each layer was inverted independently. Following Oswald et al. (2003), we therefore applied regularization to obtain smoother water content profiles. For this, an additional term was added to the objective function OF:

$$OF = OF_1 + \lambda OF_2 \tag{4.18}$$

where OF_1 is a measure of the quality of the fit, which is quantified by the sum of squared residuals between measured and modeled TDR waveforms, OF_2 is a measure of the smoothness of the fitted solution, which is quantified by the sum of the absolute values of the first derivative of the fitted water content profile with respect to depth and λ is a weighting factor. If a high value is selected for λ, the minimization of OF will lead to an overly smooth solution because of the emphasis on OF_2, whereas a low value for λ will lead to the same erratic solution as in the case of no regularization. By systematically varying λ for a number of independent TDR measurements, it was determined that $\lambda = 0.05$ resulted in an adequate compromise solution that provided a good fit to the TDR waveforms using a reasonably smooth water content profile.

A second sequential inversion approach considered here uses the cumulative infiltration determined from the average water content measured by TDR. As argued before, traditional tangent line analysis to determine the average dielectric permittivity is not straightforward for TDR measurements made during infiltration (Parkin et al., 1995). In our case, analysis is even more complicated because of the air gap and ponding depth near the head of the probe (see Figure 4.1). Huisman et al. (2002) showed that TDR waveforms can be analyzed using an inverse modeling approach with a one-layer model. Their inverse modeling results were almost identical to the water content averages determined using direct travel time analysis. In this study, the average water content of the soil in the vicinity of the TDR probe is determined by averaging the water content profiles obtained as described above.

iii) Coupled inversion of TDR measurements

In coupled inversion, the hydraulic parameters are directly estimated from the TDR measurements without first inverting them into water content averages or profiles (e.g. Looms et al., 2008; Hinnell et al., 2010; Huisman et al., 2010). This is achieved by coupling the multi-section scatter function (Eq. 4.4) to the hydrological model (HYDRUS1D). By perturbing the hydraulic parameters using the SCE-UA algorithm, water content profiles are simulated in the hydrological model and converted to permittivity profiles using the equation of Topp et al. (1980). The simulated permittivity profiles are used to simulate TDR measurements which are then compared to the measured TDR data until a close fit is found. Unlike the sequential approach where the ponding depth has to be prescribed during the inversion of TDR data to water content averages or profiles, in the coupled approach, the ponding depths are obtained from the hydrological model during the inversion for soil hydraulic parameters. In this way hydrological information (ponding depths) is directly used to constrain the inversion for soil hydraulic properties without any need for measuring the ponding depths.

iv) Multi-step outflow experiment

A multi-step outflow (MSO) experiment was conducted to determine an independent set of estimates for the hydraulic parameters. A plexiglass cylinder with a height of 6.8 cm and an internal diameter of 9.4 cm equipped with a tensiometer at 4.4 cm above the lower boundary was used in the MSO experiment. This column was packed with the Millisil W3 material to a similar bulk density as used in the falling head infiltration experiment previously described. The sample was saturated to a water content of about 0.326 cm^3cm^{-3} with degassed tap water and placed on a hanging water column. Six suction increments were applied over 15 hours while outflow and matric head readings were recorded at 30 second intervals using pressure transducers. These data were later on filtered and used

for the estimation of the parameter vector p (α, n, K_s) by inverse modeling using HYDRUS1D and the SCE-UA optimization algorithm. The filtering was such that the number of measurements during a pressure step was proportional to the length of the pressure step and the frequency of measurements was inversely proportional to the square root of time. This resulted in a measurement scheme that emphasized those parts of the flow process where flux rates and hence information content was highest. In addition to inverse modeling, the K_s value was also determined directly using the constant head method as described by Klute and Dirksen (1986).

4.2.7. Numerical experiments

Prior to the actual experiments, the feasibility of obtaining plausible estimates of α, n and K_s from TDR measurements made during falling head infiltration was numerically investigated for an initially dry sandy loam (θ_s = 0.41 cm^3 cm^{-3}, θ_r = 0.034 cm^3 cm^{-3}, α = 0.036 cm^{-1}, n = 1.56, K_s = 1.04 cm h^{-1} and l = 0.5). The numerical experiments were performed for two types of initial conditions. In the first case, a uniform initial water content equal to the residual water content was assumed. In the second case, a uniform initial matric potential of -10^5 cm (pF = 5) was assumed to be representative for air dried sandy loam. Matric potentials of this magnitude have been measured in air-dried sandy loam (e.g. Lu et al., 2007). For each of these initial conditions four inversion variants using different data were considered: i) cumulative infiltration from ponding depth, ii) cumulative infiltration from average water content obtained with TDR, iii) soil water content profiles obtained from TDR through independent inversion, and iv) the actual TDR measurements used in the coupled inversion approach. Falling head infiltration was simulated for the experimental conditions of the actual experiment using HYDRUS1D. Synthetic cumulative infiltration data for pre-defined measurement times was obtained. Similarly, synthetic water content averages and profiles were obtained. The synthetic water content profiles were converted to synthetic TDR data using the TDR wave propagation model described by Eq. 4.4.

For more realistic numerical experiments, noise was added to the synthetically generated measurements. In the case of cumulative infiltration from ponding depth, Gaussian noise with a mean of zero and a standard deviation of 0.05 cm was added to the synthetic cumulative infiltration. This error level is justified considering that real measurements are done with a graduated ruler with units of 0.1 cm. The same error level was assumed for cumulative infiltration determined from average water content determined with TDR. Soil water content measured by TDR is typically affected by an error level of 0.01 to 0.02 cm^3 cm^{-3}. Therefore, Gaussian noise with a mean of zero and a standard deviation of 0.01 cm^3 cm^{-3} was added to the simulated soil water content profile. From an analysis of reflection coefficient at long times measured in demineralized water, Huisman et al. (2004) proposed a standard deviation of 6.5 x 10^{-4} for TDR data. Likewise, Gaussian noise with this standard deviation was added to the synthetic TDR data.

The four data types were then used to compute the objective function (Eq. 17) response surfaces in the α-K_s, α-n and K_s-n parameter planes. In the computations, θ_r, θ_s, l and one of the other three parameters (α, n and K_s) were kept constant at their "true" value while the other two were systematically varied between the bounds shown in Table 4.1. For each parameter, the range was divided in 50 equidistant parts, which means that a single response surface consists of 2601 objective function evaluations.

4.3. Results and Discussion

4.3.1 Numerical Experiment

Figures 4.2 and 4.3 show the objective function response surfaces obtained from the numerical experiment using initial conditions in water content and matric potential respectively. Because the objective function response surfaces obtained using cumulative infiltration based on ponding depth and TDR average water content were the same, only one of them is presented (first column of Figure 2 and 3). The α-K_s response surfaces for all the inversion types show an error landscape in the vicinity of the objective function minimum which is almost perpendicular to the K_s axis at the point where K_s is equal to its true value. This indicates that adequate estimates of K_s are possible with all the data types from a 1D falling head infiltration experiment. This finding is also supported by the response surfaces of the n-K_s parameter plane.

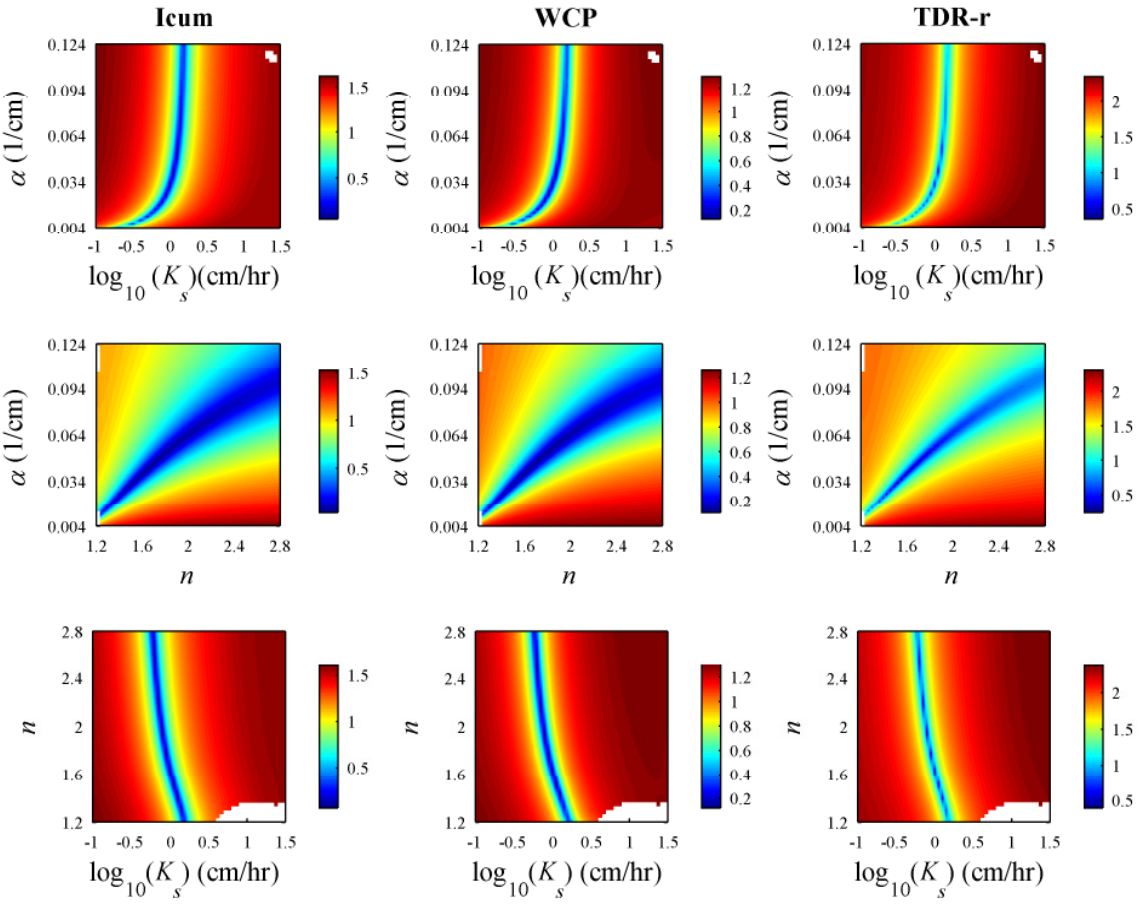

Figure 4.2: Objective function response surfaces with initial condition in water content (0.03 cm^3cm^{-3}). Columns 1, 2 and 3 respectively show the responses surfaces obtained using synthetic cumulative infiltration (Icum), water content profiles (WCP) and TDR reflection coefficients (TDR-r, also called TDR data). The white spaces indicate parameter combinations for which the hydrological model does not converge. Colour scale shows objective function values (normalized by the standard deviation of the measurement error) for various parameter combinations

The plausibility of the parameter estimates for the α and n parameters will mostly depend on the information content of the data used in the different inversion types. As can be seen in Figure 4.2, the α-n error landscape for all inversion types shows an elongated valley and a positive correlation

between α and n when the initial conditions are specified in terms of water content. This implies that the data do not contain sufficient information to simultaneously constrain the inversion for α and n from a 1D falling head infiltration experiment with initial conditions specified in water content. However, when initial conditions are specified in matric potential (Figure 4.3), it is observed that the objective function minimum in the α- n parameter plane is constrained in a smaller space for all the data types. These findings highlight the importance of at least one pressure head measurement when estimating soil hydraulic parameters from a 1D falling head infiltration experiment. The added value of pressure head measurements has also been reported by Simunek and van Genuchten (1996) and Vereecken et al. (2008). Although they are not yet common and readily commercially available, the multi-purpose TDR probe of Baumgartner et al. (1994) which can simultaneously measure matric potential and water content can be used to obtain this information.

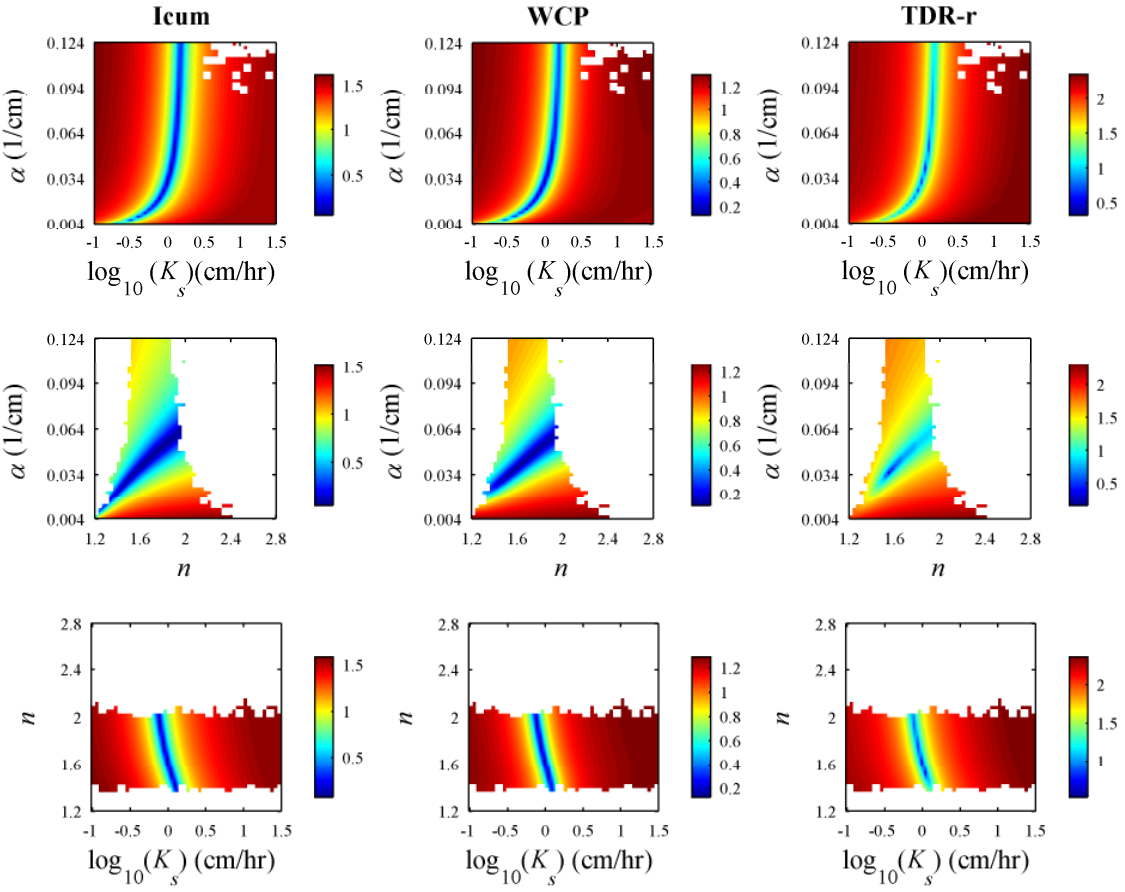

Figure 4.3: Objective function response surfaces with initial condition in water matric head. Columns 1, 2 and 3 respectively show the responses surfaces obtained using synthetic cumulative infiltration (Icum), water content profiles (WCP) and TDR reflection coefficients (TDR-r). The white spaces indicate parameter combinations for which the hydrological model does not converge. Colour scale shows objective function values (normalized by the standard deviation of the measurement error) for various parameter combinations.

It is worth noticing that in the α-n parameter plane for both types of initial conditions (Figure 4.2 and 4.3), the objective function minimum is constrained in a smaller space for the coupled approach than for the two sequential approaches. This indicates that the coupled approach is potentially less uncertain than the sequential approaches. Although the topography of 2D objective function response surfaces provide valuable insights into parameter correlation and sensitivity for designing an efficient

optimization strategy, it should however be noted that the plots cannot demonstrate uniqueness when three parameters are fitted simultaneously.

4.3.2. Laboratory experiments

Figure 4.4 presents the measured outflow and pressure head for the MSO experiment. The model predictions based on the optimized hydraulic parameters provided in Table 4.3 are also shown. Clearly, the fit is excellent. In addition, the optimized K_s value (1.01 cm h^{-1}) from the MSO data compares well with the K_s value directly determined using the constant head method (0.80 cm h^{-1}). In the remainder of this study, the hydraulic parameters obtained from these MSO data are considered as a reference for comparison with the other inversion types under investigation.

The measured cumulative infiltration determined from ponding depth (I-pond) and the average water content measured with TDR (I-TDR-awc) is presented in Figure 4.5. Clearly, there is an excellent agreement between both data types, which indicates that infiltration was reasonably homogeneous and that preferential infiltration along the wires of the TDR probe during ponded infiltration can be excluded. Table 4.3 shows the optimized hydraulic parameters (α, n and K_s) and their 95 % confidence interval in parenthesis in addition to the fixed parameters (θ_r, θ_s and l). The predicted cumulative infiltration corresponding to the model parameters of Table 4.3 is also presented in Figure 4.5. The modeling results correspond to the case in which the initial conditions are specified in water content (0.03 cm^3 cm^{-3}). It can be seen that there is excellent fit between the observations and the predictions based on hydraulic parameters determined from cumulative infiltration data obtained from ponding depth and average water content measured with TDR.

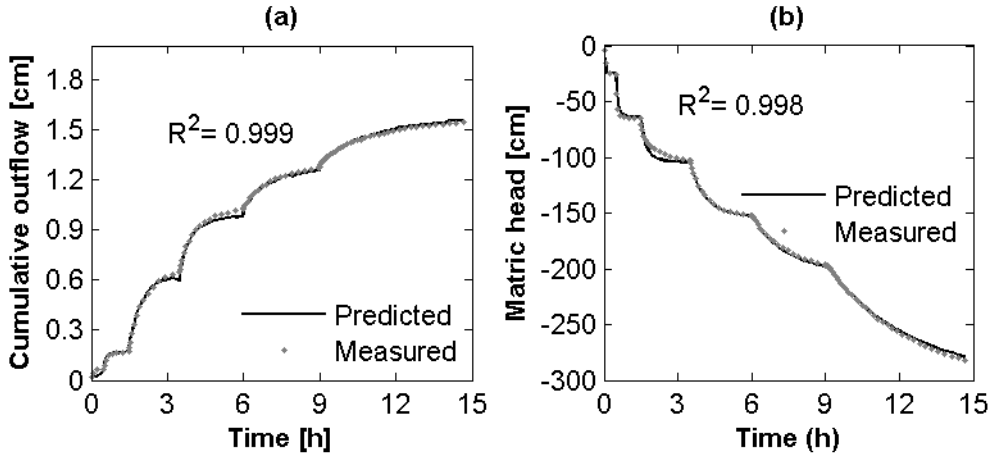

Figure 4.4: Measured versus predicted cumulative outflow (a) and matric heads (b) from the MSO experiments.

Table 4.3: Optimum parameters using the different data types

Data†	Parameters					
	¶ θ_r [cm^3cm^{-3}]	¶ θ_s [cm^3cm^{-3}]	α [cm^{-1}]	n [-]	Ks [$cm\ h^{-1}$]	¶ τ [-]
I-pond	0.030	0.326	0.047 (0.045 - 0.049)	2.693 (2.680 - 2.706)	1.157 (1.137 - 1.177)	0.5
I-TDRawc	0.030	0.326	0.037 (0.035 - 0.039)	2.462 (2.437 - 2.487)	1.028 (1.009 - 1.048)	0.5
TDR-wcp	0.030	0.326	0.025 (0.023 - 0.027)	2.686 (2.616 - 2.756)	0.863 (0.835 - 0.891)	0.5
TDR-r	0.030	0.326	0.043 (0.043 - 0.044)	2.339 (2.338 - 2.340)	1.165 (1.161 - 1.169)	0.5
MSO-d	0.030	0.326	0.009 (0.008 - 0.009)	2.482 (2.393 - 2.570)	1.009 (0.917 - 1.101)	0.5

¶ Fixed during optimization

† I-pond is the cumulative infiltration measured from ponding, I-TDRawc is the cumulative infiltration obtained from TDR-inferred average moisture content, TDR-wcp is the TDR water content profile, TDR-r is TDR reflection coefficients (also called TDR measurements or TDR data), and MSO-d is muti-step outflow data (cumulative outflow and matric head

A selection of the soil water content profiles obtained by inversion of the TDR measurements is shown in Figure 4.6. Despite the use of the regularization approach, it can be seen that the inverted water content profiles show a sharp infiltration front indicating that regularization was not overly strong. However, there is some variability in the top and the bottom of the profile, possibly indicating inversion artifacts during the conversion of the TDR measurements to water content profiles. The water content profiles were used to inversely estimate hydraulic parameters ('sequential approach') and the predicted water content profiles associated with the optimized hydraulic parameters presented in Table 4.3 are also shown in Figure 4.6. At early times, the fit between inverted and predicted water content profiles is good, but at later times (i.e. 54 minutes) the predicted water content profile is steeper than the inverted profile, perhaps indicating that the inverted water content profile is too smooth due to the regularization. Figure 4.5 shows the cumulative infiltration associated with the hydraulic parameters determined from fitting the water content profiles obtained by inversion of the TDR measurements. It can be seen that the predicted cumulative infiltration is too large as compared to the measurements and the other predictions. It is interesting to note that these inverted water content profiles were used to obtain the average water content used to determine cumulative infiltration from TDR, which well matched the measured cumulative infiltration determined from ponding depth, as discussed earlier. Again, this is an indication that the distribution of water content obtained from TDR inversion might be troubled by inversion artifacts introduced by the ill-posedness of the inverse problem and the regularization required to stabilize the solution of the inverse problem.

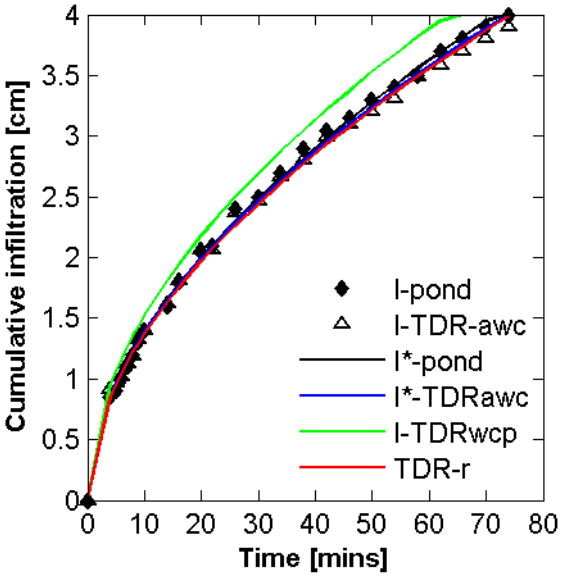

Figure 4.5: Comparison of measured infiltration with the predicted cumulative infiltration using four data types. I-pond is the measured cumulative infiltration from ponding depth and I-TDRawc is the measured cumulative infiltration from TDR average water content while, I*-pond, I*-TDRawc, I*-TDRwcp and I*-TDR-r, are respectively the simulated cumulative infiltrations using the optimized parameters from I-pond, I-TDR-awc, TDR water content profile (TDR-wcp) and TDR reflection coefficients (TDR-r, also called TDR measurements)

To overcome the propagation of inversion artifacts when using a sequential inversion strategy as outlined above, the coupled inversion strategy was proposed. Figure 4.7 shows measured and modeled TDR data for four selected times obtained using the coupled inversion approach. The key features of the measured TDR data are clearly well captured. In particular, it is worthwhile to note the complicated shape of the TDR measurement near the reflection of the end of the probe due to the infiltration front in dry soil for the measurements after 4 and 20 minutes. The modeled TDR data nicely capture the reflections from the infiltration front and the end of the probe (see Figure 4.7a), whereas a traditional travel time analysis would have had great difficulty in correctly interpreting these TDR measurements. The hydraulic parameters obtained by directly fitting the TDR measurements using a coupled inversion approach are presented in Table 3. The calculated confidence intervals for α and n for this approach are narrower than those for the sequential approaches. This confirms the findings of the numerical experiment where the objective function minimum in the α-n parameter plane was constrained in a smaller space for the coupled approach than for the sequential approaches.

Although the measured ponding depths were not an input in the coupled hydrogeophysical inversion procedure because the ponding depth was simulated by the hydrological model, the simulated cumulative infiltration matches very well with the observed infiltration from ponding depth (see Figure 4.5). This indicates that the TDR measurements can be used to simultaneously monitor ponding depth and infiltration when the measurements are interpreted using a coupled inversion approach. This implies that the method has a potential for rapid, accurate and automatic monitoring of falling head infiltration in the field. This is particularly advantageous when estimates of soil hydraulic parameters in relatively larger surface areas are desired. With TDR multiplexing and automatic data logging, several ring infiltrometers can be installed in the field for fast and cost effective estimation of soil hydraulic parameters. Additionally, the ability to remotely monitor

ponding depths using the coupled approach stretches the potential applications of our system to include flood management by earth dams and also flood irrigation management for instance.

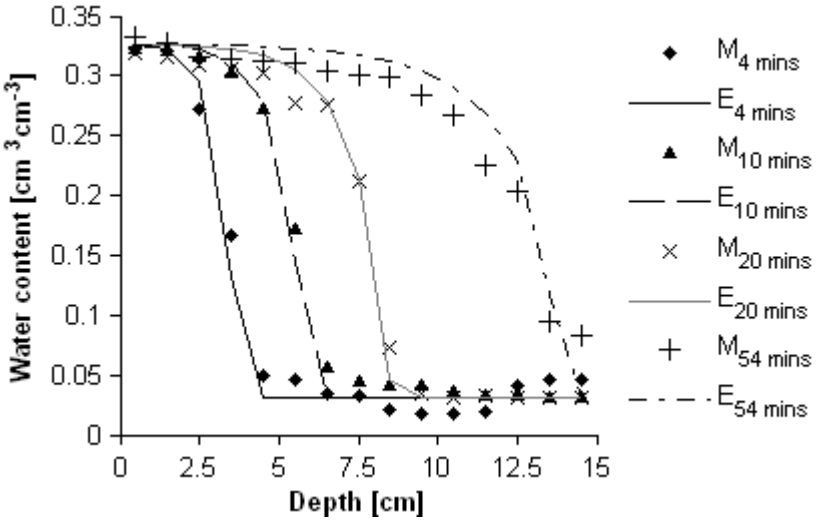

Figure 4.6: Measured versus predicted Water content profiles for four measurement times. M_{4mins}, $M_{10\ mins}$, $M_{20\ mins}$, and $M_{54\ mins}$ are the measured water content profiles at 4, 10, 20 and 54 minutes while $E_{4\ min}$, $E_{10\ mins}$, $E_{20\ mins}$ and $E_{54\ mins}$ are the corresponding simulations from the estimated hydraulic parameters.

From Table 4.3, it can be observed that the K_s values obtained in all four inversions compare well with the MSO data and the constant head method (0.8 cm h^{-1}). This confirms the findings from the numerical experiment which showed that all the data types contain adequate information on K_s. Within the limits of their uncertainties, all four inversion types also have optimal n values that compare well with those obtained from the MSO experiment. The optimal α values from all the four inversion types represent an overestimate compared to those from MSO. This implies that only two of the MVG parameters (K_s and n) can be successfully estimated using the four inversion types in a 1D falling head infiltration experiment. Russo et al. (1991) and Simunek and Van Genuchten (1996) also showed that using cumulative infiltration data alone, only two hydraulic parameters can be estimated by inverse modeling. While it seems reasonable to expect more information in the water content profiles and the full TDR measurements than in cumulative infiltration data alone in the case of a 1D falling head infiltration experiment, the difference in information content is minimal especially when the initial conditions are specified in water content. Using these initial and experimental conditions, all four inversion types produce similar results as can be seen from the hydraulic conductivity and water retention functions in Figure 4.8.

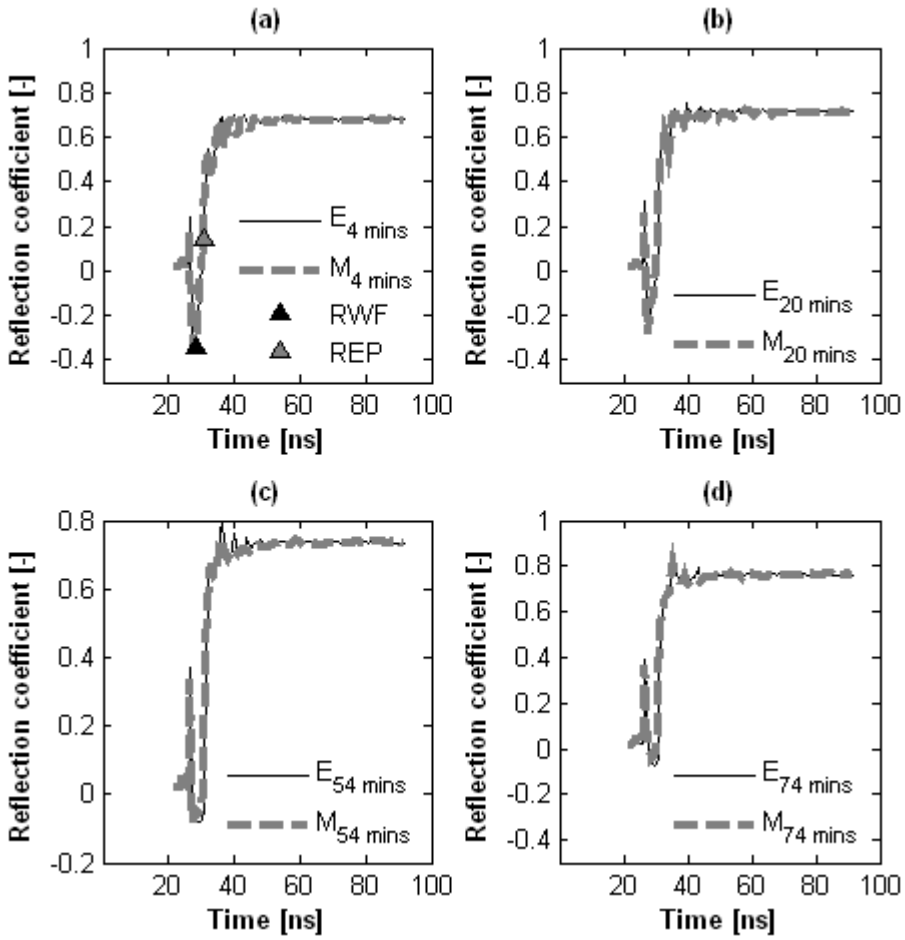

Figure 4.7: Measured versus predicted TDR waveforms four measurement times. M_{4mins}, $M_{20\ mins}$, $M_{54\ mins}$, and $M_{74\ mins}$ are the measured water content profiles at 4, 20, 54 and 74 minutes while $E_{4\ mins}$, $E_{20\ mins}$, $E_{54\ mins}$ and $E_{74\ mins}$ are the corresponding predictions from the estimated hydraulic parameters. REP is the reflection at the end of the probe while RWF is the reflection at the wetting front

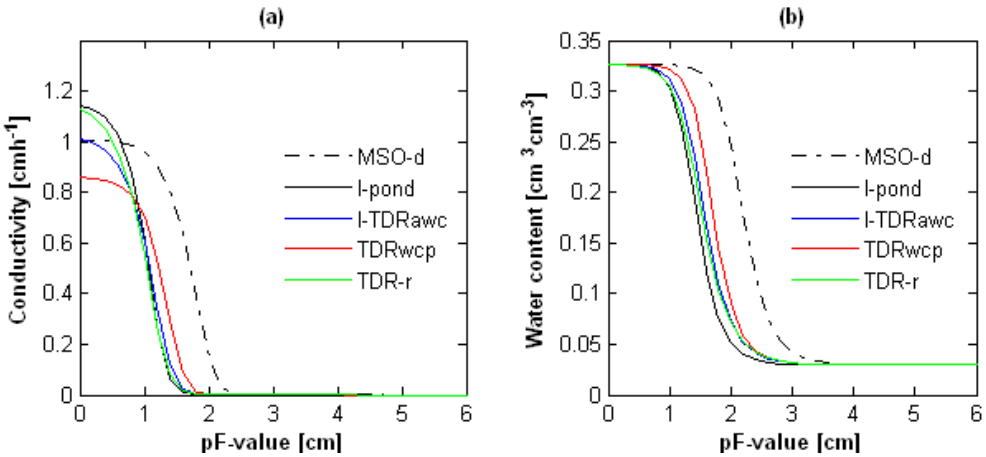

Figure 4.8: Comparison of hydraulic conductivity (a) and water retention (b) functions from optimized parameters using multi-step out flow data (MSO-d), infiltration from ponding depth (I-pond), Infiltration from TDR average water content (I-TDRawc), TDR water content profiles (TDR-awc), and TDR reflection coefficients (TDR-r, also called TDR measurements)

4.4. Conclusions

Using an artificial quartz substrate as test material and a relatively simple experimental set up consisting of a single laboratory column and a single trifilar TDR probe connected to a cable tester, we demonstrated the feasibility of using TDR data obtained under falling head infiltration to infer three topsoil MVG parameters. Three TDR-based data sets were used during inversion for hydraulic parameters: i) cumulative infiltration from average water content measured with TDR ('sequential approach'), ii) soil water content profiles obtained from TDR inversion ('sequential approach') and iii) direct inversion of TDR measurements using a coupled inversion approach. The results were compared with those from inversions using: i) cumulative infiltration from ponding depth, and ii) multi-step out flow data

When initial conditions are specified in water content, a numerical experiment revealed a positive correlation between α and n for both the sequential and coupled inversion approaches. This implied that the simultaneous estimation of α and n is not feasible in a 1D falling head infiltration experiment using this initial condition. The results also indicated that all the inversion strategies can lead to plausible estimates of K_s. On the other hand, it was numerically proven that the coupled inversion of TDR measurements can provide enough information to constrain the inversion for α, n and K_s when the initial conditions are specified in matric potential. The use of the multi-purpose probes of Baumgartner et al. (1994) which simultaneously measure matric potential and water content in combination with the coupled inversion approach of TDR measurements therefore appears as a potential and practical field method for the estimation of α , n and K_s necessitating further investigations.

In a laboratory experiment in which only the initial water content distribution was known the three TDR-based inversion strategies gave plausible estimates of n and K_s comparable with those from an MSO experiment and cumulative infiltration from ponding depth. The three TDR-based inversion strategies and the inversion using cumulative infiltration from ponding depth however ovestimated α when compared to the MSO result. This implied that under a 1D falling head infiltration with initial condition in water content all the other four inversion strategies produce similar results with minor differences. This may not be the case in multi-dimensional (2D or 3D) infiltration where the shape of the infiltrating bulb may also contain additional information on the hydraulic parameters. This should be explored in future studies.

Although the sequential and coupled inversion strategies produced similar results, the coupled inversion approach has a distinct advantage because it can be used to simultaneously monitor ponding depth and water infiltration. This avoids the laborious task of manually measuring the ponding depths and can thus enable automatic measurements of ponded infiltration for multiple rings through TDR multiplexing. This allows rapid estimation of the soil hydraulic parameters over relatively large surface areas with less human effort and resources. The code required to perform the sequential and coupled inversion are available from the first author upon request.

5. Synthesis

5.1 Final conclusions

Efficient soil and water management warrants a good knowledge of soil hydraulic parameters. From the view point of cost, spatial coverage, rapidity, accuracy and environmental safety, one way of estimating soil hydraulic parameters is to perform an inverse modeling in which geophysical data acquired from the monitoring of a hydrologic experiment are directly used to constrain a hydrologic model describing the experiment. This inverse modeling approach is referred to as coupled hydrogeophysical inversion. The objectives of this PhD work were to develop coupled hydrogeophysical inversion schemes and estimate soil hydraulic parameters using actual data from:

a) An ERT-monitored constant head infiltration experiment in the field
b) A column scale SP-monitored drainage experiment in the laboratory
c) A column scale TDR-monitored falling head infiltration experiment in the laboratory

ERT proved to be a valuable method for non-destructive monitoring of constant head infiltration in the field. Several methods of combining inflow and ERT data within the objective function for the estimation of soil hydraulic parameters using 3D coupled hydrogeophysical inversion were investigated. For an objective function defined as the sum of the root mean square error of both data types normalized by the respective standard deviations of the measurements, three key Mualem-Genuchten parameters (α, n and K_s) comparable to those obtained from a multi-step outflow experiment were obtained from coupled hydrogeophysical fusion of inflow and ERT data (electrical resistances). This showed that ERT and inflow data contain enough information to constrain the inversion for these parameters. The ability of the coupled hydrogeophysical inversion scheme to retrieve this information for parameter estimation depends on the choice of an appropriate objective function. Moreover, while it took about two months to obtain MSO data from destructive sampling of the field site, the ERT and inflow data were non-destructively acquired over a period of three hours and coupled hydrogeophysical inversion of the data took 2 days. Coupled hydrogeophysical inversion of geophysical data obtained in transient hydrologic experiments is therefore a rapid and cost-effective way of estimating soil hydraulic properties.

Coupled hydrogeophysical inversion of the streaming potential component of SP measurements obtained during primary drainage of a sandy soil column provided estimates of three key Mualem-van Genuchten parameters (α, n and K_s) comparable to those obtained from the inversion of tensiometric data. In addition, an estimate of Archie's saturation exponent close to the independently determined value could be obtained. However because SP measurements usually contain contributions other than streaming potential, efficient pre-processing of the SP data is necessary to extract the streaming potential component prior to coupled hydrogeophysical inversion. While this is can be achieved for SP data acquired under controlled laboratory conditions, it is far from trivial under field conditions. The successful inversion of streaming potential data required an adequate model for the voltage coupling coefficient at partial saturation. From a comparison of several such models with the experimental data, it was shown that models that consider the relative permeability of the porous medium in addition to water saturation were most appropriate.

Unlike coupled hydrogeophysical inversion, uncoupled hydrogeophysical inversion is an inverse modeling method which involves an intermediate inversion step. A comparison of the feasibility of both approaches to infer three key Mualem-van Genuchten parameters (α, n and K_s) of a sandy loam

from a falling head infiltration experiment monitored with a single vertically inserted TDR probe revealed that the coupled hydrogeophysical inversion approach is less uncertain and more practical. It was shown that coupled hydrogeophysical inversion enables simultaneous monitoring of ponding depth and water infiltration. This implies that with TDR multiplexing, ponded infiltration can be automatically monitored in rings at several locations within a field for accurate, rapid and cost-effective estimation of topsoil hydraulic parameters. Additionally, from synthetic experiments it was observed that the information retrieval capability of the coupled hydrogeophysical inversion of TDR waveforms for soil hydraulic properties depends on the initial conditions. Better results are obtained when initial conditions are defined in matric head than in water content. We propose to use multi-purpose TDR probes that measure water content in addition to matric potential in combination with the coupled hydrogeophysical inversion approach for improved estimates of the hydraulic parameters.

5.2 Outlook

5.21. Initial and boundary conditions and unrepresented processes.

Successful coupled hydrogeophysical inversion for soil hydraulic parameters requires the definition of a hydrologic model which is representative of the underlying physical system. At times the definition of appropriate initial and boundary conditions is not trivial. This problem sometimes leads to an initial condition paradox in which tomographic inversion is used to define the initial conditions in the forward hydrologic model used in coupled hydrogeophysical inversion. Research is needed on how to alleviate the issue of prescribing an appropriate initial condition. Although hydrologic model spin-ups with atmospheric boundary conditions have been proposed as a solution in synthetic experiments, the reliability of the approach to real field conditions still remains questionable. The hydrologic model can only provide reliable mass balance constraints on geophysical inversion when the model can reproduce the key processes under investigation. This implies that in the presence of subsurface processes like preferential flow, a hydrologic model which does not account for it can lead to erroneous interpretations of geophysical observations using the coupled hydrogeophysical inversion approach. Despite the quantitative bottlenecks associated with subsurface tomograms, the qualitative insights they can provide on unrepresented processes like preferential flow paths, can be used in defining an appropriate hydrologic model under such circumstances.The application of the coupled hydrogeophysical inversion approach to study complex flow and transport processes which are not usually accounted for in commonly used hydrologic models like HYDRUS is a therefore a challenging domain worth exploring.

5.2.2. Petrophysical parameters and spatially varying hydraulic properties

Although coupled hydrogeophysical inversion is a promising method for subsurface hydraulic characterization, there are a number of issues which must be properly addressed in order to reap its full potential. In this PhD, coupled hydrogeophysical inversion was used to estimate effective hydraulic properties and a common assumption was that the petrophysical properties that ensure the coupling between the hydrologic and geophysical forward models were spatially constant. While the results seem to justify this assumption, it is yet to be confirmed when the estimation of spatially varying hydraulic parameters is the objective of coupled hydrogeophysical inversion. Moreover the susceptibility of these petrophysical parameters to change with soil structure and temperature and the corresponding influence on the estimated hydraulic parameters still requires profound investigation.

5.2.3. Computational speed and parameter uncertainty estimation

Throughout this PhD work, a global optimizer was used to minimize the objective function for the estimation of soil hydraulic properties and the uncertainty on the parameters was determined based on first order approximation. Compared to first order approximations, a better way to characterize the uncertainty is to determine posterior probability distributions of these inverted parameters using MCMC algorithms. This can however be achieved only at a higher computational cost, typically requiring tens or hundreds of thousands of forward model runs to converge to the posterior distribution. In the 3D coupled hydrogeophysical inversion with ERT and inflow measurements a good computational speed was achieved by the use of a parallel code for the forward hydrologic model. It will be interesting to also incorporate a parallel code for the electrical flow problem within the coupled hydrogeophysical inversion scheme. Research is therefore needed on different ways of improving the computational speed.

5.2.4. Coupled hydrogeophysical data fusion - a holistic approach to subsurface characterization

The flexibility of the coupled hydrogeophysical inversion schemes allows for the integration of multiple geophysical and hydrologic data sets for subsurface characterization. If research is needed on how to combine different geophysical and hydrologic data sets, even the choice of the different geophysical and hydrologic methods requires a holistic approach. Ideally coupled hydrogeophysical data fusion for subsurface characterization should involve a combination of methods which are economically viable, technically feasible and environmentally safe. This therefore calls for stake holder participation from economic policy makers, hydrologists, geophysicists and environmentalists. Further development of the coupled hydrogeophysical inversion approach will depend on a strong collaboration between these stake holders. In this way many other exciting applications of the approach will spring up besides subsurface hydraulic characterization. For instance, the approach can be used to study root water uptake due to the strong mass balance constraints on geophysical inversion provided by the hydrologic model.

References

Allègre, V., L. Jouniaux, F. Lehmann and P. Sailhac. 2010. Streaming potential dependence on water-content in Fontainebleau sand. Geophysical Journal International 182:1248-1266.

Al-Saigh, N.H., Z.S. Mohamed, and M.S. Dahham. 1994. Detection of water leakage from dams by self-potential method. Engineering Geology 37:115-121.

Amin M.H.G., R.J. Chorley, K.S. Richards, B.W. Bache, L.D. Hall,. and T.A. Carpenter 1993. Spatial and temporal mapping of water in soil by magnetic resonance imaging. Hydrological Processes 7: 279-286.

Antraygues, P., and N. Aubert. 1993. Self potential signals generated by two phase flow in a porous medium: Experimental study and volcanological applications. Journal of Geophysical Research 98:22273-22281.

Archie, G.E.,. 1942. The electrical resistivity log as an aid in determining some reservoir characteristics. Transactions of the American Institute for Mining, Metallurgical, and Petroleum Engineers 146: 54–62.

Bänninger, D, H. Wunderli, M. Nussberger , and H. Flühler. 2008. Inversion of TDR signals-Revisited. Journal of Plant Nutrition and Soil Science 171:137-145.

Bänninger D., H. Wunderli., M. Nussberger,. and H. Flühler. 2009. Apparent electrical conductivity integrated from layered soil profiles. Journal of Plant Nutrition and Soil Science 172: 180-185.

Ball, J.A.R. 2002. Characteristic impedance of unbalanced TDR probes. IEEE Transactions on Instrumentation and Measurement 51:532-536.

Batlle-Aguilar, J., S. Schneider, M. Pessel, P**.** Tucholka, Y. Coquet, and P. Vachier. 2009. Axisymmetrical infiltration in soil imaged by noninvasive electrical resistimetry. Soil Science Society of America Journal 73: 510-520.

Baumgartner, N., G.W. Parkin, and D.E. Elrick. 1994. Soil water content and potential measured by hollow time domain reflectometry probe. Soil Science Society of America Journal 58:315-318

Behaegel, M., P. Sailhac and G. Marquis. 2007. On the use of surface and ground temperature data to recover soil water content information. Journal of Applied Geophysics 62(3): 234-243.

Binley, A., and K. Beven. 2003. Vadose zone flow model uncertainty as conditioned on geophysical data. Ground Water 41(2): 119-127.

Binley, A., B. Shaw and S. Henry-Poulter. 1996a. Flow pathways in porous media: electrical resistance tomography and dye staining image verification. Measurement Science and Technology 7: 384-390.

Binley, A., G. Cassiani, R. Middleton, and Winship, P. 2002a. Vadose zone model parameterisation using cross-borehole radar and resistivity imaging. Journal of Hydrology 267: 147–159.

Binley A., P. Winship, L.J. West, M. Pokar, and R. Middleton. 2002. Seasonal variation of moisture content in unsaturated sandstone inferred from borehole radar and resistivity profiles. Journal of Hydrology 267: 160–172.

Binley, A., S. Henry-Poulter, and B. Shaw.1996. Examination of solute transport in an undisturbed soil column using electrical resistance tomography. Water Resources Research 32: 763–769.

Bogoslovsky, V.A., and A.A. Ogilvy. 1973. Deformation of natural electric fields near drainage structures. Geophysical Prospecting 21:716-723.

Bolève, A., A. Revil, F. Janod, J.L. Mattiuzzo and J.-J. Fry. 2009. Preferential fluid flow pathways in dams imaged by self-potential tomography. Near Surface Geophysics 7:447-462.

Brocca, L., R. Morbodelli, F. Melone, and T. Moramarco. 2007. Soil moisture spatial variability in experimental areas of Italy. Journal of Hydrology 333: 356-373.

Brooks, R.H., and A.T. Corey. 1964. Hydraulic properties of porous media. Colorado Univiversity Hydrology Paper No. 3. Colorado State University. Fort Collins. CO.

Burdine, N.T. 1953. Relative permeability calculations from pore size distribution data. Transactions of the American Institute for Mining, Metallurgical, and Petroleum Engineers 198: 71-77.

Campbell, J.E. 1992. Dielectric properties and influence of conductivity in soils at one to fifty megahertz, soil Science Society of America Journal 54:332-334.

Carsel R.F., and R.S. Parish. 1988. Developing joint probability distributions of soil water retention characteristics. Water Resources Research 24: 755-769.

Cassiani, G., and A. Binley. 2005. Modeling unsaturated flow in a layered formation under quasi-steady state conditions using geophysical data constraints. Advances in Water Resources 28: 467–477.

Cassiani, G., and M.A. Medina, 1997. Incorporating auxiliary geophysical data into ground-water estimation. Ground Water 35(1): 79-91.

Cassiani, G., G. Bohm, A. Vesnaver, and R. Nicolich. 1998. A geostatistical framework for incorporating seismic tomography auxiliary data into hydraulic conductivity. Journal of Hydrology 206(1-2): 58-74.

Chen, J.S., S. Hubbard, and Y. Rubin. 2001. Estimating the hydraulic conductivity at the South Oyster Site from geophysical tomographic data using Bayesian techniques based on the normal linear regression model. Water Resources Research 37(6): 1603-1613.

Chen, J.S., S. Hubbard, Y. Rubin, E. Roden, and T. Majer. 2004. Geochemical characterization using geophysical data and Markov Chain Monte Carlo methods: A case study at the South Oyster bacterial transport site in Virginia. Water Resources Research 40: 10.1029/2003WR002883.

Chen, J.S., S. Hubbard, J. Peterson, K. Williams, M. Fienen, P. Jardine, and D. Watson. 2006. Development of a joint hydrogeophysical inversion approach and application to a contaminated fractured aquifer. Water Resources Research 42: W06425, doi:10.1029/2005WR004694.

Clément, R., M. Descloitres, T. Günther, C. Oxarango, J. Morra, L.P. Laurent, and J.P. Goura. 2009. Improvement of electrical resistivity tomography for leachate injection monitoring. Waste management 30: 542-462.

Dahlin, T. and B. Zhou. 2004. A numerical comparison of 2D resistivity imaging with 10 electrode arrays. Geophysical Prospecting 52: 379-398.

Daily, W.A., D. Ramirez, D. LaBreque, and J. Nitao. 1992. Electrical resistivity tomography of vadose water movement. Water Resources Research 28, 1429–1442.

Darnet, M., and G. Marquis. 2004. Modeling streaming potential (SP) signals induced by water movement in the vadose zone. Journal of Hydrology 285:114-124.

Darnet, M., G. Marquis and P. Sailhac. 2003. Estimating aquifer hydraulic properties from the inversion of subsurface streaming potential (SP) anomalies. Geophysical Research Letters 30(13):1679

Day-Lewis, F., J.W Lane Jr., and S.M. Gorelick. 2004. Combined interpretation of radar, hydraulic and tracer data from a fractured-rock aquifer. Hydrogeological Journal 13: 10.1007/s10040-004-0372-y.

Day-Lewis, F.D., K.Singha, and A.M. Binley. 2005. Applying petrophysical models to radar travel time and electrical resistivity tomograms: Resolution-dependent limitations. Journal of Geophysical Research-Solid Earth 110:10.1029/2004JB003569

DeGroot-Hedlin, C., and S.Constable. 1990. Occam's inversion to generate smooth, two dimensional models from magnetotelluric data. Geophysics 55: 1613-1624.

Deiana, R., G. Cassiani, A. Kemna, A. Villa, V. Bruno and A. Bagliani. 2007. An experiment of non-invasive characterization of the vadose zone via water injection and cross-bore hole timelapse geophysical monitoring. Near Surface Geophysics 5: 183-194.

Duan, Q., S. Sorooshian,. and V. Gupta. 1993. Shuffled complex evolution approach for effective and efficient global minimization. Journal of Optimization Theory and applications 76: 501-521.

Dukhin, S. S. and B.V. Derjaguin. 1974. Electrokinetic phenomena. pp. 322. *In* Matijevic, E (ed.) Surface and Colloids Science, Vol. 7. John Wiley and Sons, New York.

Ersahin, S., and A.R. Brohi. 2006. Spatial variability of soil water content in topsoil and subsoil of a typic ustifluvent. Agriculture and Water Management 83: 79-86.

Eching, S.O., and J.W. Hopmans. 1993. Optimization of hydraulic functions from transient outflow and soil water pressure data. Soil Science Society of America Journal 57: 1167-1175.

Faybishenko, B. 2000. Tensiometer for shallow and deep measurements of water pressure in vadose zone. Soil Science 165: 473-482.

Feng, W., C.P. Lin, R.J. Deschangs, and V.P. Drnevich. 1999. Theoretical model of a multisection time domain reflectometry measurement system. Water Resources Research 35:2321-2331.

Ferre, T.P.A., L. Bentley, A. Binley, N. Linde, A. Kemna, K. Singha, K. Holliger, J.A. Huisman, and B. Minsley. 2009. Critical steps for the continuing advancement of hydrogeophysics. Eos Transactions of American Geophysical Union 90:10.1029/2009EOS230004.

Ferré, P.A., D.L. Rudolph, and R.G. Kachanowski. 1996. Spatial averaging of water content by time domain reflectometry: implications for twin rod probes with and without dielectric coatings. Water Resources Research 32(2): 271-279.

Finizola, A., F. Sortino, J.F. Lénat, and M. Valenza. 2002. Fluid circulation at Stromboli volcano from self-potential and CO2 surveys. Journal of Volcanology and Geothermal Research 116:1-18.

Flury, M., H. Fluhler, W.A. Jury, and J. Leuenberger. 1994. Susceptibility of soils to preferential flow of water: A field study. Water Resources Research 30: 1945-1954.

French, H.K., C. Hardbattle, A. Binley, P. Winship, and L. Jakobsen. 2002. Monitoring snowmelt induced unsaturated flow and transport using electrical resistivity tomography. Journal of Hydrology 267: 273–284.

Friedman, S. 2005. Soil properties influencing apparent electrical conductivity: A review. Computer and electronics in Agriculture 46: 45-70.

Fuentes, C., R. Haverkamp, and J.Y. Parlange. 1992. Parameter constraints on closed-form soil water relationships. Journal of Hydrology 134: 117-142.

Furman, A., T.P.A. Ferré, and A.W. Warrick. 2003. A sensitivity analysis of electrical resistivity tomography array types using analytical element modelling. Vadose Zone Journal 2:416-423.

Gallardo, L.A., and M.A. Meju. 2003. Characterization of heterogeneous near surface materials by joint 2D inversion of dc resistivity and seismic data. Geophysical Research Letters 30(13):10.1029/2003GL017370.

Gallardo, L.A. and M.A. Meju. 2004. Joint two-dimensional DC resistivity and seismic travel time inversion with cross-gradients constraints. Journal of Geophysical Research 109: B03311

Gérald-Marchant, P., R. Angulo-Jaramillo, R. Haverkamp, M. Vauclin, P. Groenevelt, and D.E. Elrick. 1997. Estimating the hydraulic conductivity of slowly permeable and swelling materials from single-ring Experiments.Water Resources Research 33 (6): 1375-1382.

Gloaguen, E., M. Chouteau, D. Marcotte and R. Chapuis. 2001. Estimation of hydraulic conductivity of an unconfined aquifer using cokriging of GPR and hydrostratigraphic data. Journal of Applied Geophysics 47: 135-152.

Gibert, D., and M. Pessel. 2001. Identification of sources of potential fields with the continuous wavelet transform: application to self-potential profiles. Geophysical Research Letters 28:1863-1866.

Glover, P. 2009. What is cementation exponent? A new interpretation. The Leading Edge 28: 82-85.

Greco, R. 2006. Soil water content inverse profiling from single TDR waveform. Journal of Hydrology 317:325-339.

Greco, R. and A. Guida. 2008. Field measurements of topsoil moisture profi les
by vertical TDR probes. Journal of Hydrology 348:442–451.

Günther, T., C. Rücker, and K. Spitzer. 2006. Three-dimensional modeling and inversion of DC resistivity data incorporating topography – II. Inversion. Geophysical Journal International 166, 506-517.

Guichet, X., L. Jouniaux, and J. Pozzi. 2003. Streaming potential of a sand column in partial saturation conditions. Journal of Geophysical Research 108(B3):2142, doi: 10.1029/2001JB001517.

Hansen, T.M., M.C. Looms and L. Nielsen. 2008. Inferring the subsurface structural covariance model using cross-borehole ground penetration radar tomography. Vadose Zone Journal 7: 249-262.

Hardelauf, H., M. Javaux, M. Herbst, S. Gottschalk, R. Kasteel, J.Vanderborght. and H. Vereecken. 2007. PARSWMS: A parallelized model for simulating three-dimensional water flow and solute transport in variably saturated soils Vadose Zone Journal 6: 255-259.

Heimovaara, T.J. 1994. Frequency domain analysis of time domain reflectometry waveforms. 1. Measurement of the complex dielectric permittivity of soils, Water Resources Research 30:189-199.

Heimovaara, T.J., and W. Bouten. 1990. A computer-controlled 36- channel time domain reflectometry system for monitoring soil water contents. Water Resources Research 26:2311–2316

Heimovaara, T.J., J.A. Huisman, J. A. Vrugt, and Bouten, W. 2004. Obtaining the spatial distribution of water content along a TDR probe using the SCEM-UA Bayesian inverse modeling scheme, Vadose Zone Journal 3:1128–1145.

Hendrickx, J.M.H., J.L. Nieber, and P.D. Siccama. 1994. Effect of tensiometer cup size on field soil water tension variability. Soil Science Society of America Journal 58: 309-315.

Hinnell, A.C., T.P.A. Ferre, J.A. Vrugt, J.A. Huisman, S. Moysey, J. Rings, and M.B. Kowalsky. 2010. Improved extraction of hydrologic information from geophysical data through coupled hydrogeophysical inversion. Water Resources Research 46: W00D40.

Hopmans, J., J. Simunek, N. Romano, and W. Durner. 2002. Simultaneous determination of water transmission and retention properties: Direct methods. *In* Dane J.H. and Topp, G.C. (eds.) Methods of Soil Analysis. Part 4. Physical Methods, Vol.5, SSSA, Madison, WI.

Hubbard, S.S., Y. Rubin, and E. Majer. 1999. Spatial correlation structure estimation using geophysical and hydrogeological data. Water Resources Research 35(6): 1809-1825.

Hubbard, S.S., and Y. Rubin. 2000. Hydrogeophysical parameter estimation using geophysical data: A review of selected techniques. Journal of Contaminant Hydrology 45: 3-34.

Hubbard, S., J.S. Chen, J. Peterson, E. Majer, K. Williams, D. Swift, B. Mailloux, and Y. Rubin. 2001. Hydrogeological characterization of the South Oyster bacterial transport site using geophysical data. Water Resources Research 37(10): 2431-2456.

Huisman, J.A., A.H.Weerts, T.J. Heimovaara., and W.Bouten. 2002. Comparison of travel time analysis and inverse modeling for soil water content determination with time domain reflectometry. Water Resources Research 38:10.1029/2001WR000259.

Huisman, J.A., C.P. Lin, L. Weihermüller, and H. Vereecken. 2008. Accuracy of bulk electrical conductivity measurements with time domain reflectometry. Vadose Zone Journal 7(2):426-433.

Huisman, J.A., J. Rings, J.A. Vrugt, J. Sorg, and H. Vereecken. 2010. Hydraulic properties of a model dike from coupled Bayesian and multi-criteria hydrogeophysical inversion. Journal of Hydrology 380: 62-73.

Huisman, J.A., S.S. Hubbard, J.D. Redman, and P. Annan. 2003. Measuring soil water content with ground penetration radar: a review. Vadose Zone Journal 2(4):476-491.

Huisman, J.A., W. Bouten, J.A. Vrugt, and T.P.A. Ferré. 2004. Accuracy of frequency domain analysis scenarios for the determination of complex dielectric permittivity. Water Resources Research 40(2): 10.1029/2002WR001601.

Hupet, F., and M. Vanclooster. 2002. Intraseasonal dynamics of soil moisture variability within a small agricultural maize cropped field. Journal of Hydrology 261: 86-101.

Hyndman, D.W., J.M. Harris, and S.M. Gorelick. 1994. Coupled seismic and tracer test inversion for aquifer property characterization. Water Resources Research 30(7): 1965-1977.

Hyndman, D.W., and S.M. Gorelick. 1996. Estimating lithologic and transport properties in three dimensions using seismic and tracer data: The Kesterson aquifer. Water Resources Research 32(9): 2659-2670.

Ishido, T., and H. Mizutani. 1981. Experimental and theoretical basis of electrokinetic phenomena in rock-water systems and its applications to geophysics. Journal of Geophysical Research 86:1763-1775.

Ishido, T., T. Kikuchi., N. Matsusshima, Y. Yano, S. Nakao, M. Sugihara, T. Tosha, S. Takakura, and Y. Ogawa. 1997. Repeated self-potential of Izu-Oshima volcano, Japan. Journal of Geomagnetism and Geoelectricity 49:1267-1278.

Jackson, M.D.,. 2008. Characterization of multiphase electrokinetic coupling using a bundle of capillary tubes model. Journal of Geophysical Research 113: B04201.

Jackson, M.D.,. 2010. Multiphase electrokinetic coupling: Insights into the impact of fluid and charge distribution at the pore scale from a bundle of capillary tubes model. Journal of Geophysical Research 115: B07206.

Jadoon, K.Z., S. Lambot, B. Scharnagl, J. van der Kruk, E.C. Slob and H. Vereecken. 2010. Quantifying field-scale soil water content from proximal GPR signal inversion in time domain. Near Surface Geophysics 8: 483-491.

Jardani, A., A. Revil, F. Akoa, M. Schmutz, N. Florsch, and J.P. Dupont. 2006. Least squares inversion of self-potential (SP) data and application to the shallow flow of ground water in sink holes. Geophysical Research Letters 33:L19306.

Jardani, A., A. Revil., A. Bolève, A. Crespy, J.-P. Dupont, W. Barrash, and B. Malama. 2007. Tomography of the Darcy velocity from self-potential measurements. Geophysical Research Letters 34:L24403.

Jougnot, D., A. Ghorbani, A. Revil, P. Leroy, and P. Cosenza. 2010. Spectral induced polarization of partially saturated clay-rocks: a mechanistic approach. Geophysical Journal International 180: 210-224.

Jardani, A., A. Revil., A. Bolève, A. Crespy, J.-P. Dupont, W. Barrash, and B. Malama. 2007. Tomography of the Darcy velocity from self-potential measurements. Geophysical Research Letters 34: L24403.

Kemna, A., J. Vanderborght, B. Kulessa, and H. Vereecken. 2002. Imaging and characterisation of subsurface solute transport using electrical resistivity tomography (ERT) and equivalent transport models. Journal of Hydrology 267(3-4): 125-146.

Klute, A., and C. Dirksen. 1986. Hydraulic conductivity and diffusivity: Laboratory methods. P. 687-734. *In* A Klute (ed.) Methods of soil analysis. Part 1. Physical and mineralogical methods. 2nd ed. ASA and SSSA. Madison I.

Kool, J.B. and J.C. Parker. 1988. Analysis of the inverse problem for transient unsaturated soil water flow. Water Resources Research 24: 817-830.

Kowalsky, M.B., S. Finsterle, and Y. Rubin. 2004. Estimating flow parameter distributions using ground-penetrating radar and hydrological measurements during transient flow in the vadose zone. Advances in Water Resources 27(6): 583-599.

Kowalsky, M.B., S. Finsterle, J. Peterson, S. Hubbard, Y. Rubin, E. Majer, A. Ward, and G. Gee. 2005. Estimation of field-scale soil hydraulic and dielectric parameters through joint inversion of GPR and hydrological data. Water Resources Research 41: W11425.

Kulessa, B., B. Hubbard, and G.H. Brown. 2003. Cross-coupled flow modeling of coincident streaming potentials and electrochemical potentials and application to subglacial self-potential data. Journal of Geophysical Research 108 (B8):2381, doi:10.1029/2001JB001167.

LaBrecque, D.J., M. Miletto, W. Daily, A. Ramirez, and E. Owen. 1996. The effects of noise on Occam's inversion of resistivity tomography data. Geophysics 61: 538-548.

Lambot, S., E.Slob, J. Rhebergen, O. Lopera, K.Z. Jadoon, and H. Vereecken. 2009. Remote estimation of the hydraulic properties of a sand using full-waveform integrated hydrogeophysical inversion of time-lapse, off ground GPR data. Vadose Zone Journal 8:743-754.

Lambot, S., E.C. Slob, M. Vanclooster and H. Vereecken . 2006. Closed loop GPR data inversion for soil hydraulic and electric property determination. Geophysical Research Letters 33: L21405.

Lénat, J.F., D. Fitterman, and D.B. Jackson. 2000. Geoelectric structure of the central zone of the Piton de la Forounaise volcano (Réunion). Bulletin Volcanologique 62(2):75-89.

Liedenberger, P., B. Oswald, and K. Roth, 2006. Efficient reconstruction of dispersive dielectric profiles using time domain reflectometry (TDR). Hydrology and Earth System Science 10:209-232.

Lin, C.P. Frequency domain versus travel time analysis of TDR waveforms for soil moisture content measurements. Soil Science Society of America Journal 67:720-729.

Lin, C.P., and S.H. Tang. 2007. Comprehensive wave propagation model to improve TDR interpretations for geotechnical applications. Geotechnical Testing Journal, 30(2): 90-97.

Linde, N.,. 2009. Comment on" Characterization of multiphase electrokinetic coupling using a bundle of capillary tubes model" by M.D. Jackson. Journal of Geophysical Research 114: B06209.

Linde, N., A. Revil. 2007. Inverting self-potential data for redox potentials of contaminant plumes. Geophysical Research Letters 34:L14302.

Linde, N., A. Binley, A. Tryggvason, L.B. Pedersen, and A. Revil. 2006. Improved hydrogeophysical characterization using joint inversion of cross-hole electrical resistance and ground-penetrating radar travel time data. Water Resources Research 42: W12404.

Linde, N., D. Jougnot, A. Revil, K. Mathäi, T. Arora, D. Renard, and C. Doussan. 2007. Streaming current generation in two-phase flow conditions. Geophysical Research Lettters 34:L03306.

Linde, N., J. Doetsch, D. Jougnot, O. Genoni, Y. Dürst, B.J. Minsley, T. Voght, N. Pasquale, and J. Luster. 2011. Self-potential investigations of a gravel bar in a restored river corridor. Hydrology and Earth System Sciences 15:729-742.

Linde, N., S. Finsterle, and S. Hubbard. 2006b. Inversion of tracer test data using tomographic contraints. Water Resources Research 42: W04410

Liu, S. and Yeh, T.C., 2004. An integrative approach for monitoring water movement in the vadose. Vadose Zone Journal 3(2): 681-692.

Loke, M.H., and T.Dahlin. 2002. A comparison of the Gauss-Newton and quasi-Newton methods in resistivity imaging and inversion. Journal of Applied. Geophysics 49:149-162.

Looms, M.C., A. Binley, K.H. Jensen, L. Nielsen, and T.M. Hansen. 2008b. Identifying unsaturated hydraulic parameters using an integrated data fusion approach on cross-borehole geophysical data. Vadose Zone Journal 7: 238–248.

Looms, M.C., K.H. Jensen, A. Binley, and L. Nielsen. 2008a. Monitoring unsaturated flow and transport using cross-borehole geophysical methods. Vadose Zone Journal 7: 227–237.

Lu, S., T. Ren, Y. Gong, and R. Horton. Evaluation of three models that describe soil water retention curves from saturation to oven dryness. 2007. Soil Science Society of America Journal 72:1542-1546.

Maineult, A., Y. Bernabé, and P. Ackerer. 2005. Detection of advected concentration and pH fronts from self-potential measurements. Journal of Geophysical Research 110: B11205.

Maineult, A., L. Journiaux, Y. Bernabé . 2006. Influence of the mineralogical composition on the self-potential response to advection of KCl concentration fronts through sand. Geophysical Research Letters 33: L24311..

Marshall, D.J., and T.R. Madden. 1959. Induced polarization, a study of its causes. Geophysics 24(4):790-816.

Martinez, G., K. Vanderlinden, J.V. Giráldez, A.J. Espejo, and J.L. Muriel. 2009. Field scale moisture pattern mapping using electromagnetic induction. Vadose Zone Journal 9: 871-881.

Mboh, C.M., J.A. Huisman, and H. Vereeecken. 2011. Feasibilty of sequential and coupled inversion of time domain reflectrometry data to infer soil hydraulic parameters under falling head infiltration. Soil Science Society of America Journal 75: 775-786.

Mboh, C.M., J.A. Huisman, N. Van Gaelen, J. Rings and H. Vereecken. 2012a. Coupled Hydrogeophysical inversion of electrical resistances and inflow measurements for topsoil hydraulic properties under constant head infiltration. Near Surface Geophysics 10: 413-426.

Mboh, C.M:, J.A. Huisman, E. Zimmermann and H. Vereecken. 2012b. Vadose Zone Journal 11(2). doi: 10.2136/vzj2011.0115.

McKenna, S.A., and E.P. Poeter. 1995. Field example of data fusion in site characterization. Water Resources Research 31: 3229– 3240.

Mertens, J., D. Jacques, J. Vanderborgt and J. Feyen. 2002. Characterisation of the field-saturated hydraulic conductivity on a hill slope: In situ single ring pressure infiltrometer measurements. Journal of Hydrology 263: 217-229.

Minsley, B.J., J. Sogade, and F.D. Morgan. 2007. Three dimensional source inversion of self-potential data. Journal of Geophysical Research 112: B02202, doi: 1029/2006JB004262.

Moysey, S., R. Knight and K. Singha. 2006. Relating geophysical and hydrologic properties using field-scale rock physics. *In*: P.J. Binning, P.K. Engesgaard, H.K. Dahle, G.F. Pinder, and W.G. Gray (eds.) Proceedings of the XVI international conference on Computational Methods in Water Resources, Copenhagen, Denmark, 8 pp.

Mualem, Y. 1976. A new model for predicting the hydraulic of unsaturated porous media. Water Resources Research 12: 513-522.

Mualem, Y. and S.P. Friedman. 1991. Theoretical prediction of electrical conductivity in saturated and unsaturated soil. Water Resources Research 27, 2271-2277.

Müller, K., J. Vanderborght, A. Englert, A. Kemna, J.A. Huisman, J. Rings, and H. Vereecken. 2010. Imaging and characterization of solute transport during two tracer tests in a shallow aquifer using electrical resistivity tomography and multilevel groundwater samplers. Water Resources Research 46: W03502

Musil, H., H.R. Maurer, and A.G. Green. 2003. Discrete tomography and joint inversion for loosely connected or unconnected physical properties: application to crosshole seismic and georadar data sets. Geophysical Journal International 153: 389-402.

Nakashima, Y., H. Zhou and M. Sato. 2001. Estimation of groundwater level by GPR in an area with multiple ambiguous reflections. Journal of Applied Geophysics 47(3-4): 241-249.

National Academy of Sciences. 2000. Seeing into the earth: Non-invasive characterization of the shallow subsurface for environmental and engineering applications, 129pp., National Academic Press, Washington, D.C.

Naudet, V., A. Revil., J.Y. Bottero, and P. Bégassat. 2003. Relationship between self-potential (SP) signals and redox conditions in contaminated groundwater. Geophysical Research Letters 30(2):2091..

Naudet, V., A. Revil., E. Rizzo, J.Y. Bottero, and P. Bégassat. 2004. Groundwater redox conditions and conductivity in a contaminant plume from geoelectrical investigations. Hydrology and Earth System Science 8(1):8-22.

Nimmo J.R. 1991. Comment on the treatment of residual water content in “A consistent set of parametric models for two-phase flow of immiscible fluids in the subsurface” by L. Lunker et al. Water Resources Research 27, 661-662.

Oldenborger, G.A., M.D. Knoll, P.S. Routh, and D.J. LaBreque. 2007. Time-lapse ERT monitoring of an injection/withdrawal experiment in a shallow unconfined aquifer. Geophysics 72(4): 177–187.

Oswald, B., H.R. Benedickter, W. Bachtold, and H. Fluhler. 2003. Spatially resolved water content profiles from inverted time domain reflectometry signals. Water Resources Research 39(12): 1357.

Overbeek, J.T.G. 1952. Electrochemistry of the electrical double layer. In Colloids Science irreversible Systems, vol. 1,:115-193.ed. Kruyt, H.R., Elsevier, New York.

Panthulu, T.V., C. Krishnaiah, and J.M. Strike. 2001. Detection of seepage paths in earth dams using self-potential and electrical resistivity methods. Engineering Geology 59: 281-295.

Parkin, G.W., G.R. Kachanoski, and D.E. Elrick. 1995. Unsaturated hydraulic conductivity measured by time domain reflectometry under a rainfall simulator. Water Resources Research 31(3): 447-456.

Parkin, G.W., D. Redman, P. v. Bertoldi, and Z. Zhang. 2000. Measurement of soil water content below a wastewater trench using ground-penetrating radar. Water Resources Research 36(8): 2147-2154.

Patella, D. 1997. Introduction to ground surface self-potential tomography. Geophysical Prospecting 45:653-681.

Pearce, F.,. 1992. The dammed; rivers, dams and the coming of water crisis. The Bodley Head, London.

Perrier, F., and P. Morat. 2000. Characterization of electrical daily variations induced by capillary flow in the non-saturated zone. Pure and Applied Geophysics 157:785-810.

Petiau , G., and A. Dupis. 1980. Noise, temperature coefficient, and long time stability of electrodes for telluric observations. Geophysical Prospecting 28(5): 792-804.

Pezard, G.E., S. Gautier, T.L. Borgne, B. Legros, and J.-L. Deltombe. 2009. Muset: A multiparameter and high precision sensor for downhole spontaneous electrical potential measurements. Comptes Rendus Geoscience 341:957-964.

Reedy, R.C., and B.R. Scanlon. 2003. Soil water content monitoring using electromagnetic induction. Journal of Geotechnical and Geoenvironmental Engineering 129: 1028-1039.

Revil, A., and A. Cerepi. 2004. Streaming potentials in two-phase flow conditions. Geophysical Research Letters 31: L11605.

Revil, A., N.Linde, A. Cerepi, D.Jougnot, S. Matthäi, and S. Finsterle. 2007. Electrokinetic coupling in unsaturated porous media. Journal of Colloid and Interface Science 313: 315-327.

Revil, A., H. Schwaeger, and P.D. Manhardt. 1999. Streaming potential in porous media: 2. Theory and application to geothermal systems. Journal of Geophysical Research 104(B49):20033-20048.

Revil, A., N. Linde, A. Cerepi, D. Jougnot, S. Matthai, and S. Finsterle. 2007. Electrokinetic coupling in unsaturated porous media. Journal of Colloid and Interface Science 313:315-327

Revil, A., and P.A. Leroy. 2004. Constitutive equations for ionic transport in porous shales. Journal of Geophysical Research 109:B03208.

Reynolds, W.D., D.E. Elrick, E.G. Youngs, A. Amoozegar, H.W.G. Booltink,. and J. Bouma. 2002. Saturated and field saturated water flow parameters. In: Methods of soil analysis. Part 4. Physical methods (ed. Dane H.J. and Topp C.G.), pp. 797-877. Soil Science Society of America, Madison, WI.

Rhoades, J.D., P.A.C. Raats, and R.J. Prather. 1976. Effect of liquid-phase electrical conductivity, water content and surface conductivity on bulk soil electrical conductivity. Soil Science Society of America Journal 40: 651-655.

Richards, L.A., 1931. Capillary conduction of liquids in porous medium. Physics 1:318-333.

Richards, K., A. Revil, A. Jardani, F. Henderson, M. Batzle, and A. Haas, 2010. Pattern of shallow ground water flow at mount Princeton hot springs, Colorado, using geoelectric methods. Journal of Volcanology and Geothermal Research. 198 (1-2): 217-232.

Rings, J., C. Hauck, K. Preko, and A. Scheuermann. 2008. Soil water content monitoring on a dike model using electrical resistivity tomography. Near Surface Geophysics 6: 123-132.

Rings, J., J.A. Huisman, and H. Vereecken. 2010. Coupled hydrogeophysical parameter estimation using a sequential Bayesian approach. Hydrology and Earth System Sciences 14: 545-556.

Rizzo, E., B. Suski and A. Revil. 2004. Self-potential signals associated with pumping tests experiments. Journal of Geophysical Research 109:B10203, doi: 10.1029./2004JB003049.

Robinson, D.A., C.S. Campbell, J.W. Hopmans, B.K. Hornbuckle, S.B. Jones, R. Knight, F. Ogden, J. Selker, and O. Wendroth. 2008. Soil moisture measurement for ecological and hydrological watershed-scale observatories. Vadose Zone Journal 7(1):358-389.

Roy, A., and M.W. Lubcynski. 2005. MRS multi-exponential decay analysis: aquifer pore-size distribution and vadose zone characterization. Near Surface Geophysics 3: 287-298.

Rubin, Y., G. Mavko, and J. Harris. 1992. Mapping permeability in heterogeneous aquifers using hydrologic and seismic data. Water Resources Research 28(7): 1809-1827.

Rücker, C., T. Günther,. and K. Spitzer. 2006. Three-dimensional modeling and inversion of DC resistivity data incorporating topography-I Modelling. Geophysical Journal International 166: 495-505.

Rucker, D.F., and T.P.A. Ferre. 2004. Parameter estimation for soil hydraulic properties using zero-offset borehole radar: Analytical method. Soil Science Society of America Journal 68(5): 1560-1567.

Russo, D., E. Bresler, U. Shani, and J.C. Parker. 1991. Analysis of infiltration experiments in relation to determining soil hydraulic properties by inverse methodology. Water Resources Research 27: 1361-1373.

Sailhac, P., and G. Marquis. 2001. Analytic potentials for forward and inverse modeling of SP anomalies caused by subsurface fluid flow. Geophysical Research Letters 28:1643-1646.

Samouelian, A., I. Cousin, A. Tabbagh, A. Bruand, and G. Richard. 2005. Electrical resistivity survey in soil science: A review. Soil and Tillage Research 83:173-193

Sato, M., and H. M. Mooney. 1960. The electrochemical mechanism of sulfide self-potentials. Geophysics 25:226-249.

Schwartz, R.C., and S.R. Evett. 2002. Estimating hydraulic properties of a fine-textured soil using a disc infiltrometer. Soil Science Society of America Journal 66:1409–1423.

Sheets, K.R., and J.M.H. Hendrickx. 1995. Noninvasive soil water content measurements using electromagnetic induction. Water Resources Research 31: 2401-2410.

Sill, W.R.,. 1983. Self-potential modeling from primary flows. Geophysics 48:76-86.

Slater, L., A. Binley, W. Daily and R. Johnson. 2000. Cross-hole electrical imaging of a controlled saline tracer injection. Journal of Applied Geophysics 44: 85–102.

Slater, L., A. Binley, R. Versteeg, G. Cassiani, R. Birken, and S. Sandberg. 2002. A 3D ERT study of solute transport in a large experimental tank. Journal of Applied Geophysics 49: 211-229.

Slater, L.,. 2007. Near surface electrical characterization of hydraulic conductivity: From petrophysical properties to aquifer geometries-A review. Surveys in Geophysics 28: 169-197.

Simunek, J., R. Angulo-Jaramillo, M.G. Schaap, J.P. Vandervaere, and M.T. van Genuchten. 1998a. Using an inverse method to estimate hydraulic properties from multiple tension disc infiltrometer data. Geoderma 86: 61-81.

Simunek, J., M.T. van Genuchten. 1996. Estimating unsaturated soil hydraulic properties from tension disc infiltrometer data by numerical inversion. Water Resources Research 32: 2683-2696.

Simunek, J., M.T. van Genuchten, M.M. Gribb, J.W. Hopmans. 1998. Parameter estimation of unsaturated soil hydraulic properties from transient flow processes. Soil and Tillage Research 47: 27-36.

Simunek, J., M.T. van Genuchten, and M. Sejna. 2008. Development and applications of the HYDRUS and STANMOD software packages and related codes. Vadose Zone Journal 7: 587-600.

Singha, K. and S.M. Gorelick. 2005. Saline tracer visualized with three-dimensional electrical resistivity tomography: Field-scale spatial moment analysis. Water Resources Research 41(5): W05023

Singha, K., and S.M. Gorelick. 2006a. Effects of spatially variable resolution on field-scale estimates of tracer concentration from electrical inversions using Archie's law. Geophysics 71(3): G83-G91.

Singha, K. and S.M. Gorelick. 2006b. Hydrogeophysical tracking of three-dimensional tracer migration: the concept and application of apparent petrophysical relationships. Water Resources Research 42: W06422.

Singha, K., and S. Moysey. 2006. Accounting for spatially variable resolution in electrical resistivity tomography through field-scale rock physics relations. Geophysics 71: A25-A28

Sisson, J.B., G.W. Gee, J.M. Hubbell, W.L. Bratton, J.C. Ritter, A.L. Ward and T.G. Caldwell. 2002. Advances in tensiometry for long-term monitoring of soil water pressures Vadose zone Journal 1: 310-315.

Slater, L. 2007. Near surface electrical characterization of hydraulic conductivity: From petrophysical properties to aquifer geometries-A review. Surveys in Geophysics 28: 169-197.

Slater, L., A. Binley, W. Daily, and R. Johnson. 2000. Cross-hole electrical imaging of controlled saline tracer injection, Journal of Applied Geophysics 44: 85–102.

Slater, L., A. Binley., R. Versteeg, G. Cassiani, R. Birken, and S. Sandberg. 2002. A 3D ERT study of solute transport in a large experimental tank. Journal of Applied Geophysics 49: 211-229.

Smoluchowski, M. 1905. Theory of electrophoretic deposition and surface conduction. (in German). Physikalische Zeitung 6:529-536.

Sprunt, E.S., T.B. Mercer, and N.F. Djabbarah. 1994. Streaming potential from multiphase flow. Geophysics 59: 707, doi: 10;1190/1.443628.

Srayeddin, I., and C. Doussan. 2009. Estimation of the spatial variability of root water uptake of maize and sorghum at the field scale by electrical resistivity tomography. Plant and Soil 319: 185-207.

Stern, O.,. 1924. Theory of the electrical double layer (in German). Electrochemistry 30:508-516.

Suski, B., A. Revil, K. Titov, P. Konosavsky, M. Voltz, C. Dagés and O. Huttel. 2006. Monitoring an infiltration experiment using self-potential method. Water Resources Research 42:W08418.

Timlin, D., and Y. Pachepsky. 1998. Measurement of unsaturated soil hydraulic conductivities using a ceramic cup tensiometer. Soil Science 163: 625-635.

Toorman, A.F., P.J. Wierenga, and R.G. Hills. 1992. Parameter estimation of hydraulic properties from one-step outflow data. Water Resources Research 28: 3021-3028.

Topp, G.C., J.L. Davis, and A.P. Annan. 1982. Electromagnetic determination of soil water content using TDR. 1. Applications to wetting fronts and steep gradients. Soil Science Society of America Journal 46:672-687.

Topp, G.C., J.L.Davis and A.P. Annan. 1980. Electromagnetic determination of soil water content: measurements in coaxial transmission lines. Water Resources Research 16(3): 574-582

Turesson, A.,. 2006. Water content and porosity estimated from ground-penetrating radar and resistivity. Journal of Applied Geophysics 58: 99–111.

Ulrich, C. and L.D. Slater. 2004. Induced polarization measurements on unsaturated, unconsolidated sands. Geophysics 69: 762-771.

van Dam, J.C., J.N.M. Stricker, and P. Droogers. 1994. Inverse method to determine soil hydraulic functions from multistep outflow experiments. Soil Science Society of America Journal 58: 647-652.

Van Gemert, M.J.C. 1973. High-frequency time-domain methods in dielectric spectroscopy, Philips Research Reports 28:530-572.

van Genuchten, M.T. 1980. A closed-form equation for predicting the hydraulic conductivity of unsaturated soils. Soil Science Society of America Journal 44: 892–89.

Van Overmeeren, R.A., S.V. Sariowan, and J.C. Gehrels. 1997. Ground penetrating radar for determining volumetric soil water content; results of comparative measurements at two sites. Journal of Hydrology 197: 316-338.

Vereeken, H., J.A. Huisman, H. Bogena, J. Vanderborght, .J.A. Vrught, and J.W. Hopmans. 2008. On the value of soil moisture measurements in vadose zone hydrology: A review. Water Resources Research 40: WD00D06.

Vereecken, H., S. Hubbard, A. Binley and T. Ferré. 2004. Hydrogeophysics: An introduction from guest editors. Vadose Zone Journal 3: 1060-1062.

Vouillamoz, J.M., A. Legchenko, L. Nandagiri. 2011. Characterizing aquifers when using magnetic resonance sounding in a heterogeneous geomagnetic field. Near Surface Geophysics 9: 135-144.

Vrugt, J.A. and B.A. Robinson. 2007. Improved evolutionary optimization from genetically adaptive multimethod search. Proceedings of the National Academy of Sciences 104: 708-711.

Vrugt, J.A., and W. Bouten. 2002. Validity of first-order approximations to describe parameter uncertainty in soil hydrologic models. Soil Science Society of America Journal 66(6):1740-1751.

Wang, D., S.R. Yates and F.F. Ernst.1998. Determining soil hydraulic properties using tension infiltrometers, time domain reflectrometry and tensiometers. Soil Science Society of America Journal 62: 318-325.

Waxman, M.H., and L.M.M. Smits. 1968. Electrical conductivities in oil-bearing shaly sands. Society of Petroleum Engineering 243: 107-122.

Weerts, A.H., J.A. Huisman, and W. Bouten. 2001. Information content of time domain reflectometry waveforms. Water Resources Research 37:1291-1299.

Wetzel, R.G. 2001. Fresh water ecosystems. Encyclopaedia of Biodiversity 3: 75-87.

Wilkinson, P.B., P.I. Meldrum, O. Kuras, J.E. Chambers, S.J. Holyoake, and R.D. Ogilvy. 2010. High-resolution electrical resistvity tomography monitoring of a tracer test in a confined aquifer. Journal of Applied Geophysics 70**:** 268-276.

Wyseure, G.C.L, and M.A. Mojid. 1997. Measurement of volumetric water content by TDR in saline soils. European Journal of Soil Science 48:348-354.

Yeh, T.C.J., and J. Simunek. 2002. Stochastic fusion of information for characterizing and monitoring the vadose zone. Vadose Zone Journal 1: 207-221.

Yeh, T.-C., S. Liu, R.J. Glass, K. Baker, R. Brainard, D. Allumbaugh, and D. LaBrecque. 2002. A geostatiscally based inverse model for electrical resistivity surveys and its applications to vadose zone hydrology. Water Resources Research 38(12): 1278, doi:10.1029/2001WR001204.

Zablocki, C.J. 1978. Streaming potentials resulting from the descent of meteoric water- A possible mechanism for the Kilauean self potential anomalies. Transactions of the Geothermal Resources Council 2:747-748.

Zhang, F.Z., R.G. Kachanoski, G.W. Parkin, and B. Si. 2000. Measuring hydraulic properties using a line source: II. Field test. Soil Science Society of America Journal 64: 1563-1569.

Zimmermann, E., A. Kemna, W. Glaas, and H. Vereecken. 2008. EIT measurement system with high phase accuracy for imaging spectral induced polarization properties of soils and sediments. Measurement Science and Technology 19:094010.